DEVELOPMENT OF A CONTROL SYSTEM TO DETERMINE INFLUENCE OF ROLLING RESISTANCE IN MANUAL WHEELCHAIR DYNAMICS AND MECHANICAL EFFICIENCY

A Thesis
Presented to
The Academic Faculty

by

Efrain Andres Teran Calle

In Partial Fulfillment
of the Requirements for the Degree
Master of Science in the
School of Mechanical Engineering

Georgia Institute of Technology
December 2014

DEVELOPMENT OF A CONTROL SYSTEM TO DETERMINE INFLUENCE OF ROLLING RESISTANCE IN MANUAL WHEELCHAIR DYNAMICS AND MECHANICAL EFFICIENCY

Approved by:

Dr. Jun Ueda, Advisor
School of Mechanical Engineering
Georgia Institute of Technology

Dr. Stephen Sprigle
School of Applied Physiology
Georgia Institute of Technology

Dr. Aldo Ferri
School of Mechanical Engineering
Georgia Institute of Technology

Date Approved: November 21, 2014

To the people of the Republic of Ecuador.

ACKNOWLEDGEMENTS

I would like thank my mother and father, without whose guidance and support I would not be here. I would also like to thank my girlfriend for her love and support during these years.

I would like to thank my advisor Dr. Jun Ueda for his continuous support, guidance and patience, my committee members for their advice, and my fellow lab members for offering me their friendship and help.

Special thanks to the government of the Republic of Ecuador for supporting my graduate studies, to the National Institute on Disability and Rehabilitation Research of the U.S. Department of Education, under grant number H133E070003, for supporting the AMPS research, and to the National Science Foundation, IIS #1316617, for supporting my summer internship.

TABLE OF CONTENTS

LIST OF TABLES

LIST OF FIGURES

LIST OF SYMBOLS AND ABBREVIATIONS

1	Subscript used for the RIGHT side of the wheelchair
2	Subscript used for the LEFT side of the wheelchair
2D	Two-dimensional
a_{cn}	Center of mass normal acceleration
a_{ct}	Center of mass tangential acceleration
a_{cx}	Center of mass linear acceleration on the x axis
a_{cy}	Center of mass linear acceleration on the y axis
a_y	Forward wheelchair acceleration on the y axis
α	Caster wheel orientation with respect to the xy frame
a_y	Forward wheelchair acceleration on the y axis
$[A]$	Motor electric current matrix
a	Linear acceleration
AMPS	Anatomical Model Propulsion System
A	Motor electric current
c	Pulse cycle duration
COT	Cost of transport
COM	Center of mass
COT_m	Cost of transport (mass)
d	Distance travelled during a pulse cycle
d_R	Distance between rear wheels
d_L	Distance between rear axis and caster pivots
d_C	Caster trail
d_F	Distance between caster forks

D	Wheelchair travelled distance
ds	Wheel linear displacement
$d\theta$	Wheel angular displacement
dS	Wheelchair linear displacement
DC	Direct current
E_{output}	System's energy output
E_{input}	System's energy input
$\emptyset$	Wheelchair orientation angle
$\dot{\emptyset}$	Wheelchair orientation angular velocity
F_y	Total force in the y direction
F_1	Force applied to the right rear wheel
F_2	Force applied to the left rear wheel
F_R	Rolling resistance force on a rear wheel
F_{TR}	Rear wheel lateral force
F_{TC}	Caster wheel lateral force
F_{Roll}	Total rolling resistance
FBD	Free-body diagram
h	Amplitude of pulse
I_o	Mass moment of inertia with respect to the point O
I_R	Mass moment of inertia of rear wheels
I_{Fork}	Mass moment of inertia of caster forks
K_t	Motor torque constant
KE_{Total}	System's total kinetic energy
KE_i	System's kinetic energycomponent
k_1, k_2, k_3, k_4	Integration constants

λ	Rolling resistance parameter
λ_R	Rolling resistance parameter of the rear wheels
λ_c	Rolling resistance parameter of the caster wheels
$[\lambda]$	Rolling resistance parameters matrix
L	Trajectory total length
m	Combined mass of the AMPS and wheelchair
M_o	Total moment of force with respect to the point O
M_R	Resistive moment of force at a rear wheel
M_c	Resistive moment of force at a caster wheel
M_C	Total moment of force about point C
NI	National Instruments
η	Energy conversion efficiency
N	Normal force
N_R	Normal force on the rear wheels
N_c	Normal force on the caster wheels
$[N]$	Normal force coefficient matrix
O	Rear axis center point
P	Motor electric power
p	Pulse duration
r_R	Rear wheel radius
R	Instantaneous radius of curvature
r_c	Caster wheel radius
r	Wheel radius
RRP	Rolling resistance parameter
T	Motor torque

t	Time
T_{res}	Total turning resistance
t_o	Initial time of pulse
t_p	Final time of pulse
$\Delta\theta$	Wheel angular displacement
$\dot{\theta}$	Wheel angular velocity
$\ddot{\theta}$	Wheel angular acceleration
$\Delta\theta_i$	Change in wheel angular displacement at step i
V_m	Velocity profile maximum velocity
V	Forward wheelchair velocity on the y axis
w	Motor angular velocity
Δx	Wheelchair displacement on the x axis
xy	Body-fixed coordinate frame
$\bar{x}$	Center of mass location on the x axis
XY	Ground-fixed absolute coordinate frame
$\dot{X}$	Absolute wheelchair velocity on the X axis
$\dot{x}$	Wheelchair velocity on the x axis
X_n	Absolute location of wheelchair on the X axis at step n
ΔX_i	Change in wheelchair absolute location on the Y axis at step i
$\bar{y}$	Center of mass location on the y axis
$\dot{Y}$	Absolute wheelchair velocity on the Y axis
$\dot{y}$	Forward wheelchair velocity on the y axis
Y_n	Absolute location of wheelchair on the Y axis at step n
ΔY_i	Change in wheelchair absolute location on the Y axis at step i
Δy	Wheelchair displacement on the y axis

SUMMARY

Manual wheelchairs are essential mobility tools for millions of people with disabilities around the world. Manufactures' ability for designing wheelchairs and users' proficiency in selecting among different models are only limited by the current understanding of wheelchair dynamics and performance. Increasing such understanding could benefit both producers and users of manual wheelchairs.

The amount of effort a person needs to perform a maneuver on a manual wheelchair directly affects their mobility. This effort depends on two major factors: the particular propulsion biomechanics of the passenger and the mechanical characteristics of the wheelchair. The latter includes rolling resistance, which is the most important resistive force affecting manual wheelchairs' dynamic behavior. Several studies have measured rolling resistance using diverse methodologies and equipment including dynamometers, treadmills and instrumented wheelchairs. Rolling resistance has been reported to depend on tire and floor materials, total loads applied to the wheels and the velocity of the vehicle, among other factors. A new approach for testing rolling resistance was used in this work. The results found here confirm previous conclusions that rolling resistance increases with velocity but also adds new evidence that rolling resistance increase significantly with acceleration on a manual wheelchair.

Another resistive effect of importance is turning resistance. This resistive moment of force is manifest when a wheelchair changes orientation and the tires scrub the floor. Published work studying turning resistance on manual wheelchairs is very scarce. The

present work also presents a new approach to estimate turning resistance in manual wheelchairs and presents evidence that it depends on the radius of rotation.

Research performed on manual wheelchairs usually involves human passengers, bringing in some unfortunate disadvantages. Experiments requiring high repetition or precise maneuver control are affected by the variability introduced by the passenger. Human test subjects differ in their disability, propulsion technique, dexterity and overall physical condition. It is therefore desirable to create a system capable of performing experiments on manual wheelchairs keeping high accuracy and repeatability. The Anatomical Model Propulsion System (AMPS) was designed to propel manual wheelchairs in a highly repeatable manner while emulating human weight distribution and force application. The AMPS is intended to become a test bed for analyzing manual wheelchair dynamics and mechanical efficiency, allowing an objective and quantitative comparison among different wheelchair models actual performance.

This thesis work presents the development of a control system for the AMPS and its application on several sets of experiments directly related to its desired application. The control system allows the AMPS to perform maneuvers with precision for different types of trajectories. A mathematical model of wheelchair kinematics and dynamics was fundamental for developing the AMPS' controller and analyzing the data collected during experiments. The AMPS' controller uses an estimation of input forces provided by the model along with real time feedback to create an appropriate maneuver control of the wheelchair.

Experiments performed over a straight path at different constant speeds confirmed that rolling resistance changes with velocity. Additional experiments show new evidence

that rolling resistance also increases significantly with acceleration on manual wheelchairs. Rolling resistance parameters were determined for front and rear wheels and later used for interpreting data from turning resistance experiments. Based on the developed dynamic model, turning resistance could be estimated by doing experiments with the wheelchair moving along a simple curvilinear path. Circular trajectory maneuvers were performed with the AMPS to estimate the total turning resistance at different radius of curvature. Results show new evidence that turning resistance increase as the radius shortens.

Besides measuring resistive forces, quantifying wheelchair efficiency was an important objective of this work. Mechanical efficiency definition is not unique however. Two particular indices, energy conversion efficiency (η) and cost of transport (COT), were selected due to their relevance for vehicles. Energy conversion efficiency was found to vary significantly during different values of acceleration. COT was measured in straight and circular maneuvers with constant linear velocity. COT was found to increase as linear velocity increased and the radius of curvature was reduced. These results were consistent with experiments showing that rolling resistance incremented with velocity and that turning resistance increased with smaller radius of curvature. Wheelchair efficiency could be used to compare the performance of different wheelchair models over common maneuvers, helping clinicians do more informed decisions for their patients.

Finally, an original type of controller was developed providing the AMPS with the ability to propel a manual wheelchair emulating human pulsatile propulsion. Frequency and duration of pulses were modified to compare the effects of various propulsion techniques. The findings on COT for these pulsatile propulsion experiments can be partially explained by the results on previous experiments. Future work could involve using

this unique kind of controller to improve our understanding of wheelchair propulsion biomechanics and efficiency.

CHAPTER 1

INTRODUCTION

1.1 Background

According to the World Health Organization around 65 million people in the world (1%) need a wheelchair to meet their mobility needs [1]. In the US alone roughly 3.5 million people are manual wheelchair users [2]. The market for manual wheelchairs offers many different brands and models, assembled with components from distinct manufacturers. Prices ranges from under $200 to several thousand dollars for a manual wheelchair, depending on many factors such as brand, frame material, wheels type, seat cushion and overall weight. However, there is not one common technical standard to compare different models and make a selection based on overall manual wheelchair performance.

A variety of research has been done attempting to determine the effort needed to ride a manual wheelchair and evaluate its performance. Two major factors affect this effort according to research: the propulsion biomechanics of the human passenger riding the wheelchair and the mechanical aspects of the wheelchair itself. Some studies focus on the movement of the passenger upper limbs and propulsion [3-4], or try to determine energy input by measuring oxygen consumption [5]. Another set of studies focus on the mechanical aspects of the wheelchair itself by measuring resistive forces such as rolling resistance [6-10]. The present work also focus on mechanical aspects, trying to establish a series of experiments that could be used as a methodology for comparing several wheelchair models based on performance.

Experiments evaluating wheelchair performance are usually made with the help of human passengers [4-6]. Unfortunately humans present some characteristics that increase the complexity of performing experiments and interpreting their results. The broad spectrum of possible body injuries and disabilities determine the patient's ability to perform maneuvers on a manual wheelchair [11]. Even when using healthy subjects, their body size, weight, physical condition and propulsion techniques can vary significantly. Additionally, an individual's precision for repeating a test is limited by his skills, available time and stamina.

In this thesis work a new approach to performing precise experiments is used to gather relevant manual wheelchair performance information without using human passengers. The Anatomical Model Propulsion System (AMPS) is a robotic device designed to act as a manual wheelchair passenger. The AMPS mimics the weight distribution of an average passenger placed on the seat [12]. It propels the wheelchair by using two electric motors engaged to the rear wheels through spur gears. The control system that governs the AMPS was developed in this work (chapter 4), achieving precision of motion used in the variety of experiments described in chapter 6. Further details on the AMPS can be found in chapter 3 of this thesis.

The user effort and wheelchair mechanical efficiency during motion are highly affected by rolling resistance, which is a resistive force depending on many factors such as vehicle speed, tire and floor materials, tire inflation pressure, loads applied to wheels, etc. [13]. The understanding of this particular force over several conditions could lead to improvements in wheelchair design and component selection. Rolling resistance fundamentals are described in more detail in appendix D. Several methodologies has been

used to measure rolling resistance over a variety of conditions. Each of these methods present some disadvantages that limit the scope of study of rolling resistance [14]. In this thesis work, a new device and methodology is introduced to study rolling resistance over a variety of conditions that wasn't possible before.

When a trajectory include direction changes, a resistive moment of force known as turning resistance affects the effort needed to maneuver a wheelchair. Little literature is known by the author regarding the study or measurement of turning resistance (see appendix D). The AMPS was used in experiments estimating turning resistance on a manual wheelchair moving along a circular trajectory.

The definition of mechanical energy efficiency for a system can vary among disciplines [15]. In general, for a mechanical system, energy efficiency involves the ratio between a 'useful output' and the amount of energy required produce it. A common metric for efficiency is the energy conversion efficiency (η). It is a ratio between the system's energy output (kinetic energy of a wheelchair) and the energy input required by the system to create such output (electric power in the case of the AMPS). For transportation vehicles one common efficiency index is the cost of transport (COT) [16]. COT relates the distance travelled by a vehicle, its mass, and the energy required to complete such task. It compares the energy consumed by different vehicles for achieving the same task.

1.2 Motivation

Any increment on our knowledge of wheelchairs is beneficial to the individuals who use them, clinicians, the industry and society in general. Better understanding wheelchair dynamics may help manufactures improve manual wheelchair design and component choices. Designers could decide which parameters are more important to improve and what choices are more globally relevant. By focusing on the factors that affect the overall wheelchair performance and efficiency, doctors and clinicians could select better wheelchair options to meet the needs of their patients. This would be an improvement over the current practice of comparing wheelchairs based on their weight.

Previous methods studying wheelchair dynamics and resistive forces present certain limitations. Some can only test the rear wheels, omitting the casters, or are limited to very specific surfaces. Others allow testing wheelchairs only on straight trajectories. An innovative method that facilitates the measurement of resistive forces over a broad spectrum of motions, trajectories and floor surfaces would certainly constitute an improvement over other previous approaches. This work is focused on implementing a new proposed method involving the AMPS and testing its capabilities through a series of experiments. The results presented here were intended to demonstrate some of the AMPS possible applications, not to provide exhaustive statistical information about any particular test.

Determining rolling resistance, turning resistance and wheelchair mechanical efficiency, allows to objectively compare different models of wheelchairs under various circumstances. Using the AMPS to provide fast and accurate results regarding rolling

resistance, turning resistance and mechanical efficiency, for a particular wheelchair model or configuration, could provide a reasonable testing platform for manufacturers.

Since tests with human passengers have repeatability and variability inconveniences, using the AMPS to isolate the mechanical aspects of a manual wheelchair would be most valuable for comparing different products. Its results are not be affected by the individuals acting as test subjects including the possible variations among them. However, a set of experiments emulating human pulsatile propulsion is highly desirable. It would allow to correlate results provided by the AMPS with tests performed with human passengers. The precise control of the propulsion pattern could shed new light on the effects of different propulsion techniques in the overall wheelchair efficiency.

1.3 Research objectives

1.3.1 General Objectives

- The primary objective of this project is to design and test a control system for the AMPS, capable of accurately producing wheelchair maneuvers.
- Experiments designed and performed by the AMPS must convey relevant information that improves our knowledge of resistive forces and overall wheelchair mechanical efficiency. Results should be quantifiable and relevant to compare among different manual wheelchairs and configurations.
- Some experiments should also include resemblance to human propulsion on manual wheelchairs, making the system relatable to actual passengers' tests and previously published studies.

To meet these objectives the following specific aims were defined:

1.3.2 Specific Objectives

- Select a mathematical model that accurately describes the AMPS-wheelchair system and use it create a feed-forward portion of the controller system.
- Develop an open-loop controller able to propel the AMPS with accurate forces regardless of the output.
- Develop a closed-loop controller that allows the AMPS to perform any given maneuver or trajectory.
- Design and perform experiments measuring rolling resistance as a function of velocity and acceleration.
- Design and perform experiments that measure turning resistance for different radios of curvature.
- Develop a controller that emulates human pulsatile propulsion including freewheeling periods. Recreate the effect of freewheeling without disconnecting any mechanical devices. Establish a methodology to create the pulses necessary for a straight maneuver.
- Select an appropriate metric for wheelchair mechanical efficiency and quantify the performance of a wheelchair over various common maneuvers, providing meaningful information useful to compare different wheelchairs.
- Compare straight path experiments, curvilinear trajectories experiments and pulsatile propulsion experiments in terms of mechanical efficiency.

CHAPTER 2

WHEELCHAIR DYNAMICS

The dynamic analysis of a manual wheelchair is fundamental to this work. The controller developed in chapter 4 uses this analysis for estimating the forces necessary to control the wheelchair through a maneuver. Additionally, experiments designed and performed in chapter 6 were based in the wheelchair model presented here. The results of such experiments were evaluated using the equations presented in this chapter.

A publication by Johnson and others [17] presented a complete dynamic analysis model for an electric wheelchair that could be conveniently adapted to the present work. Several other dynamic models has been released over the years [14, 18] by making different assumptions and simplifications. However, the basic model elements remain the same and has created a common representation and understanding of manual wheelchairs among researchers. The dynamic model of a wheelchair used in this work identify resistive forces such as rolling resistance, turning resistance and friction, and neglects minor resistive effects such as air drag. It also assumes the wheelchair frame as perfectly rigid and regards the location of the center of mass (COM) with respect to the rear axis wheel as constant.

Rolling resistance and turning resistance directly affects the dynamic behavior of wheelchairs in addition to the vehicle's inertial properties. The accurate study of these resistive forces requires a dynamic model able to identify their effects and quantitatively estimate their value through experiments. Equations and relations determined in this chapter permits the later analysis of experimental data to characterize rolling resistance and turning resistance.

The development of a controller in chapter 4 requires a kinematic and dynamic model that is accurate enough to predict the forces needed by the wheelchair to perform a proposed maneuver. Kinematic modeling of a wheelchair is the analysis that describes the

motion of the vehicle without considering forces or inertial properties. Calculating the entire motion of the wheelchair by knowing the angular changes in the rear wheels is identified as forward kinematics. The opposite process, i.e. calculating the angular changes of the rear wheels by knowing the final motion of the wheelchair, is identified as inverse kinematics. Both approaches are used throughout this work. Considering the forces and inertial properties of the wheelchair producing its motion is known as dynamic analysis. Forward dynamic analysis determines the final wheelchair motion starting from the knowledge of the forces acting on it. Inverse dynamic analysis consists in determining the forces that act on the vehicle by knowing its motion. Once again, both approaches are important to this work. Inverse dynamics is used in the AMPS controller while forward dynamics is used to analyze experimental data.

Kinematic and dynamic analysis complement each other by fully describing the motion of the wheelchair and the forces producing it. Each of the next sections present a part of the total wheelchair analysis in detail and describes what it is used for in this work. Due to the length of the analysis and for sake of clarity, some details have been moved to appendices.

2.1 Wheelchair forward kinematics

Forward kinematics is the description of the wheelchair's complete motion over the floor starting with the knowledge of the rear wheels' angular displacement, velocity and acceleration. It was deemed appropriate to spare this section from some of the details of this analysis by presenting only the most relevant results. The complete derivation of equations is detailed in appendix A.

Manual wheelchairs have two wheels attached to the rear axis at each side of the passenger's seat. They are pushed by the wheelchair passenger producing their rotation and

the motion of the wheelchair. Two front casters wheels are passive elements that support part of the wheelchair weight and facilitate turning by changing their orientation as the wheelchair turns. The distance between wheels, casters and axes, among other wheelchair dimensions, need to be identified for beginning the kinematic analysis. Wheelchair dimensions relevant to the present analysis are shown in figure 2.1.

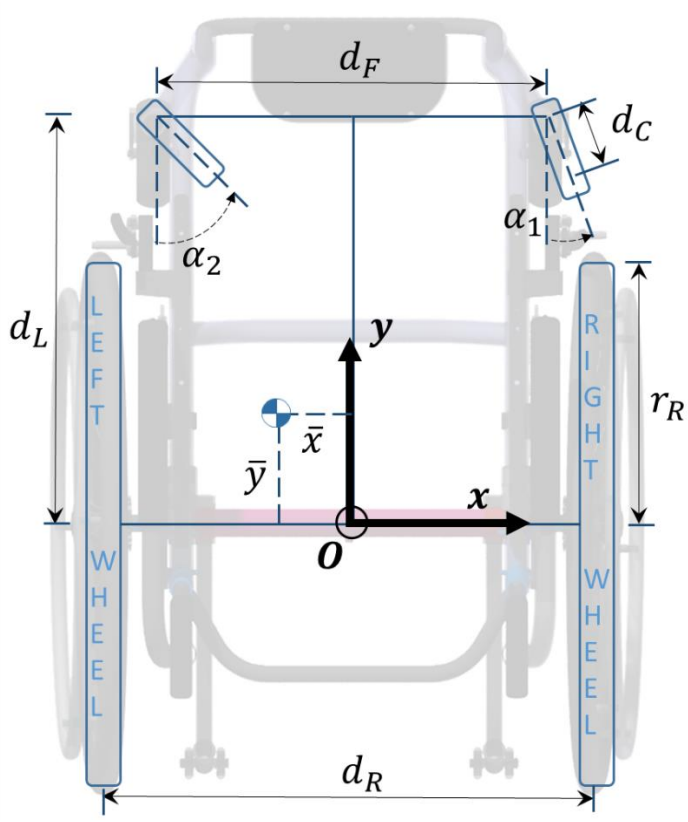

Figure 2.1 Top view of a manual wheelchair showing dimensions.

The particular name for each symbol in figure 2.1 describing the geometry of a manual wheelchair, and subsequent figures, can be found on the 'List of symbols' section in the initial pages of this document. Throughput this work the subscript 1 refers to the right side of the wheelchair while the subscript 2 refers to the left side.

The coordinate frame xy is fixed to the rear wheels axis center point, which is named O. The center of mass (COM) is located at coordinates $(-\bar{x}, \bar{y})$ on the xy frame.

Throughout this analysis it is assumed that the wheelchair does not move laterally. This means that velocity and acceleration on the body-fixed x direction is always zero.

The following figure shows a top view of a manual wheelchair moving on a 2D plane with a general curvilinear trajectory.

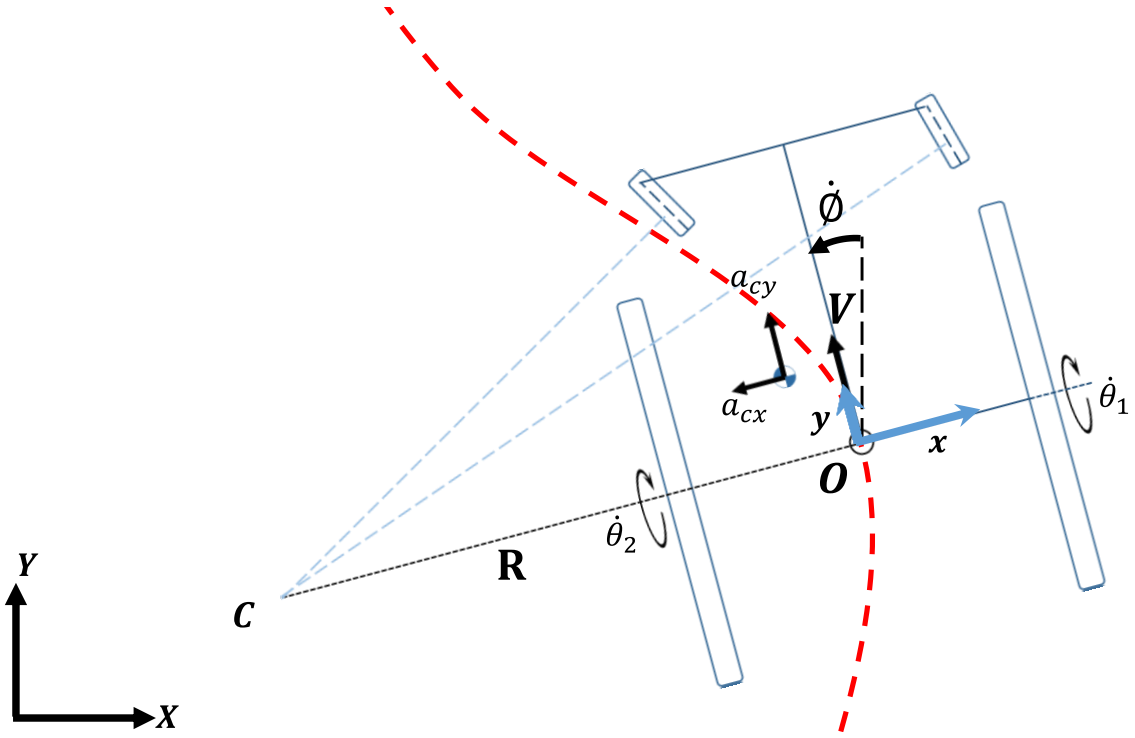

Figure 2.2 Kinematic model of a manual wheelchair.

Figure 2.2 shows the kinematic description of a wheelchair following a general curvilinear path over the floor (shown in red). xy is a coordinate frame fixed to the wheelchair body, while XY is a global (absolute) reference frame fixed to the ground, from which the absolute position and orientation of the wheelchair are measured. V represents the linear velocity of the wheelchair. Notice that from, the xy frame perspective, V always points in the forward y direction. The angle $\emptyset$ represents the orientation of the wheelchair with respect to the global reference vector Y, and $\dot{\emptyset}$ represents the angular velocity (orientation change) of the wheelchair with respect to the XY reference frame. $\dot{\theta}_1$ and $\dot{\theta}_2$

are the angular velocities of the rear wheels measured with respect to the xy frame. R is the instantaneous radius of curvature of the trajectory about the instantaneous center C.

From appendix A, the following equations relate the rear wheels angular velocities with the linear velocity of the wheelchair and its orientation angular velocity:

$$V = \frac{1}{2} r_R (\dot{\theta}_1 + \dot{\theta}_2) \tag{2.1}$$

$$\dot{\phi} = \frac{(\dot{\theta}_1 - \dot{\theta}_2)}{d_R} \tag{2.2}$$

$$\dot{\phi} = \frac{V}{R} \tag{2.3}$$

For the dynamic analysis (section 2.3) accelerations at point O and the COM are required. The equations describing such accelerations are:

$$a_y = \frac{1}{2} r_R (\ddot{\theta}_1 + \ddot{\theta}_2) \tag{2.4}$$

$$a_{cx} = -\bar{y} \frac{r_R}{d_R} (\ddot{\theta}_1 - \ddot{\theta}_2) \tag{2.5}$$

$$a_{cy} = \frac{r_R}{2}\left(1 - \frac{2\bar{x}}{d_R}\right)\ddot{\theta}_1 + \frac{r_R}{2}\left(1 + \frac{2\bar{x}}{d_R}\right)\ddot{\theta}_1 \tag{2.6}$$

As stated at the beginning of the chapter, in the kinematic analysis, the rear wheels' displacement are used to determine the movement of the wheelchair. The trajectory of the wheelchair can be accurately determined from the angular position and velocity of the rear

wheels assuming there is no slip between tires and floor. A positive angular change in both wheels displace the whole wheelchair in the 'forward' direction, which corresponds to the body-fixed y axis. A difference between the angular velocities of the wheels generates a change of wheelchair orientation $\emptyset$.

To calculate the absolute position and velocities of the wheelchair's O point with respect to the ground-fixed XY reference frame the following equations are used:

$$\dot{Y} = \dot{y} \cos\emptyset = V \cos\emptyset \tag{2.7}$$

$$\dot{X} = \dot{x} \sin\emptyset = V \sin\emptyset \tag{2.8}$$

$$Y_n = \sum_{i=1}^{n} \Delta Y_i = \sum_{i=1}^{n} \frac{1}{2} r_R (\Delta\theta_{1i} + \Delta\theta_{2i}) \cos\left(\frac{r_R}{d_R}(\Delta\theta_{1i} - \Delta\theta_{2i})\right) \tag{2.9}$$

$$X_n = \sum_{i=1}^{n} \Delta X_i = \sum_{i=1}^{n} \frac{1}{2} r_R (\Delta\theta_{1i} + \Delta\theta_{2i}) \sin\left(\frac{r_R}{d_R}(\Delta\theta_{1i} - \Delta\theta_{2i})\right) \tag{2.10}$$

Regarding the caster wheels work published by Chenier and others [19] offered simplified equations to estimate their orientation during a maneuver.

$$\dot{\alpha}_1 = \frac{\dot{\emptyset}}{d_C}\left(d_L \cos\alpha_1 - \frac{d_F \sin\alpha_1}{2} - d_C\right) - \frac{V}{d_C}\sin\alpha_1 \tag{2.11}$$

$$\dot{\alpha}_2 = \frac{\dot{\emptyset}}{d_C}\left(d_L \cos\alpha_1 + \frac{d_F \sin\alpha_2}{2} - d_C\right) - \frac{V}{d_C}\sin\alpha_2 \tag{2.12}$$

However, a practical approximation for determining the caster orientation is to consider that the casters align themselves tangentially to the instantaneous center of rotation of the wheelchair.

2.2 Wheelchair inverse kinematics

Inverse kinematics is the process of determining the position, velocities and acceleration of the rear wheels from the trajectory and velocity profile of the wheelchair during a maneuver. The detailed equation derivation of this section can be found in appendix B.

The inverse kinematics calculation process starts by defining a trajectory and velocity profile as shown in figures 2.3 and 2.4.

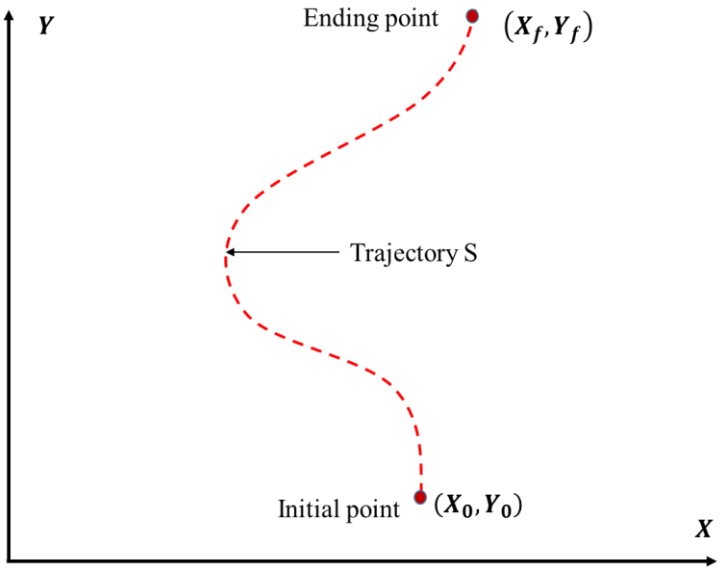

Figure 2.3 Wheelchair trajectory used in the inverse kinematics calculation process.

Wheelchair orientation along the path is easily determined by calculating the tangent of the curve at any given point of the trajectory. The total length of the curve can be determined by adding up the infinitesimal distances between each point on the curve. Having the total length of the curve and a velocity profile allows us to assign a linear velocity to each point along the path. Additionally, since each of these locations along the curve is already related to a wheelchair orientation, now the orientation is defined a function of time. Both velocity and orientation can be differentiated to obtain linear and angular acceleration. This means that, starting from a known trajectory and velocity profile, it is possible to determine $y(t)$, $\emptyset(t)$, $V(t)$, and $\dot{\emptyset}(t)$. $y(t)$ is the displacement of the wheelchair along its body-fixed y axis and $V(t)$ is the linear velocity along the same direction. $\emptyset(t)$ is the orientation of the wheelchair with respect to the ground-fixed XY frame and $\dot{\emptyset}(t)$ is the rate of change of that orientation.

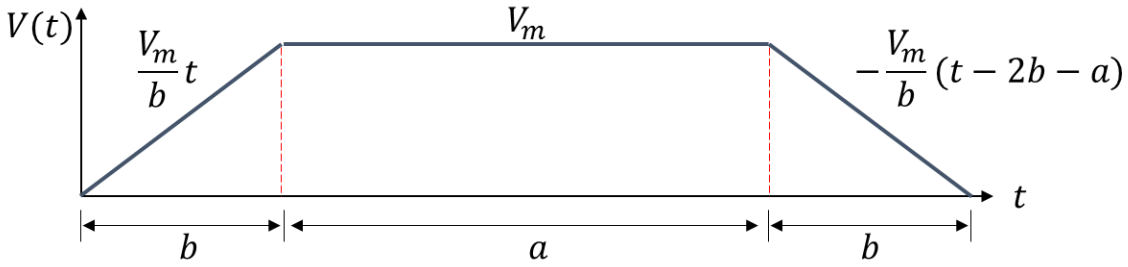

Figure 2.4 Wheelchair velocity profile used in the inverse kinematics calculation process.

The following sets of equations show how to calculate the rear wheels angular velocities and acceleration.

$$\dot{\theta}_1 = \frac{V}{r_R} + \frac{\dot{\emptyset}\, d_R}{2r_R} \tag{2.13}$$

$$\dot{\theta}_2 = \frac{V}{r_R} - \frac{\dot{\phi}\, d_R}{2r_R} \tag{2.14}$$

$$\ddot{\theta}_1 = \frac{a_y}{r_R} + \frac{\ddot{\phi}\, d_R}{2r_R} \tag{2.15}$$

$$\ddot{\theta}_2 = \frac{a_y}{r_R} - \frac{\ddot{\phi}\, d_R}{2r_R} \tag{2.16}$$

2.3 Wheelchair forward dynamics

Dynamics is the branch of mechanics that studies forces and their effect on a body's motion. For a wheelchair passenger system, the dynamic analysis includes inertial properties (such as mass and mass moment of inertia) and resistive forces (such as rolling resistance, bearing resistance, tire friction and air drag).

Figure 2.3 presents a free body diagram (FBD) of a wheelchair. Air drag force is not included since previous studies demonstrate that, for the velocity range used in manual wheelchairs, it is negligible [20]. In addition to that, the frictional resistance created by the bearings in the wheels' joints are not included since it manifest in the wheels and is undistinguishable from the effect of rolling resistance.

The following dynamic equations can be directly written from the FBD:

$$\sum F_y = ma_{cy} = (F_1 + F_2) - (F_{R1} + F_{R2}) - (F_3 + F_4) \tag{2.17}$$

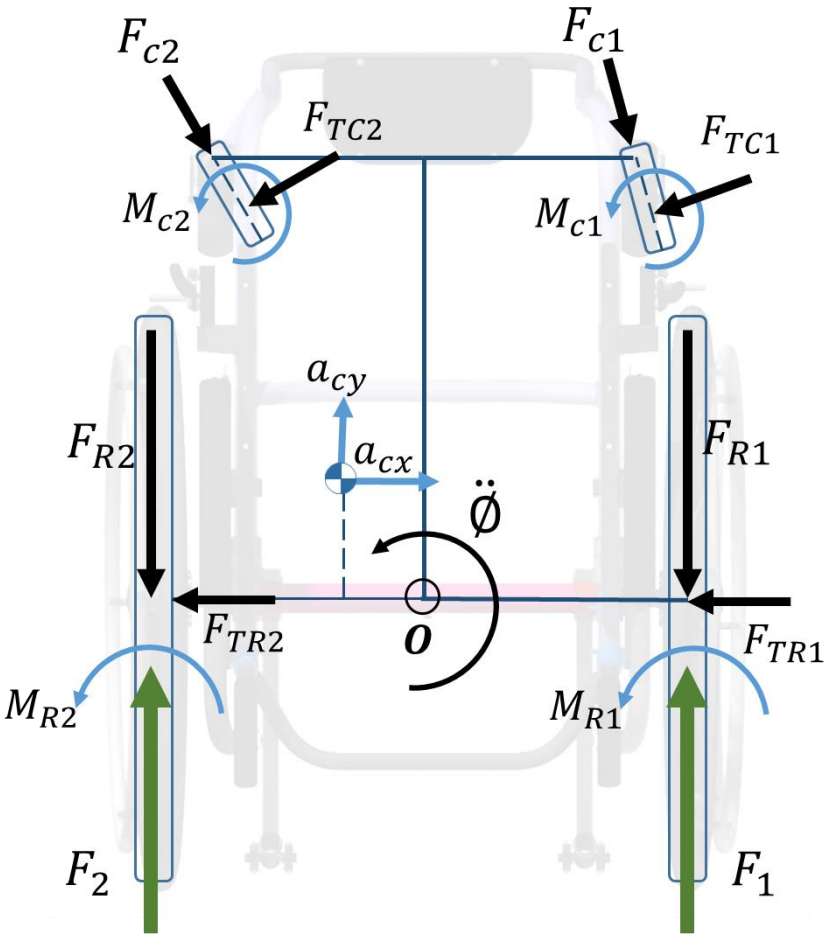

Figure 2.5 Wheelchair free body diagram.

$$\sum M_o = I_o\ddot{\emptyset} - \bar{x}ma_{cy} - \bar{y}ma_{cx} \tag{2.18}$$

$$= (F_1 - F_2 + F_{R1} - F_{R2})\frac{d_R}{2} + (F_3 - F_4)\frac{d_F}{2}$$

$$+(F_5 - F_6)\frac{d_L}{2} - (M_{R1} + M_{R2} + M_{c1} + M_{c2})$$

Where I_o is the mass moment of inertia and m is the mass of the system. $F_1$and F_2 are the input forces applied to the wheelchair; F_{R1}, F_{R2}, F_{c1}, and F_{c2} are the rolling resistance

produced by the rear wheels and casters; M_{R1}, M_{R2}, M_{c1} and M_{c2} are the turning resistance created by each wheel; F_{TR1}, F_{TR2}, F_{TC1}, and F_{TC2} are the tangential frictional forces preventing wheelchair slip. For convenience and brevity of equations the following algebraic grouping was introduced.

$$F_3 = F_{R1}\cos\alpha_1 + F_{TC1}\sin\alpha_1 \tag{2.19}$$

$$F_4 = F_{R2}\cos\alpha_2 + F_{TC2}\sin\alpha_2 \tag{2.20}$$

$$F_5 = F_{R1}\sin\alpha_1 + F_{TC1}\cos\alpha_1 \tag{2.21}$$

$$F_6 = F_{R2}\sin\alpha_2 + F_{TC2}\cos\alpha_2 \tag{2.22}$$

In the forward dynamic analysis, linear and angular accelerations are calculated by considering the forces acting on the system. The following equations conclude the forward dynamic analysis.

$$\ddot{\emptyset} = \frac{1}{I_o}\,[\bar{x}ma_{cy} + \bar{y}ma_{cx} \tag{2.23}$$

$$-(F_1 - F_2 + F_{R1} - F_{R2})\frac{d_R}{2} - (F_3 - F_4)\frac{d_F}{2}$$

$$-(F_5 - F_6)\frac{d_L}{2} + \ (M_{R1} + M_{R2} + M_{c1} + M_{c2})\ ]$$

$$a_{cy} = \frac{1}{m}[(F_1 + F_2) - \ (F_{R1} + F_{R2}) - \ (F_3 + F_4)] \tag{2.24}$$

$$a_{cx} = \frac{1}{m}[-(F_{TR1} + F_{TR2}) - (F_5 + F_6)] \tag{2.25}$$

2.4 Wheelchair inverse dynamics

The purpose of inverse dynamics is to determine the forces needed by the passenger to create the desired trajectory. From the previous dynamic model equations, the forces can be determined by using some algebraic rearrangement.

$$F_1 = \frac{I_o\ddot{\emptyset}}{d_R} - (F_5 - F_6)\frac{d_L}{2d_R} - \frac{\bar{y}ma_{cx}}{d_R} + \frac{1}{d_R}(M_{R1} + M_{R2} + M_{c1} + M_{c2}) + ma_{cy}\left(\frac{1}{2} - \frac{\bar{x}}{d_R}\right) + F_3\left(\frac{1}{2} - \frac{2d_F}{d_R}\right) + F_4\left(\frac{1}{2} + \frac{2d_F}{d_R}\right) \tag{2.26}$$

$$F_2 = (F_{R1} + F_{R2}) + (F_3 + F_4) + ma_{cy} - F_1 \tag{2.27}$$

Notice that the difficulty in using inverse dynamics equations to determine input forces belies in the amount of information they require. Inertial properties and dimensions are obtained by direct measurements, accelerations are estimated by the inverse kinematics process, and resistive forces have to be estimated or measured. By restricting the motion of the wheelchair to certain kind of trajectories, some of the terms of these equations disappear or can be neglected. In chapter 6 these restrictive conditions are used to measure rolling resistance and turning resistance.

CHAPTER 3

THE ANATOMICAL MODEL PROPULSION SYSTEM (AMPS)

The Anatomical Model Propulsion System, or AMPS, is a robotic device designed as a tool to test manual wheelchairs. Its main advantages are high repeatability and controllability when compared with human subject tests. Human drivers differ significantly in body size, weight, sitting position, type of disability, propulsion technique, and physical fitness. This inconvenient level of human variability can be solved by replacing the human passenger with a robotic device able to propel the wheelchair. AMPS body is modular, allowing control over weight distribution, and its propulsion technique can be programmed as desired.

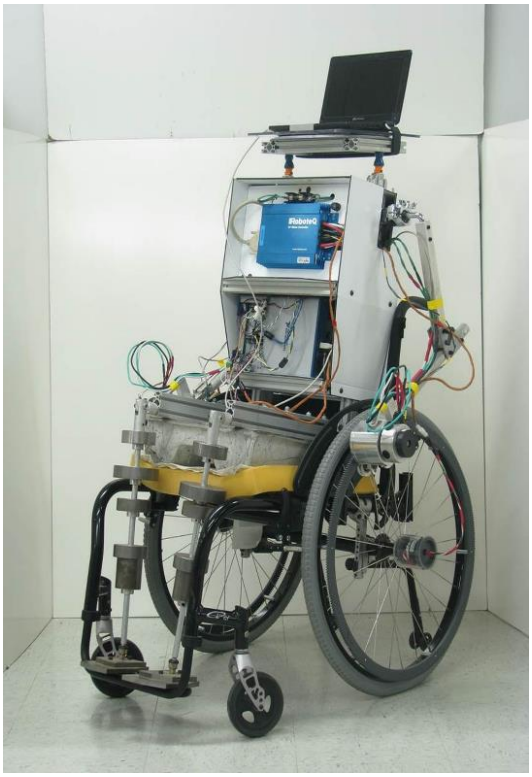

Figure 3.1 The Anatomical Model Propulsion System (AMPS).

3.1 Description of the AMPS

The AMPS' main structure (figure 3.2) is made out of steel or aluminum bars and disks. Limbs and main body resembles the geometry and weight distribution of an average person sitting on a manual wheelchair. Weight can added at will to change the weight distribution and center of gravity of the whole system.

The AMPS has two electric DC brushless motors as main actuators to propel the wheelchair. They are attached tangentially to the rear wheels handrims, resembling the location of a passenger's hands while propelling a wheelchair. In order to transmit torque from the motors to the rear wheels, the handrims on the rear wheels need to be replaced with custom spur gears. They engage with other smaller gears attached to the motors' shafts.

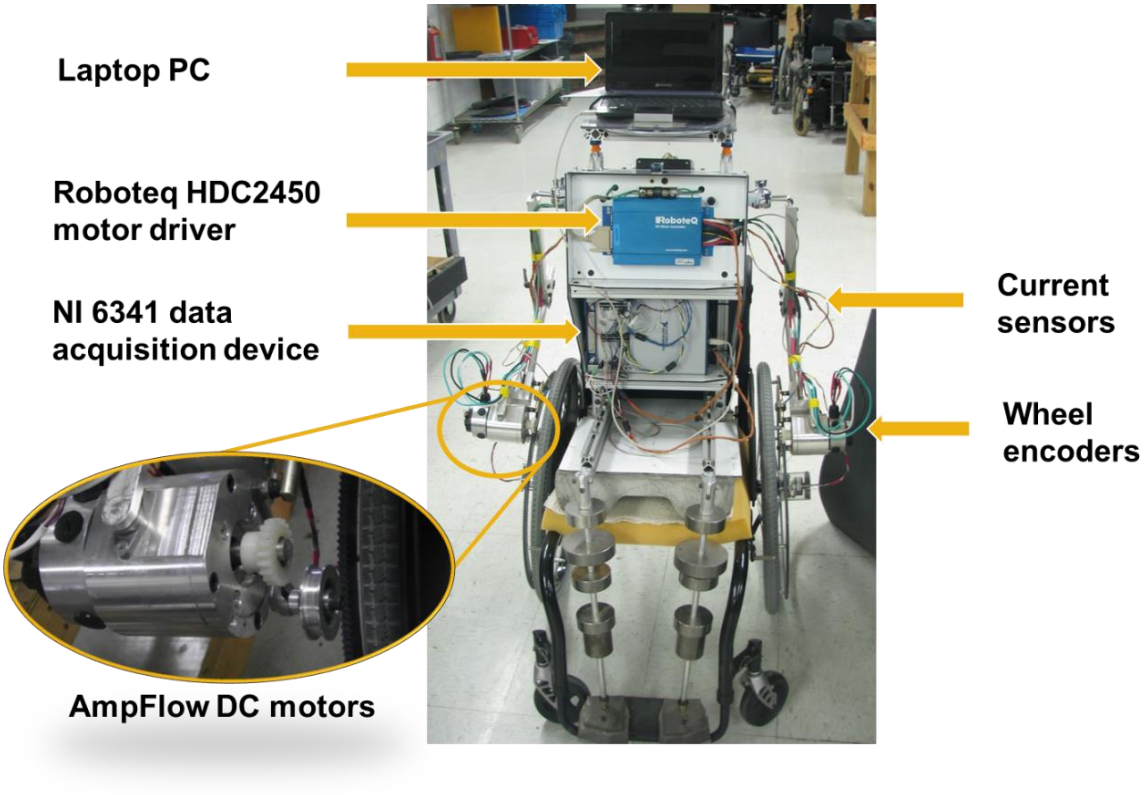

Figure 3.2 AMPS components detail.

Optical rotary encoders are attached to the rear wheels' axels to measure the angular position of the wheels. The data gathered by these encoders are used to control the AMPS trajectory and velocity in real time.

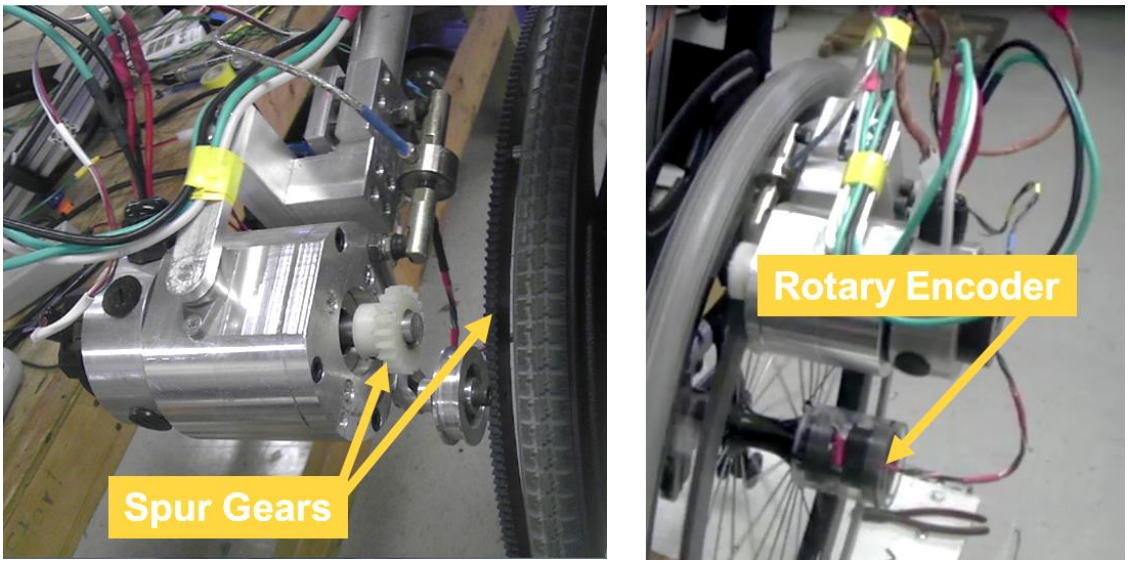

Figure 3.3 Detail of AMPS' motors, gears and rear wheel encoder.

The motors are powered by a Roboteq motor driver which receives analog commands between 0 and 5 Volts. The driver controls the voltage applied to the motors based on the command signal. To measure the electric current flowing through the motors' coils two Hall-effect current sensors are attached to the power wires. A NI USB-6341 data acquisition card manages the command signals sent to the motor driver and collects data provided by the wheel encoders and current sensors. Finally, a laptop computer runs the main control program using LabVIEW 2012 and communicates with the data acquisition card via USB interface.

3.2 AMPS specifications

From the dynamic analysis of the wheelchair-passenger system it is evident that geometric and inertial properties need to be determined for making calculations. The dimensions of the wheelchair can be found in the product technical sheet or measured directly with simple instruments. However, measuring inertial properties such as location of center of gravity (COM) or the mass moment of inertia about the COM requires more complex equipment. A pendulum platform (figure 3.4) is a device capable of measuring the mass moment of inertia of an object resting on top of it [21].

Figure 3.4 Pendulum platform used measure AMPS inertial properties

The procedure includes adjusting the wheelchair location on the platform until the COM aligns with the center of the platform. This way, the distance from the COM to the center of the rear axis can be measured directly. The platform is later disturbed and forced to oscillate around its center. The mass moment of inertia of the wheelchair can be determined by measuring the vibration frequency of the pendulum platform.

The following table presents the measured geometric and inertial properties of the AMPS-wheelchair combination used in experiments in chapter 6.

Table 3.1 AMPS-wheelchair geometric and inertial properties

Parameter	**symbol**	**unit**	**Value**
Radius of rear wheel	rR	m	0.3047
Radius of caster wheel	rC	m	0.1012
Rear wheels distance (at floor contact points)	dR	m	0.5334
Caster forks centers distance	dF	m	0.435
Distance from rear axis to caster forks center	dL	m	0.4445
Caster trail	dC	m	0.0371
Distance from rear axis to COM (frontal)	$\bar{y}$	mm	115.9
Distance from rear axis to COM (lateral)	$\bar{x}$	mm	5.1
Mass of system (wheelchair + AMPS)	m	kg	107.42
Mass moment of inertia about the COM	Io	$kg \cdot m^2$	7.06

3.3 Limitations of the AMPS

Despite the many advantages of using the AMPS to test manual wheelchairs, there are some limitations to consider when designing experiments and interpreting the results. The AMPS propulsion is achieved via DC motors which propel the wheel handrims tangentially, as a human passenger would do. However, the dexterity of the human hand

and the complexity of its motion cannot obtained with the AMPS. The AMPS' motors are engaged with the handrims in a single location and cannot be disconnected. In contrast, a person's hand grabs the wheel handrim in one location and travels with it for a short distance before letting go the grip for some time until the next propulsion cycle. In chapter 6 a procedure is used to emulate the natural deceleration condition, or 'free-wheeling', of the wheelchair by artificially cancelling the motors inertia.

While propelling a manual wheelchair, the upper body of a human passenger changes its shape. The amount of this change depends on the propulsion technique used by the passenger and his particular disabilities. By doing this, the COM location and mass moment of inertia of the wheelchair-passenger system with respect to the point O varies during the propulsion. The AMPS cannot emulate this behavior since its rigid body is fixed to the wheelchair. This fact could be considered both an advantage and a disadvantage. Since the AMPS body doesn't change, the variation of inertial properties (COM location and mass moment of inertia) occurring in human propulsion cannot be emulated. However, the dynamic analysis becomes simpler and more accurate since the aforementioned properties remain constant.

CHAPTER 4

AMPS CONTROL SYSTEM

As any robotic device, the AMPS requires a control system capable of performing different tasks. The AMPS was designed to provide a controlled push to a manual wheelchair and achieve a certain desired maneuver. Some experiments may require the AMPS to push the wheelchair independently of the outcome in terms of trajectory and velocity profile. In others, the input push would need to self-adjust in real time so to match a desired trajectory and velocity.

This chapter describes the development of the AMPS control system. An open-loop control was created to provide accurate propulsion to the wheelchair regardless of the outcome. A closed-loop control was also created to perform a maneuver matching a specific trajectory and velocity profile. Both controllers use feed-forward and feedback modules for achieving the required task. Feed-forward predicts the necessary currents applied to the motors based on the dynamic model developed in chapter 2. Current feedback is necessary to ensure matching the desired propulsion created by the motors. Velocity and orientation feedback was further implemented so the AMPS would match a desired trajectory and velocity profile.

4.1 Current control

The essential control for the AMPS is current control. There exist a direct relationship between the current passing through a motor and the torque delivered at the shaft. This torque directly determines the input force of the system. Thus, by controlling current, the torque and forces applied to the wheelchair are controlled as well. Manufacturers tests their motors in special dynamometers to measure motor parameters including the torque constant, K_t, which describes the linear mapping between current and torque. Figure 4.1 shows the actual technical information provided by the AMPS' motors manufacturer including current and torque relationship. By measuring the actual current with the help of sensors, the torque and forces delivered by the motors are determined.

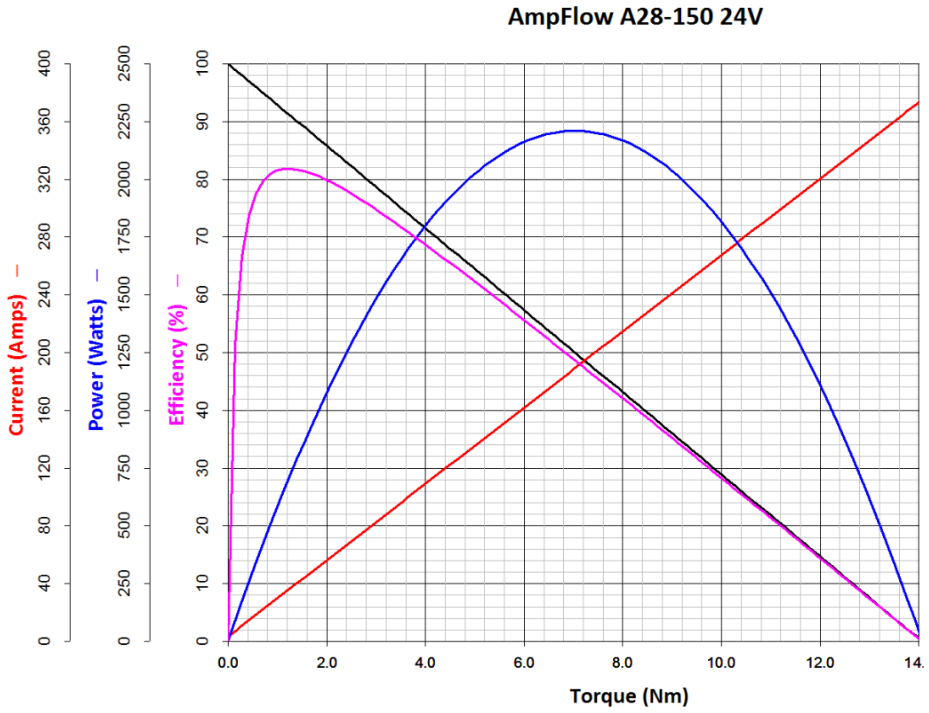

Figure 4.1 Torque-current curve for the electric motors used in the AMPS [22].

Current control relies in two modules to effectively control current and, consequently, control the torque applied to the wheelchair. The first module, feed-forward, calculates the desired current to be applied. The second module, feedback, makes sure the desired current is actually matched by the motor driver.

In general, feed-forward refers to the determination of a system input needed to perform a specific task. In the AMPS, the task is defined by a trajectory and associated velocity profile and wheelchair orientation, which fully define the desired maneuver. The feed-forward controller module must determine the required input to the system to create such desired maneuver. It uses inverse kinematics and inverse dynamics analysis as presented in chapter 2. Figure 4.2 shows a block diagram of the AMPS' feed-forward module. At the beginning of the diagram, a desired maneuver is defined by a series of trajectory points, a velocity profile and orientation through the path. Inverse kinematics and inverse dynamics are used to determine the currents required by the motors to create such desired maneuver. These current profiles are finally delivered to the controller governing the AMPS.

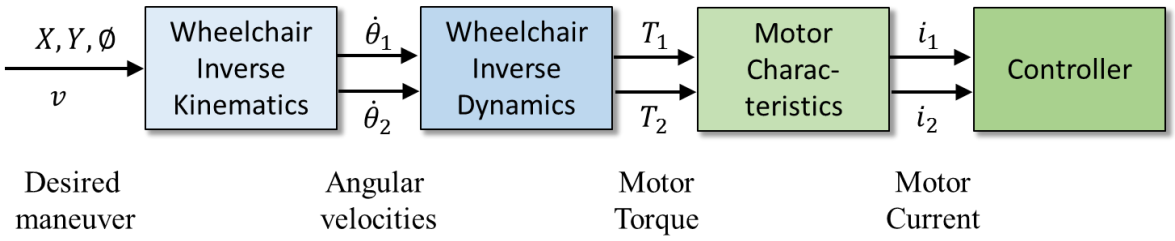

Figure 4.2 AMPS feed-forward module block diagram.

The controller sends an analog command signal to the motor driver. This device changes the voltage applied to the motor circuit based on the signal received. The voltage

then induces a current in the circuit, which increases or decreases depending on the mechanical load attached to the motor. Therefore, controlling the voltage in the circuit is not enough to ensure a particular current and torque output. This is the reason why feedback is necessary to perform current control. Two current sensors where inserted in the circuit to measure the actual current flowing through the motors in real time. This real time measurement data is then sent back to the controller. By calculating the error between the desired current and the real one, a proportional correction signal can be generated and added to the original command sent to the driver in order to achieve the desired current, resulting in the desired torque output. Figure 4.3 show a block diagram of the current control system including feed-forward and feedback.

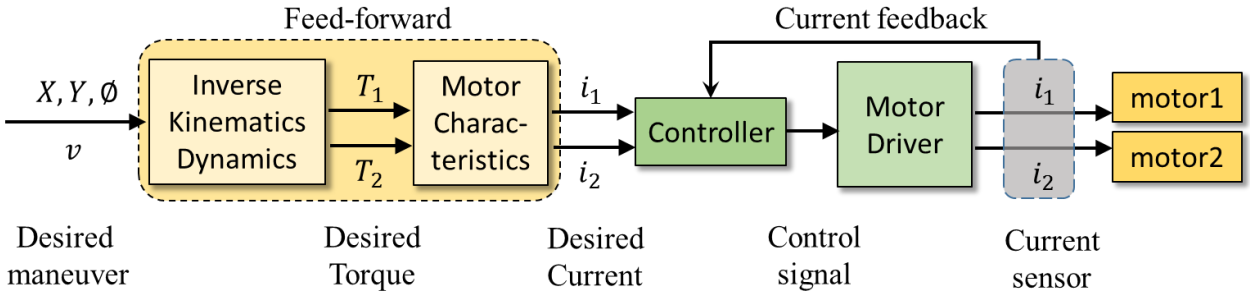

Figure 4.3 AMPS current control block diagram.

This control strategy is known as *P* control, since the feedback correction signal is proportional to the error. An additional correction term was added based on the accumulated error, thus introducing what is known as *I* control. A more detailed block diagram of the feedback calculation done by the controller is shown in figure 4.4.

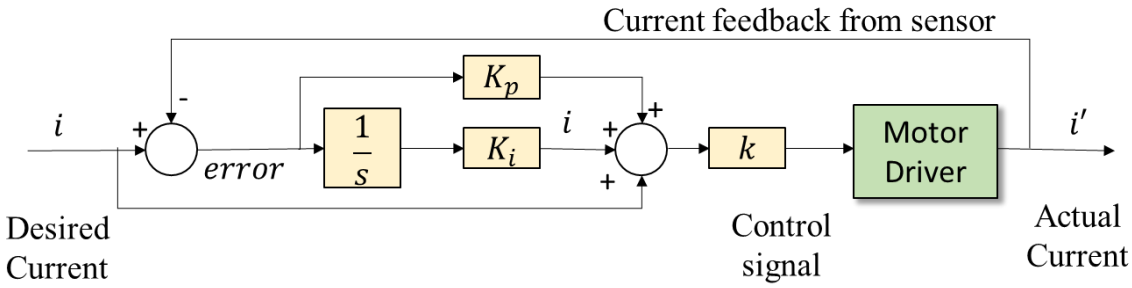

Figure 4.4 Current feedback control detail.

Notice that this control approach is meant to guarantee that the motors receive the current stablished by the feed forward calculation. There is no feedback or signal correction based on how the wheelchair actually moves. Thus, from the perspective of the wheelchair system, this is open-loop control. By using current control we regulate the torques and forces applied to the wheels, which is the input to the system. The resulting motion of the wheelchair, the system's output, does not change the input forces in any way when using solely the current control described so far. The next section presents a closed-loop control approach, in which the actual wheelchair motion outcome is used to correct the input torques and forces.

4.2 Closed-loop control

Most experiments performed with manual wheelchairs require it to move along a specific trajectory with a particular velocity. Thus, the AMPS controller needs to be able perform such a task. In closed-loop control, additional feedback of velocity and orientation is included in the AMPS' control to guarantee the outcome trajectory and velocity profile during a wheelchair maneuver. The feed-forward part is given by the model-based input estimation as described previously. Current control makes sure that the desired current is

met. Finally, trajectory and velocity are determined in real time from the wheel encoders and used as feedback to correct the input signal. The previously estimated value of current is now corrected to match the desired trajectory and velocity of the wheelchair. This way the input to the wheelchair (torque) is modified to match a desired output. This closed-loop control strategy is shown in figure 4.5.

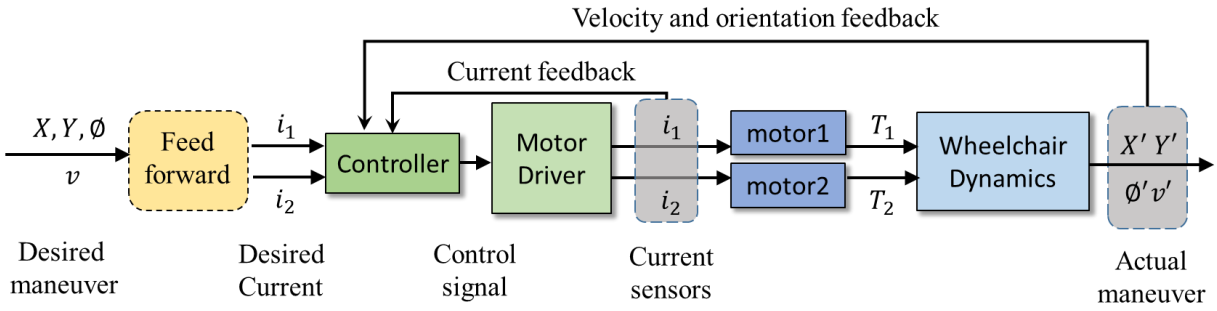

Figure 4.5 AMPS trajectory and velocity control block diagram.

Figure 4.6 offers a more detailed block diagram describing the calculation made by the closed-loop controller.

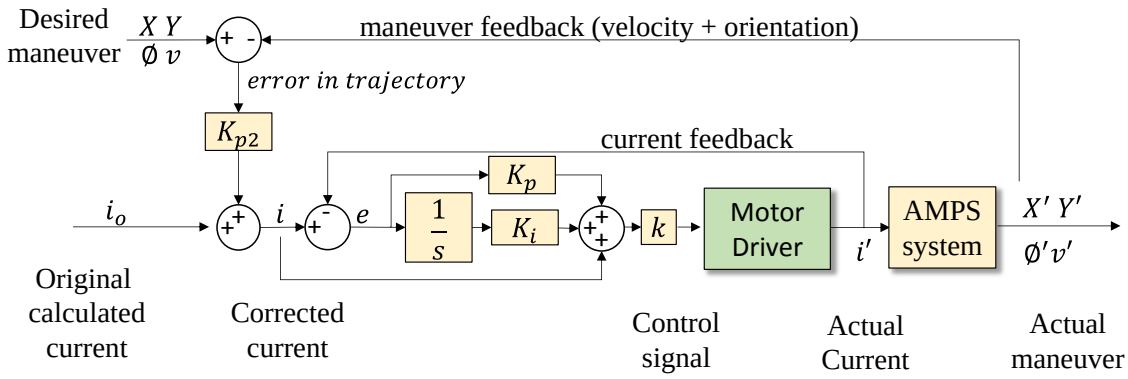

Figure 4.6 AMPS closed-loop velocity and trajectory feedback detail.

4.3 Computer implementation

The computer implementation of AMPS' control system is separated in two sections. Feed-forward calculations are executed in Matlab (The Mathworks, LLC) determined the current needed by the motors. Those calculations are fed to the laptop computer commanding the AMPS on real time by executing a closed-loop control implemented in LabVIEW.

Feed-forward calculation in Matlab required writing code that contained all the equations from wheelchair kinematic and dynamic analysis. The determination of motor torques and currents based on a desired trajectory (inverse dynamics) was implemented as a graphical user interface (GUI) to visually appreciate the different stages of the process. Figure 4.6 shows the GUI used to generate a slalom curvilinear trajectory.

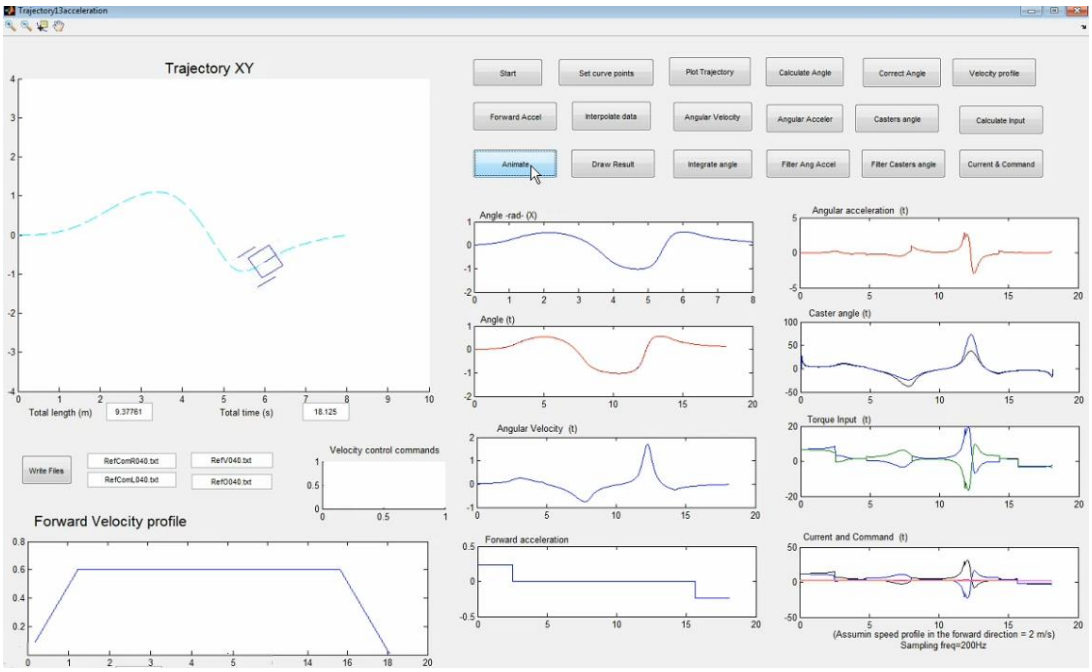

Figure 4.7 Feed-forward process in a Matlab GUI.

In the GUI, the process begins by determining a trajectory and associated linear velocity profile. To facilitate the definition of a curvilinear trajectory, the programs only requests a finite number points within the path. It later uses a B-spline function to connect the points creating a smooth trajectory. This initial definitions are followed by the inverse kinematics and inverse dynamics calculations. Once the currents of the motors are determined the process ends. The final step is to export four files containing the current input for right and left motor, the wheelchair velocity profile and required orientation throughout the trajectory. These files are used later in the closed-loop controller that governs the AMPS motion.

The closed loop control program was developed in LabVIEW 2012, which is a system-design platform that uses a visual programming language (figure 4.7). The program is able to read signals from sensors and send commands to the motors' driver through a NI USB 6341 data acquisition device.

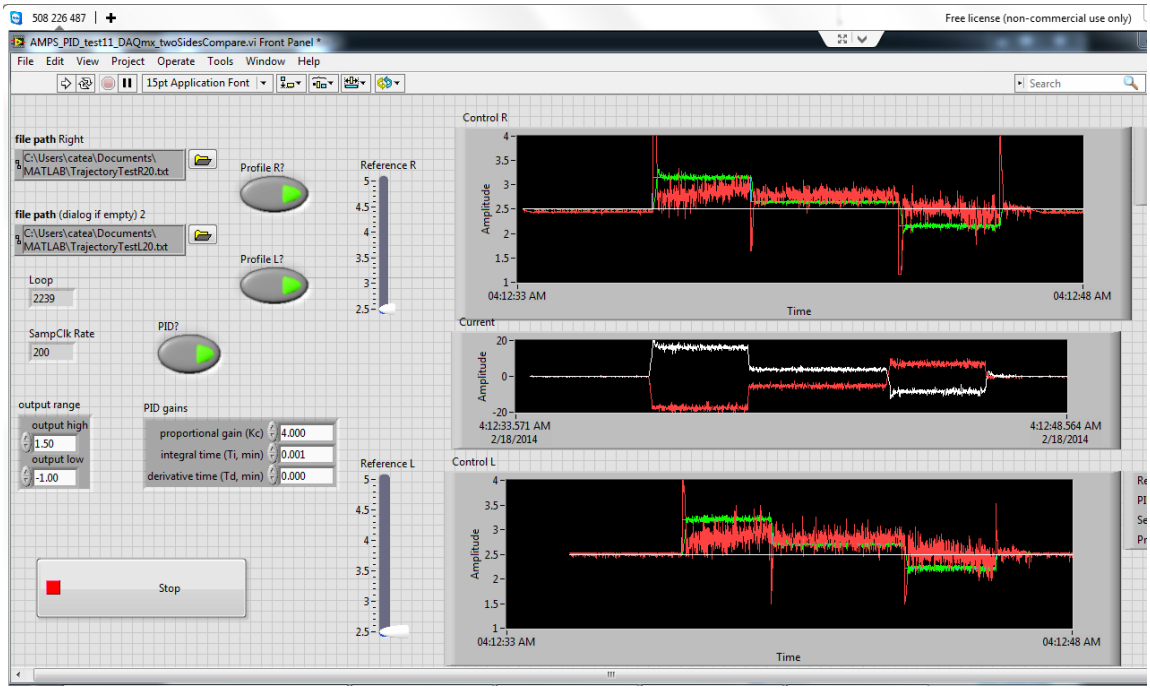

Figure 4.8 AMPS control program executed on LabVIEW 2012.

The control program was written to run at 200 samples per second, which is the maximum velocity obtainable with the AMPS' hardware and software. This operation speed has proven to be the minimum necessary to maintain a stable current control feedback loop. At the beginning of execution, the program reads the files containing information of current, velocity and orientation determined previously through the inverse dynamic analysis in Matlab. During program execution it collects real-time information coming from the current sensors and encoders. Encoder data is processed with the forward kinematics equations to determine the wheelchair's velocity, orientation and absolute position. By calculating the error between desired and actual current, orientation and velocity, the command input signal is corrected and sent to the driver to power the motors.

The control program was tested successfully for a variety of maneuvers including the ones used on experiments in chapter 6. Nevertheless, some discussion is in place regarding the design and selection of this control strategy. The AMPS control developed here uses a model-based input estimation of the currents required by the motors. This estimation is corrected to match a desired velocity profile and trajectory of the vehicle. It is possible, nonetheless, to achieve such maneuver without having an input estimation. The controller could supply current to the motors based only on the error between desired and actual velocity profile, and the error between desired and actual wheelchair orientation. This method, however, is highly dependent in the selection of 'gains' which are the factors dictating how much correction in input is needed proportionally to the measured error.

Figure 4.9 shows the motor current for a straight trajectory achieved with only error-based control. With inappropriately selected (or tuned) gains, the controller changes drastically the applied currents in order to achieve the desired maneuver. This strategy is said to produce a large 'control effort' since the amplitude of the correction is relatively large. In figure 4.9 the gains have been 'tuned' and so the control effort is decreased considerably to achieve the same maneuver. Tuning these gains takes time and is an empirical process.

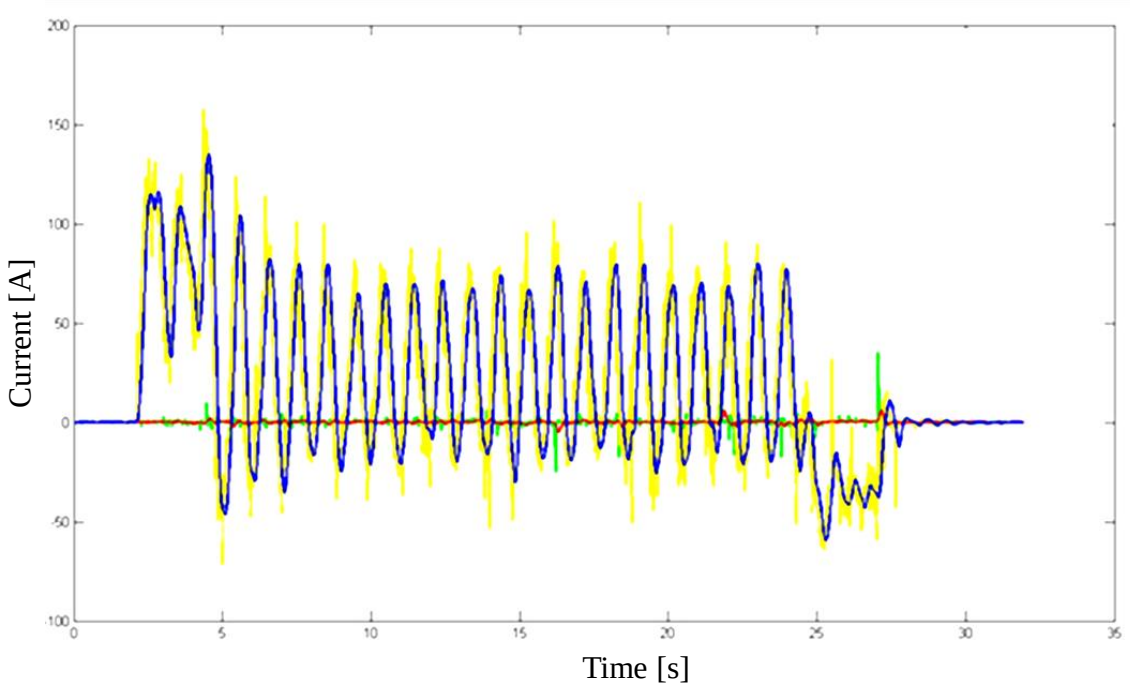

Figure 4.9 Motor current from an error-based control test with un-tuned gains.

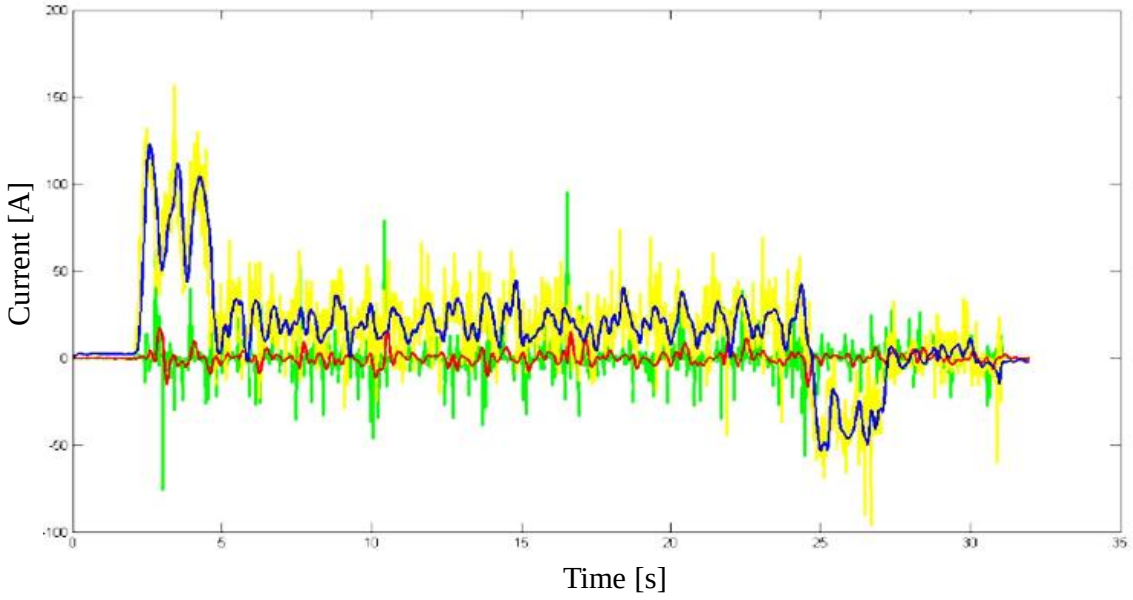

Figure 4.10 Motor current from an error-based control test with tuned gains.

The model-based controller developed in this section has shown very little sensitivity to the error-correction gains. The model-based controller provides an estimation of the input reducing significantly the amount of correction, or control effort, needed to match the specified trajectory and velocity. The more accurate the estimation, the lower the output error and the lower the correction necessary to match it. Figure 4.10 shows a model-based estimated input control where the motor current variation has decreased significantly.

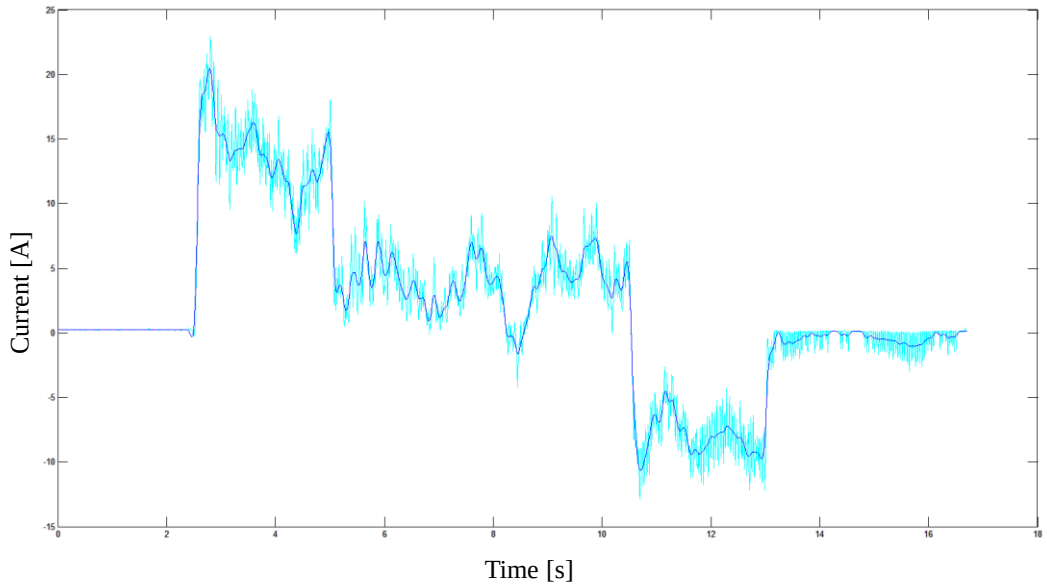

Figure 4.11 Motor current from an input estimation control test.

One simple analogy can be made with the difference between two people driving a new car model for the first time. One of them has never driven a car before while the other is an experienced driver. They are requested to maneuver the car through a course in a limited time by using the gas and brake pedals. The inexperienced driver has to constantly press the gas and brake pedals, struggling to control the vehicle through the assigned path in time. Differently, the experienced driver smoothly passes through the course barely

making any corrections. The main difference is based in the previous knowledge each of them has regarding the input required to drive the system.

Another difference found with the model-based controller is the accuracy of response to rapid changes in the wheelchair velocity. Figures 4.11 through 4.14 shows the results of a straight path maneuver using different control methods. The first two figures show the results when using model-based estimation of the input. The last two show the result when only using feedback for error correction.

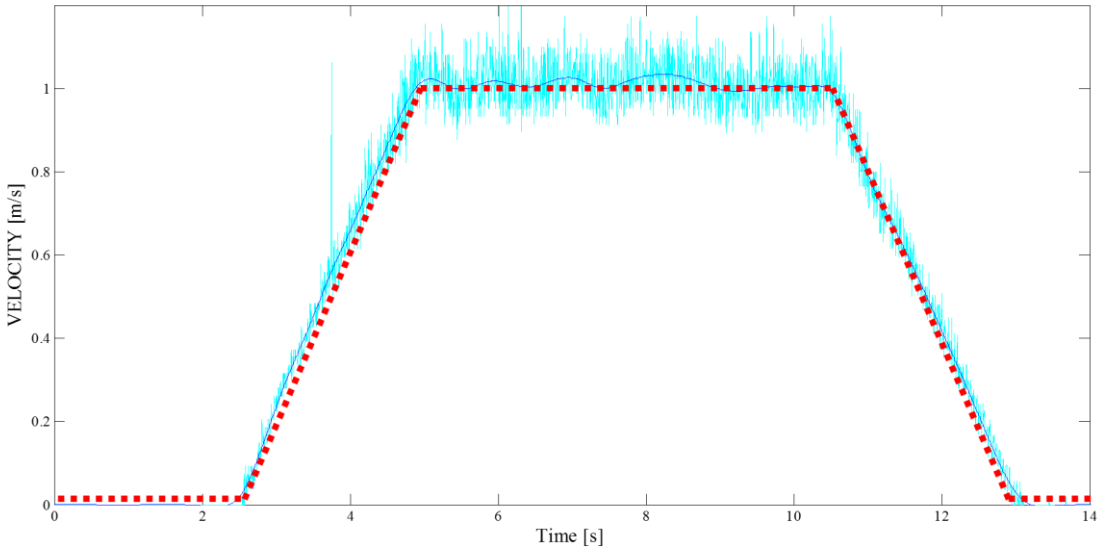

Figure 4.12 Wheelchair velocity profile using model-based input estimation. Red dotted line shows the desired profile

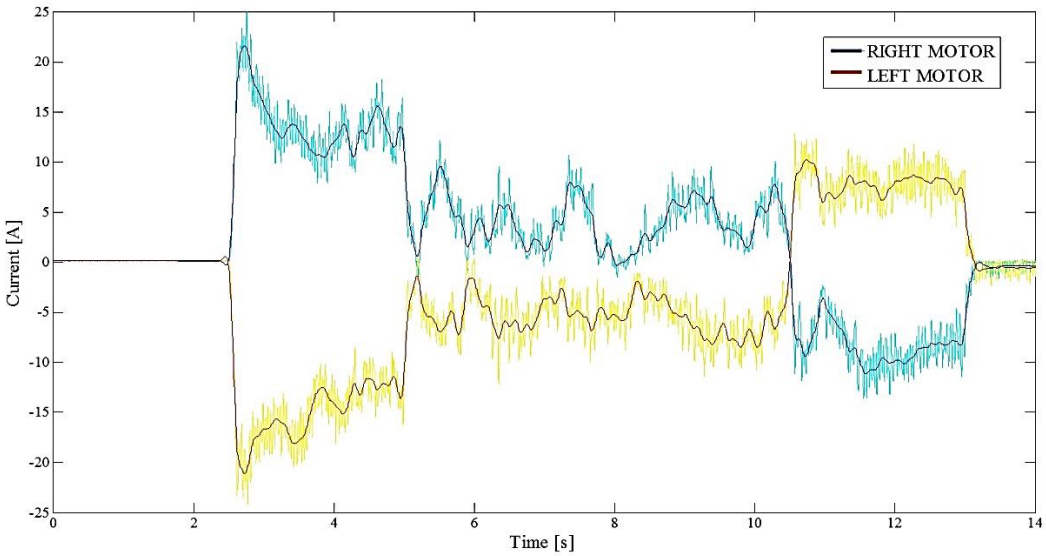

Figure 4.13 Motors' currents using model-based input estimation.

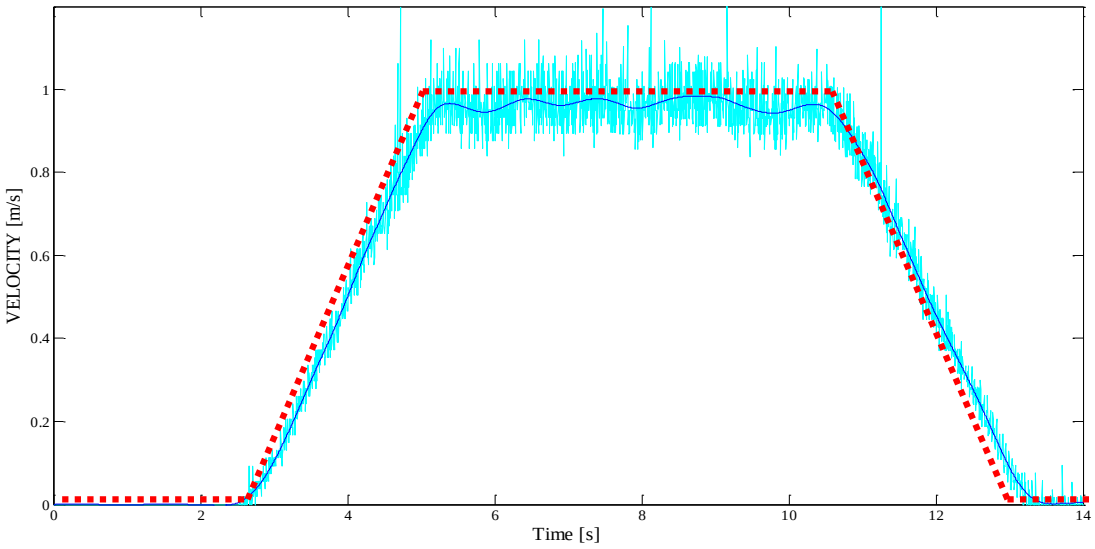

Figure 4.14 Wheelchair velocity profile using pure error-based correction.

Red dotted line shows the desired profile

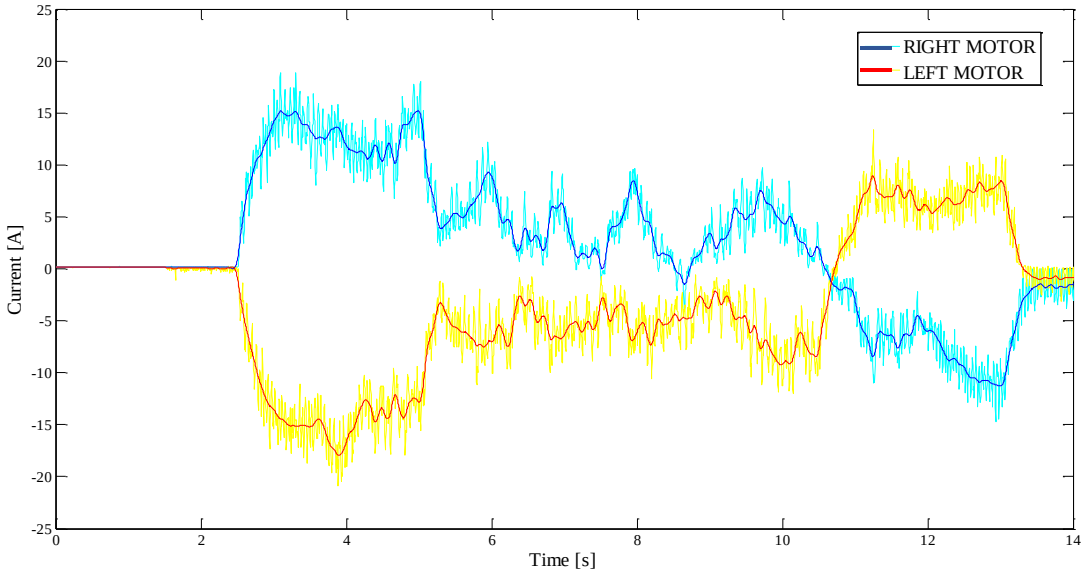

Figure 4.15 Motors' currents for a test using pure error-based correction.

It can be seen that the model-based input estimation controller is more effective to track the desired velocity profile. This happens because the controller doesn't need to wait for an error in velocity to react and make input corrections. The slower development in velocity is also evident in the current used by the motors. The model-based controller supplies the appropriate amount of current to the motor faster without waiting for a mismatch in velocity.

CHAPTER 5

WHEELCHAIR MECHANICAL EFFICIENCY

In general terms, mechanical efficiency is the ratio between the 'useful output' of a system or process and the energy input required by it [15]. Many particular definitions are used among different disciplines since the idea of 'useful output' of a process depends on what is meaningful output for a certain audience.

For vehicles, two definitions of mechanical efficiency are considered in this work. The first is a classical definition of energy efficiency used in energy conversion machines. The second is used primarily in transportation vehicles. Both were used to characterize wheelchair mechanical efficiency in different experiments in chapter 6. The next sections describe in more details the referred mechanical efficiency definitions.

5.1 Energy conversion efficiency

Energy conversion efficiency, η, is the ratio between the output of an energy conversion machine and the input, both in energy terms.

$$\eta = \frac{E_{output}}{E_{input}} \tag{5.1}$$

For a wheelchair moving along a path, the energy output E_{output} is the total kinetic energy of the system, KE_{Total}, which includes kinetic energy from translation and rotation of the different elements of the wheelchair. Equations 5.2 and 5.3 describe the total kinetic energy in more detail.

$$E_{output} = KE_{Total} \tag{5.2}$$

$$KE_{Total} = KE_1 + KE_2 + KE_3 + KE_4 + KE_5 \tag{5.3}$$

Where KE_1 is the system's overall translation energy, KE_2 is the system's rotational overall energy, KE_3 is the rear wheels' rotational energy, KE_4 is the caster forks' rotational energy, and KE_5 is the caster wheels' rotational energy.

By placing the appropriate terms for each kinetic energy we obtain

$$E_{output} = \frac{1}{2}mV^2 + \frac{1}{2}I_o\dot{\emptyset}^2 + \frac{1}{2}I_R\left(\dot{\theta}_{R1}^2 + \dot{\theta}_{R2}^2\right) + \frac{1}{2}I_{Fork}(\dot{\alpha}_1^2 + \dot{\alpha}_2^2) + \frac{1}{2}I_C(\dot{\theta}_{C1}^2 + \dot{\theta}_{C2}^2) \tag{5.4}$$

Where m is the mass of the system, V is the linear velocity of the center of mass, I_o is the mass moment of inertia of the system about the rear axis center, $\dot{\emptyset}$ is the wheelchair orientation angular velocity, I_R is the rear wheels mas moment of inertia about their center axis, $\dot{\theta}_R$ is the rear wheel angular velocity about the rear axis, I_{Fork} is the caster's mass moment of inertia about the caster fork joint center, $\dot{\alpha}$ is the caster orientation angular velocity, I_C is the mass moment of inertia of the caster wheels about their center axis, and $\dot{\theta}_C$ is the caster wheels angular velocity about their center axis. All these terms require inertial properties measurement or estimation. Additionally, several linear and angular velocities values can be obtained from the kinematic analysis presented in chapter 2.

The energy input of the system used in equation 5.1 can be obtained by integrating the mechanical power delivered by the motors through their shafts throughout the maneuver. Equation 5.5 details this calculation.

$$E_{input} = \int_0^t P(t)dt = \int_0^t T(t)w(t)dt = \int_0^t A(t)\, K_t\, w(t)dt \qquad (5.5)$$

Where P is mechanical power, T is torque output, w is the angular velocity of the shaft, A is the current consumed by the motor, and K_t is the motor torque constant that relates current and torque for an electric motor. Replacing these terms in equation 5.1 results in

$$\eta = \frac{E_{output}}{E_{input}} = \frac{KE_{Total}}{\int_0^t A(t)\, K_t\, w(t)dt} \qquad (5.6)$$

5.2 Cost of transport

The cost of transport (COT) quantifies the energy efficiency of transporting a vehicle from one point to another. The greater the COT the less efficient a vehicle is since it requires more energy to perform the same task. The COT is calculated in the following way:

$$COT_m = \frac{E_{input}}{mD} \qquad (5.7)$$

Where E_{input} is the energy input to the system, calculated in the same way as in section 5.1, D is the total travelled distance and m is the total mass of the system, both easily measured.

5.2.1 Cost of transport for a straight maneuver

It is of interest to determine a relationship between COT and rolling resistance. For the simplest case, a straight maneuver, let's consider the cost of transport equation.

$$COT = \frac{E_{input}}{mD} \tag{5.8}$$

Terms can be replaced with equivalent integral expressions.

$$COT = \frac{\int_0^t P(t)dt}{m\int_0^t V(t)dt} = \frac{\int_0^t T(t)w(t)dt}{m\int_0^t V(t)dt} \tag{5.9}$$

Where T is the torque provided by the motors, w is the angular velocity of the motor shafts and V is the linear velocity of the wheelchair. A simple application of the law of conservation of energy let us find that

$$T(t)w(t) = V(t)F(t) \tag{5.10}$$

Where F is the total force applied to the wheelchair. Replacing this in the COT equation we find

$$COT = \frac{\int_0^t V(t)F(t)dt}{m\int_0^t V(t)dt} \tag{5.11}$$

We also know that for a straight maneuver the force F is

$$F(t) = F_{Roll}(V, a_y) + ma_y(t) \tag{5.12}$$

So, replacing again

$$COT = \frac{\int_0^t V(t) F_{Roll}(V, a_y) dt + m \int_0^t a_y(t) V(t) dt}{m \int_0^t V(t) dt} \tag{5.13}$$

This last expression relates the cost of transport with the mass of the system, the rolling resistance affecting the wheelchair, velocity and acceleration of the wheelchair throughout a straight maneuver.

For the especial case when measuring COT for a straight trajectory with constant velocity, the rolling resistance force can be considered constant $\bar{F}_{Roll}$, yielding the following expressions.

$$COT = \frac{\bar{F}_{Roll} \int_0^t V(t) dt}{m \int_0^t V(t) dt} + \frac{\int_0^t V(t) a_y(t) dt}{\int_0^t V(t) dt} \tag{5.14}$$

$$COT = \frac{\bar{F}_{Roll}}{m} + \frac{1}{D} \int_0^t V(t) a_y(t) dt \tag{5.15}$$

This result means that for a straight trajectory maneuver with constant speed, the cost of transport depends directly on the rolling resistance. An additional term $\int_0^t V(t) a_y(t) dt$ is part of the calculation.

For a straight trajectory at constant speed, since acceleration is very close to zero, it could be expected that the term $\int_0^t V(t) a_y(t) dt$ would be close to zero. This means that the calculated COT for a given constant velocity maneuver should be close to the value of rolling resistance at such speed. Results in section 6.3 illustrate this result better.

CHAPTER 6

EXPERIMENTS AND RESULTS

The whole purpose of the AMPS is becoming a tool to perform experiments on manual wheelchairs and provide useful information regarding their dynamic behavior and mechanical efficiency. In this thesis work, different experiments were designed to address specific questions about wheelchair dynamics and characterize its overall mechanical performance under various circumstances. Some of the experiments were intended to characterize rolling resistance dependency on velocity and acceleration. Others, to identify turning resistance in curvilinear trajectories with various radios of curvature. A different set of experiments were designed to study the manual wheelchair behavior under a pulsatile propulsion resembling a human passenger's propulsion. Other class of experiments measured wheelchair mechanical efficiency under different metrics.

The sequence of experiments was determined logically, in order of complexity and interdependency of the results. Experiments identifying rolling resistance required the wheelchair to move on a straight line, the simplest case, where no other resistive forces intervenes in the system dynamics. Turning resistance experiments required previous estimation of rolling resistance tests for doing calculations. The last set of experiments considered two different metrics of overall system mechanical efficiency and applied them to straight motion, circular motion and pulsatile propulsion.

All experiments used a Quickie GT (Sunrise Medical, LLC) manual wheelchair equipped with Primo Orion 24x1-3/7 pneumatic rear wheels (inflated to recommended pressure of 75psi) and Primo urethane casters. Detail of dimensions and inertial properties of this setup was already presented in table 3.1. Experiments were performed indoors, over tile surface which is a very common type of flooring. This work

doesn't pretend to be an exhaustive characterization of manual wheelchairs in all possible combinations of tires and floors, or under all available different configurations within the same wheelchair. It is intended to determine a methodology to characterize manual wheelchairs' performance by using the AMPS as a tool of measuring forces and efficiency. This methodology could be used in future work to compare among different wheelchairs and possible configurations

This chapter contains many figures for easily visualizing the experimental results. Tables with original data used to create such graphs are presented in appendix E.

6.1 Rolling resistance experiments

6.1.1 Constant velocity experiments

The first set of experiments were designed to measure rolling resistance during constant velocity straight motion. As shown in figure 6.1 the AMPS was used to follow a straight path while controlling its velocity.

Figure 6.1 AMPS performing a straight trajectory experiment.

Many previous publications [8-10] demonstrate that rolling resistance increments non-linearly with velocity in wheelchairs. However, their methodology usually limits the estimation of rolling resistance to specific cases as described in appendix D. Using the AMPS is a novel methodology that allows testing a manual wheelchair on any selected floor while accurately controlling velocity. It was found that results obtained with the AMPS in this section are consistent with previous published work.

For the experiments in this section the wheelchair moved over a straight trajectory of 8 meters with a period of constant velocity motion. Considering the common range of human-driven wheelchair velocities, the AMPS performed straight maneuvers including segments travelling at constant velocities from 0.4 to 1.2 m/s, in 0.1 m/s increments. One trial was performed in both directions of the same track for each velocity. The velocity profile followed by the AMPS in this set of experiments is shown in figure 6.2.

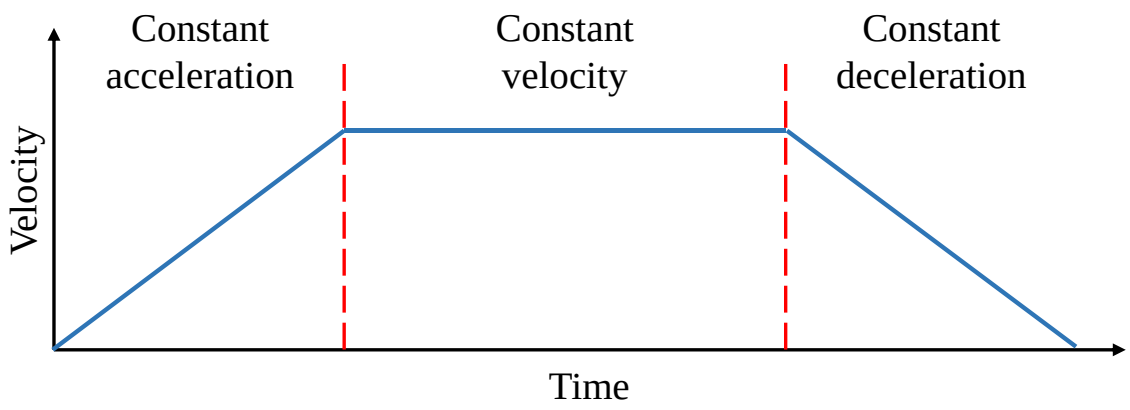

Figure 6.2 Velocity profile used in rolling resistance experiments.

During each run, the current flowing through the motors was measured by the sensors and recorded. From this, motor torque input was determined by using the motor torque constant, K_t, found in the motor specifications sheet. The motor torque constant relates the amount of current flowing through the motor coil and the torque output delivered at the shaft. Simultaneously, the rear wheels' encoders recorded their angular position as a function of time. By processing this data it was possible to determine the velocity of the wheelchair at any given time during the run. Since the wheels are constantly engaged to the AMPS' motors through spur gears, data from the wheel encoders could also be used to determine the angular velocity of the motors during the experiments, something useful in supplementary data analysis.

Based on the dynamic model presented in chapter 2, the total rolling resistance affecting a manual wheelchair moving along a straight path is determined from the following equations:

$$ma_y = F_1 + F_2 - F_{R1} - F_{R2} - F_{c1} - F_{c2} \tag{6.1}$$
$$= (T_1/r_R + T_2/r_R) - F_{Roll}$$

Rearranging equation 6.1 lets us find the appropriate expression to calculate rolling resistance.

$$F_{Roll} = (T_1/r_R + T_2/r_R) - ma_y \tag{6.2}$$

Where F_{Roll} represents the total rolling resistance force created by all four wheels. The torque applied by the left and right motors (T_1 and T_2) is calculated with the following equations:

$$T_1 = A_1 K_t \tag{6.3}$$

$$T_2 = A_2 K_t \tag{6.4}$$

For the first set of experiments the forward acceleration approximates zero ($a_y = 0$) when travelling closely to constant velocity. Thus, the final equation for determining total rolling resistance during a straight maneuver is:

$$F_{Roll} = (A_1 + A_2) K_t/r_R \tag{6.5}$$

Figure 6.3 shows the velocity of the wheelchair's rear center axis during a straight maneuver. The AMPS kept the maximum velocity within a range of ±5%. Figure 6.4 shows the current needed by the motors to achieve such maneuver.

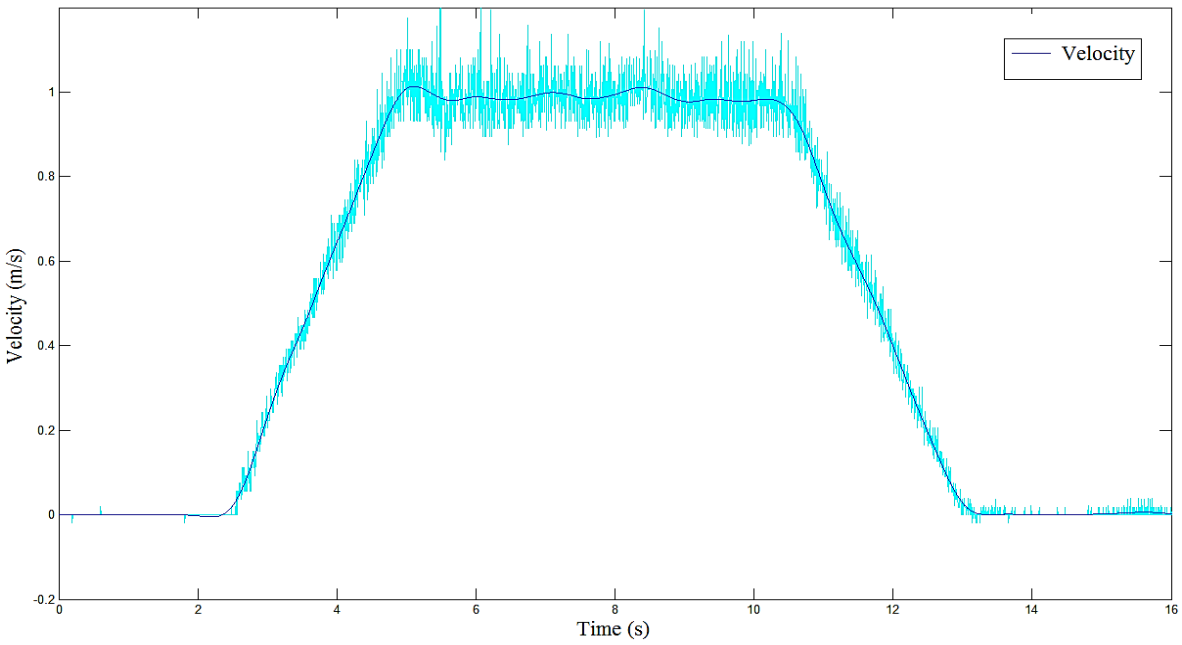

Figure 6.3 AMPS velocity profile during a straight trajectory experiment.

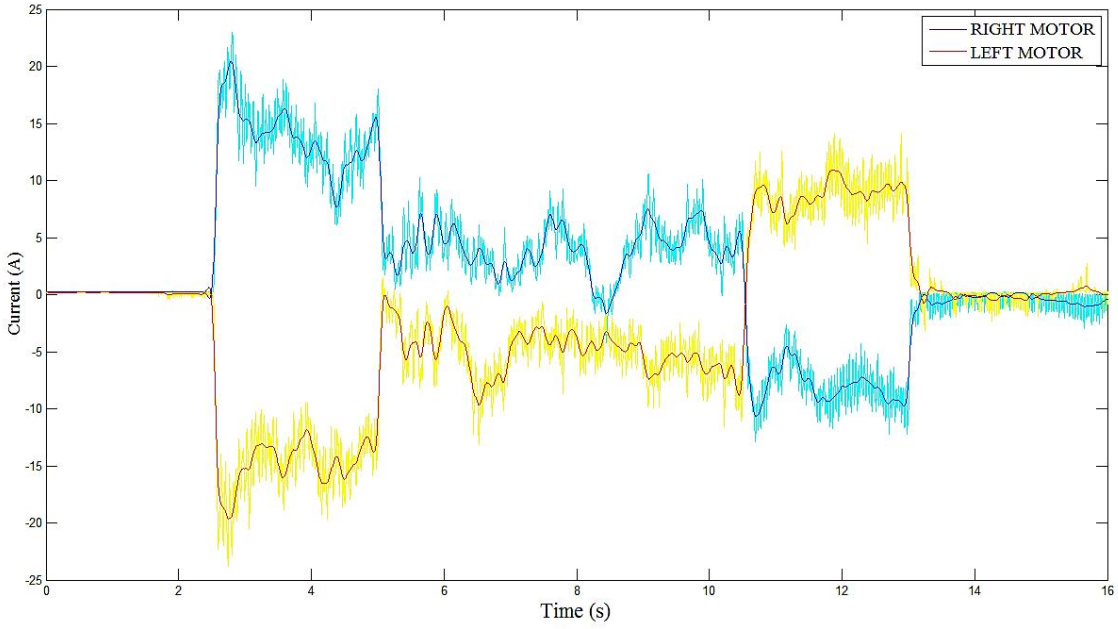

Figure 6.4 Motor currents recorded during a straight trajectory experiment.

Figures 6.3 and 6.4 show raw and filtered data superimposed. The need for filtering is different for both sets of data. On the one hand, electric current data is recorded directly

but need filtering due to noise created by the sensors. On the other hand, velocity is calculated by numerically differentiating encoder recorded data of wheels' angular displacement in time. The encoder resolution creates a discretization error when measuring angle displacement on wheels. Additionally, the sampling time of the data acquisition device is not exact and thus introduces an additional error.

As can be seen from figure 6.4 the current needed by the AMPS to maintain a near constant speed oscillates significantly. Several factors could create this oscillation, including: the control effort from the AMPS' controller, floor imperfections, frame and wheels' elasticity that create oscillations in the wheelchair structure as it travels.

In figure 6.4 the current for the left motor appears inverted relative to the right one, despite both motors propelling the wheelchair in a forward direction. Because of the location on the motors on the AMPS, they have rotate in opposite directions with respect to their stators to create overall wheelchair forward motion. The current used in equation (6.5) are the average values recorded during the constant velocity period of the maneuver.

The usual protocol for rolling resistance tests performed on the ground requires each maneuver to be repeated in opposite directions of the same track. This is made to compensate for the possible slopes and irregularities existing on the testing floor. The final calculated value of rolling resistance is the arithmetic average of the measurements made in each direction. Results for total rolling resistance are presented in the following graph.

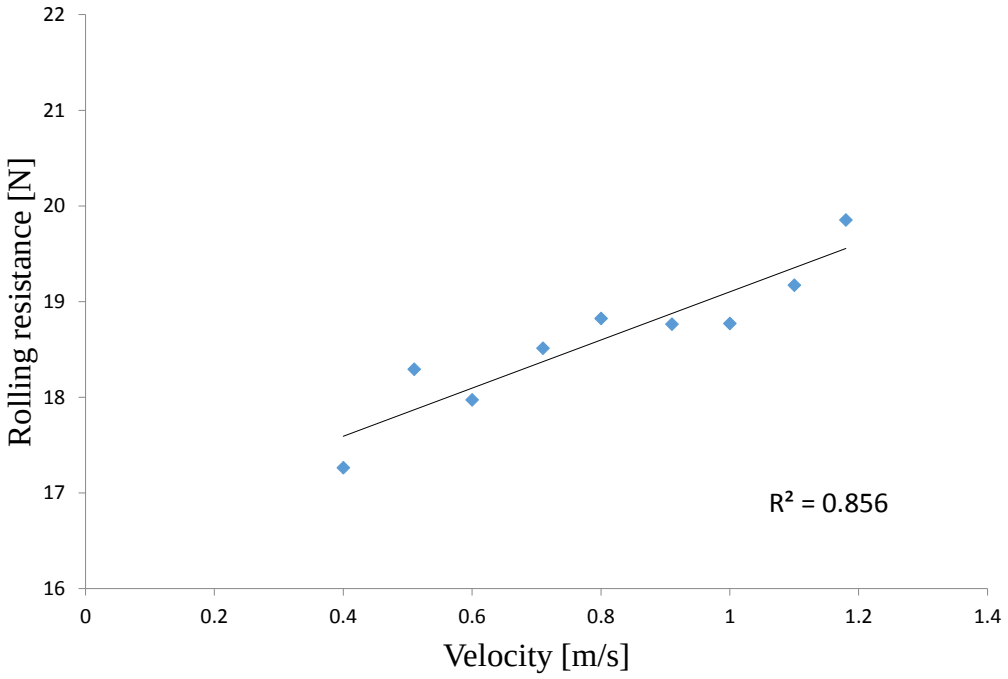

Figure 6.5 Rolling resistance measured at different constant velocities on a straight path.

Figure 6.5 shows total rolling resistance acting on the wheelchair at different velocities within the normal human use range. Rolling resistance varies from 17.3 to 19.9 N within a velocity range between 0.4 to 1.2 m/s. The correlation coefficient is 0.856 for the trend line shown. Rolling resistance increases 2.6 N (15%) for a 0.8 m/s change. These experiments show that rolling resistance increases with velocity, something consistent with previous published material by other authors [8, 9, 13]. This demonstrates that using the AMPS is an effective alternative to other methodologies in measuring rolling resistance. Repeating the experiments several times would provide more precise data along with statistical information. However, tests in this chapter are focused on demonstrating the AMPS applications and resistive forces tendencies, rather than providing accurate values.

Another three sets of data were collected for a straight path with constant velocity. An extra 11 kg (about 10% of the original weight) was added on different locations of the wheelchair to obtain different weight distributions. The experiments were repeated by

adding weight on the front, center, and rear segments of the wheelchair. Tables E.2 through E.5 in the appendix section details the different weight distributions used here and the experiment results.

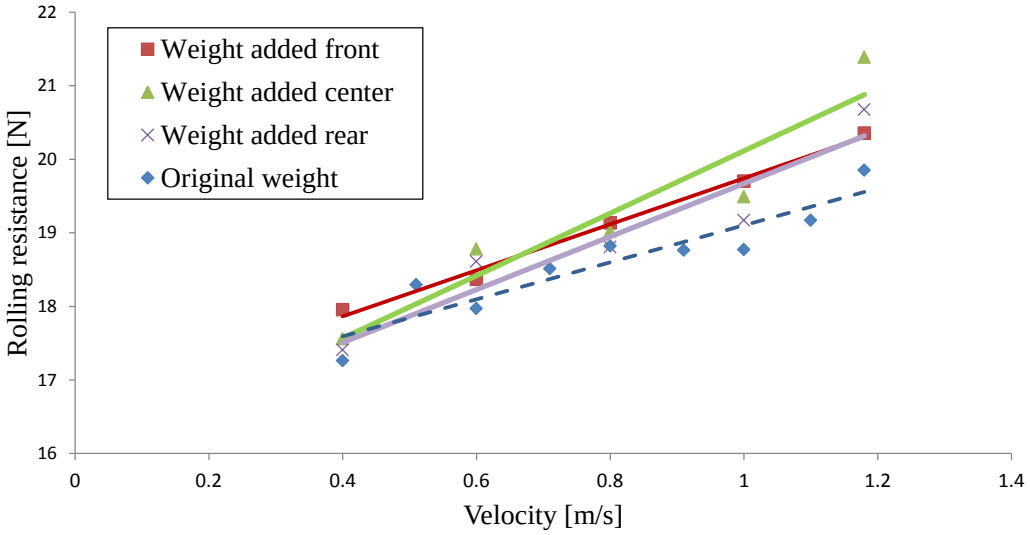

Figure 6.6 Rolling resistance for different velocities and weight distributions along a straight path.

Figure 6.6 shows rolling resistance for three different weight distributions with added weight. The data of the original weight test is also shown in blue for comparison. The tests were performed once in each direction of the same track. The average from both directions is shown of fig. 6.6. It can be observed from the results that, at different velocities, rolling resistance tends to increase with the increment in total weight on the wheelchair. Once again this is consistent with previously published work describing rolling resistance as increasing with total load applied on wheels [8]. The difference on trend lines slopes could be explained by the small amount of data points. Additionally, since the rear and caster wheels are made from different materials, total weight affects total rolling resistance depending on the distribution of such weight.

6.1.2 Rolling resistance parameters determination

A complementary task after measuring rolling resistance is to determine the rolling resistance parameters (RRPs) for the rear and caster wheels. For the turning resistance experiments presented later, it is necessary to predict rolling resistance for each wheel individually. The total rolling resistance acting on a wheelchair is the addition of the individual rolling resistance affecting the two rear wheels and the two front caster wheels.

From appendix D, rolling resistance for an individual wheel is usually described by the following equation:

$$F(V) = \frac{\lambda(V)\, N}{r} \tag{6.6}$$

Where $F(V)$ is the rolling resistance at the wheel, N is the normal force, r is the radius of the wheel, and λ is the rolling resistance parameter (RRP). The RRPs are affected by many factors such as velocity and the wheel and floor materials.

Placing this representation on the dynamic equation for a wheelchair moving at constant velocity, we have:

$$ma_y = F_1 + F_2 - F_{R1} - F_{R2} - F_{c1} - F_{c2} \tag{6.7}$$

$$\frac{(A_1 + A_2)\, K_t}{r_R} = F_{R1} + F_{R2} + F_{c1} + F_{c2} \tag{6.8}$$

$$\frac{(A_1 + A_2)\, K_t}{r_R} = \frac{\lambda_{R1}\, N_{R1}}{r_{R1}} + \frac{\lambda_{R2}\, N_{R2}}{r_{R2}} + \frac{\lambda_{c1}\, N_{c1}}{r_{c1}} + \frac{\lambda_{c2}\, N_{c2}}{r_{c2}} \tag{6.9}$$

Assuming that both rear wheels and both casters have the same RRPs the equation is further simplified.

$$\frac{(A_1 + A_2)\, K_t}{r_R} = \frac{2\lambda_R\, N_R}{r_R} + \frac{2\lambda_c\, N_c}{r_c} \tag{6.10}$$

In this last equation only the two rolling resistance parameters are unknown. Hence, a minimum of two independent equations are necessary to calculate the RRPs. By testing at least two different weight distributions the problem can be solved.

The referred system of two equations and its solution can be represented with matrices as:

$$\begin{bmatrix} \frac{2\lambda_R\, N_{R1}}{r_R} & \frac{2\lambda_c\, N_{c1}}{r_c} \\ \frac{2\lambda_R\, N_{R2}}{r_R} & \frac{2\lambda_c\, N_{c2}}{r_c} \end{bmatrix} \begin{bmatrix} \lambda_R \\ \lambda_C \end{bmatrix} = \begin{bmatrix} A_R \\ A_C \end{bmatrix} \tag{6.11}$$

$$[N][\lambda] = [A] \tag{6.12}$$

$$[\lambda] = [N]^{-1}[A] \tag{6.13}$$

The precision of estimation of the RRPs can be incremented by adding more experimental results represented by extra equations. The addition of more equations creates an overdetermined system, where $[N]$ is no longer square and, thus, also not invertible. However, a solution of linear least square regression [14] can be obtained by using the pseudo inverse:

$$[\lambda] = ([N]^T[N])^{-1}\ [N]^T\ [A] \tag{6.14}$$

This analysis was used to determine the RRPs for the rear wheels and front caster wheels. Original data used in this calculation is the same presented in table E.2 through

E.5. Figure 6.6 shows RRPs calculated for different velocities on the straight path experiments.

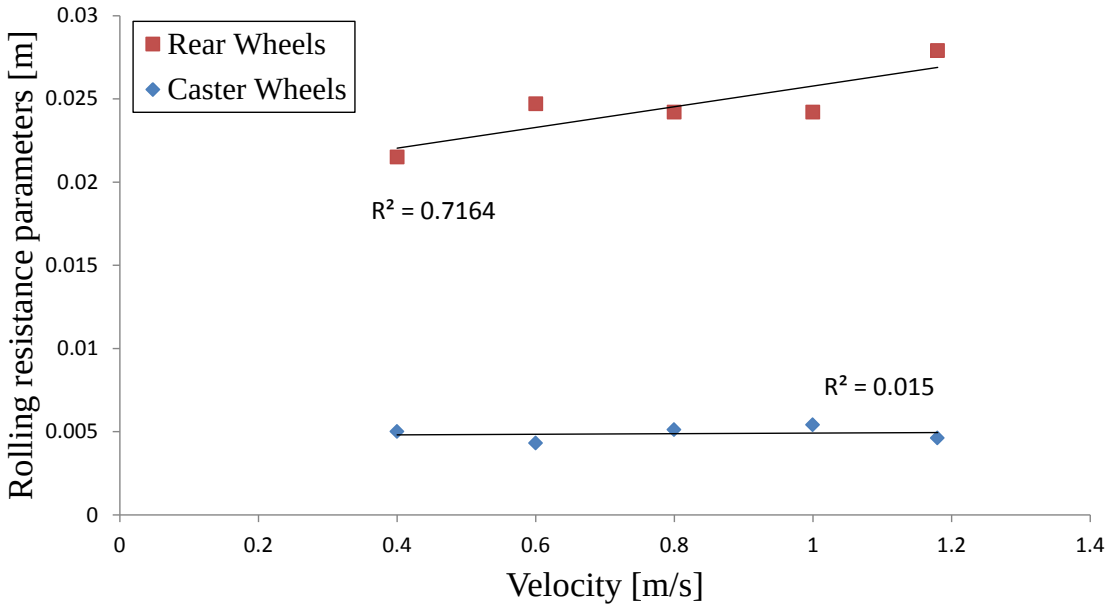

Figure 6.7 Estimated rolling resistance parameters (RRPs) at different velocities.

6.1.3 Constant acceleration experiments

This set of experiments consisted in driving the wheelchair on a straight path at different values of constant acceleration. The velocity profile needed for these tests was similar to the previous section, but the constant velocity section remained unchanged. Only the acceleration magnitude was varied from 0.12 to 0.48 m/s^2. The test track remained the same and each experiment was repeated once in both directions to compensate for the ground irregularities and slope.

The result from a constant acceleration experiment is shown in the next figures, including velocity, acceleration and current fed to the motors.

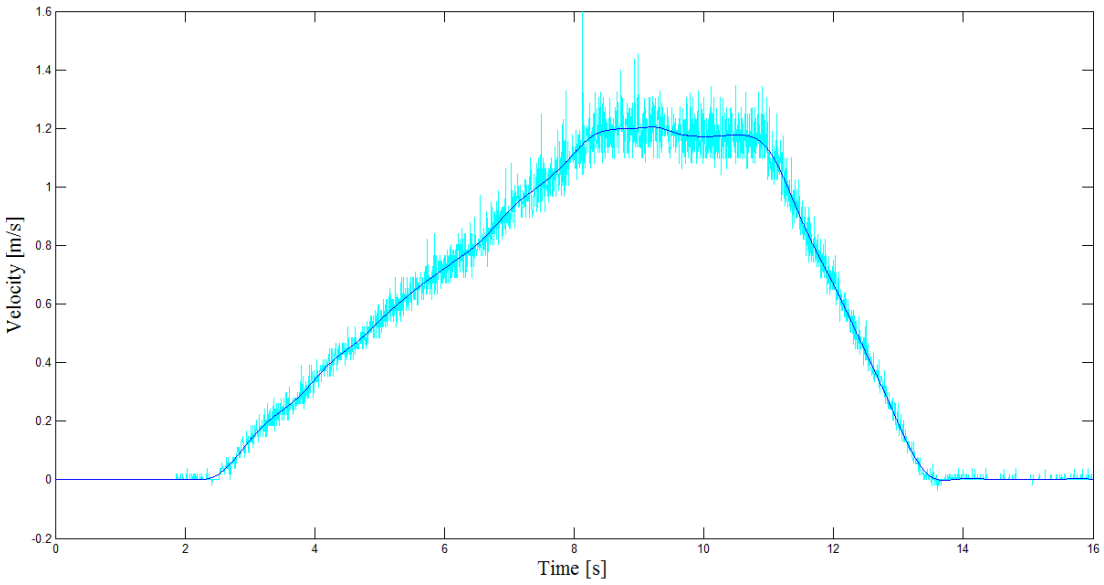

Figure 6.8 AMPS velocity profile during a constant acceleration experiment.

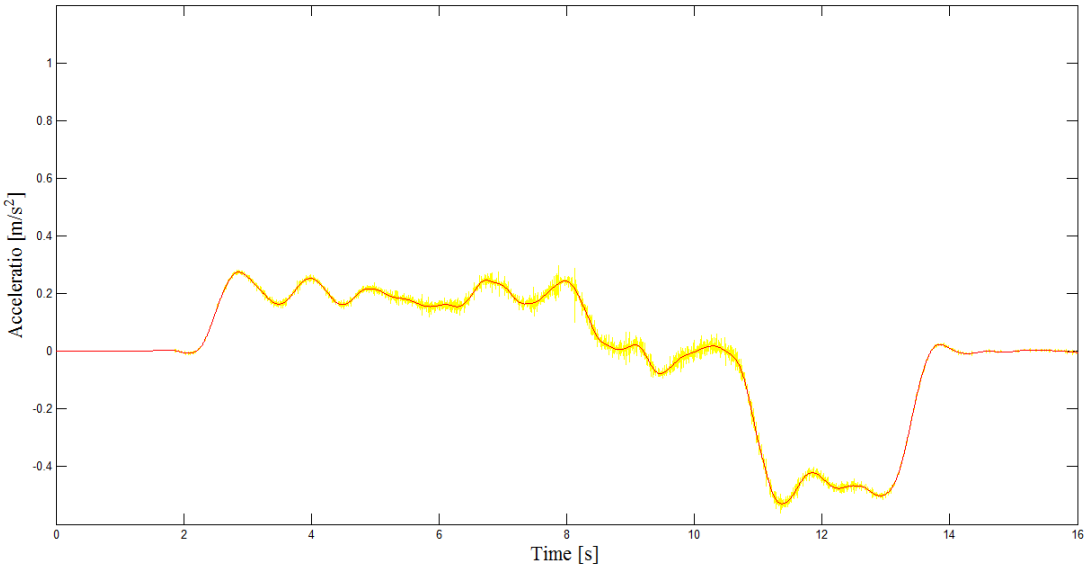

Figure 6.9 AMPS acceleration profile during a constant acceleration experiment.

Obtained by numerically differentiating the velocity profile.

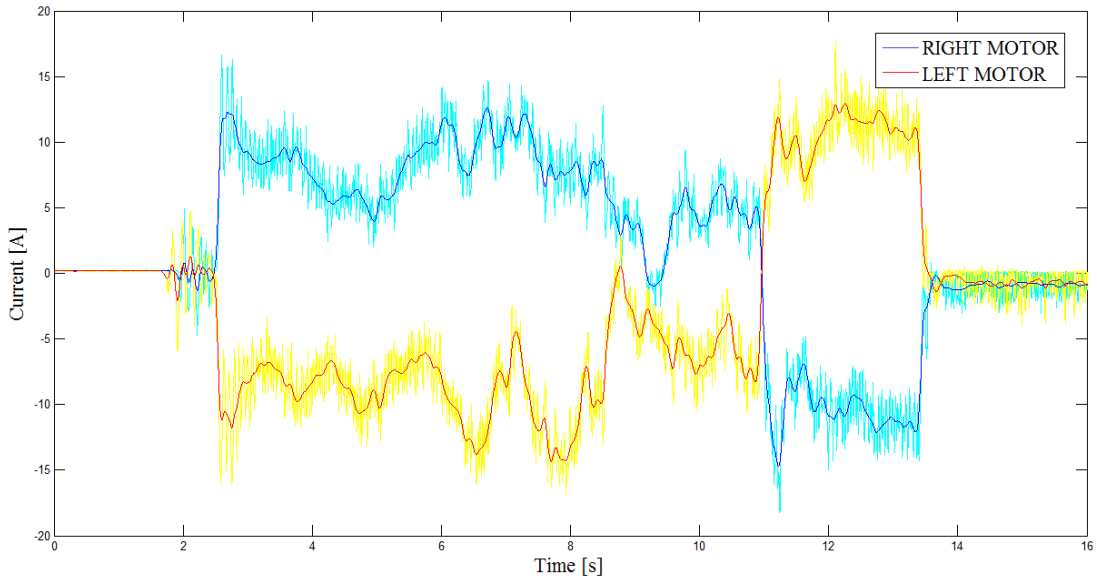

Figure 6.10 Motor currents recorded in a constant acceleration experiment.

To calculate rolling resistance during acceleration we need to refer to the same equations presented in section 6.1.1. In this case the acceleration term is not equal to zero and accordingly it must be considered. To obtain the total rolling resistance during a constant acceleration experiment the following relations were used:

$$F_{Roll} = (F_1 + F_2) - ma_y \tag{6.15}$$

$$F_{Roll} = (T_1/r_R + T_2/r_R) - ma_y \tag{6.16}$$

$$F_{Roll} = (A_1 + A_2)\, K_t/r_R - ma_y \tag{6.17}$$

Average values of current and acceleration were obtained for the period of interested and used in the calculations. The results for the tests are presented in the following figure.

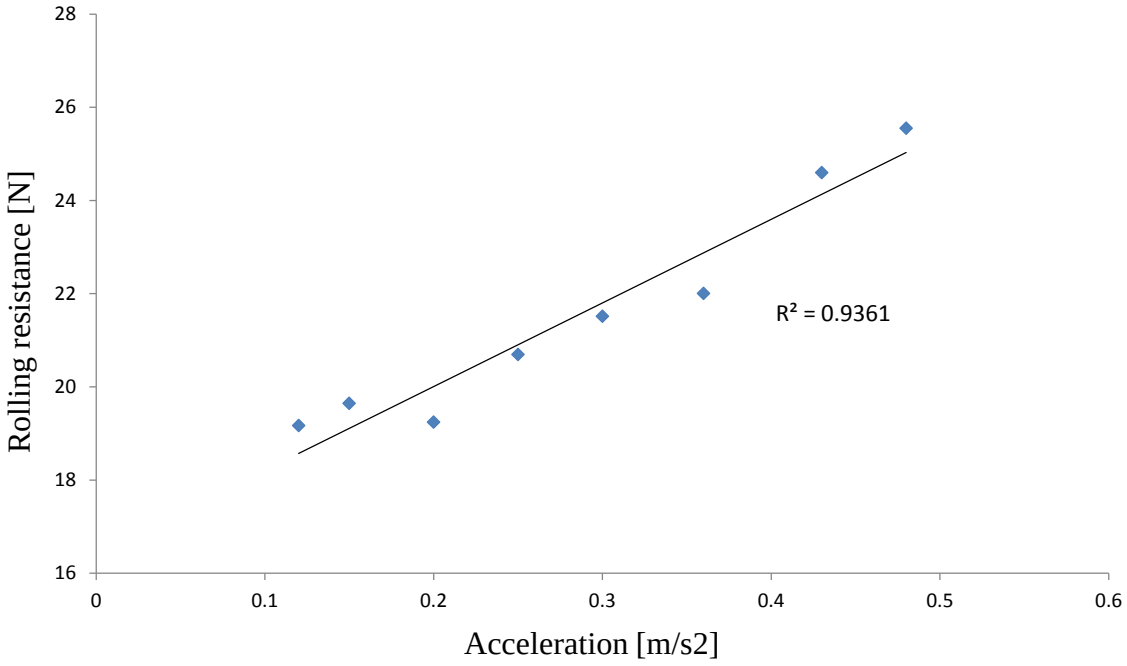

Figure 6.11 Rolling resistance for different acceleration values.

Figure 6.11 shows rolling resistance for several values of acceleration during a straight maneuver. Rolling resistance varies from 17.2 to 25.6 N in a range of accelerations from 0.12 to 0.48 m/s^2. The correlation coefficient is 0.9631 for the trend line shown. Rolling resistance increases 8.4 N (49%) for a 0.36 m/s^2 change.

In the previous experiment rolling resistance force ranged from 16.5 to 20.1 N at constant speeds of 0.4 to 1.2 m/s. Rolling resistance surpassed those values during acceleration. This means that the rolling resistance experienced by the wheelchair not only increases with velocity as previously known, but the acceleration has an effect on it. This acceleration tests has not been performed before in previous publications except by one by the same author of this work [23]. That set of experiments used an open-loop torque control to match an acceleration profile to get a similar result as shown here.

We can further analyze the collected data to determine average rolling resistance at different velocities during the acceleration maneuver. For example, for determining an approximate rolling resistance at 0.6 m/s during a constant acceleration test, the motors

current used from the 0.55 to 0.65 m/s period could be averaged. This process can be repeated for each of the constant acceleration experiments, obtaining a cloud of data points that estimate rolling resistance for different values of velocity and acceleration on a straight trajectory. Figure 6.12 show the calculated points. A pink surface has been added as a visual aid to locate the data points on a three-dimensional space where the axes are velocity, acceleration and rolling resistance.

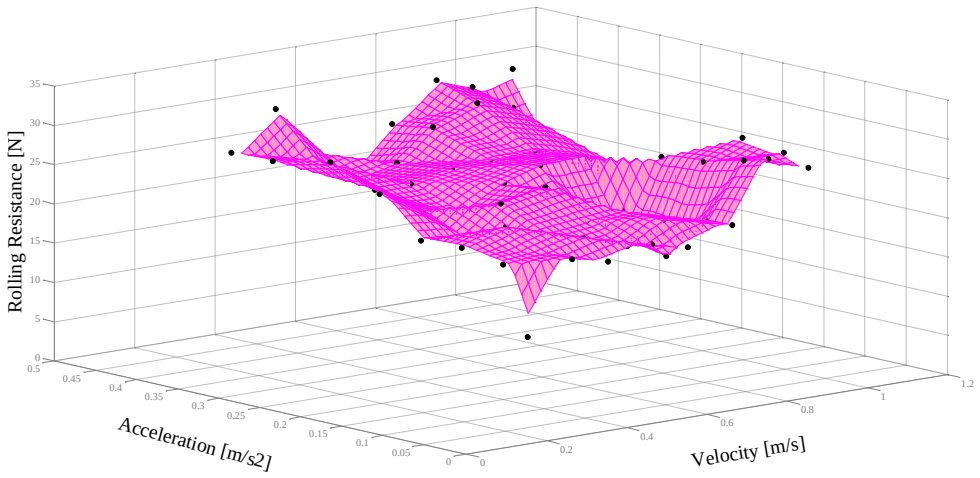

Figure 6.12 Estimated rolling resistance at different velocities and accelerations.

Similar to what has been done to other experimental results throughout this work, a linear regression plane can be calculated to show the overall tendency of the data points. This ‘best fit plane’ can be observed in figure 6.13. Each point represent a certain average value of rolling resistance for a specific velocity during a constant acceleration maneuver.

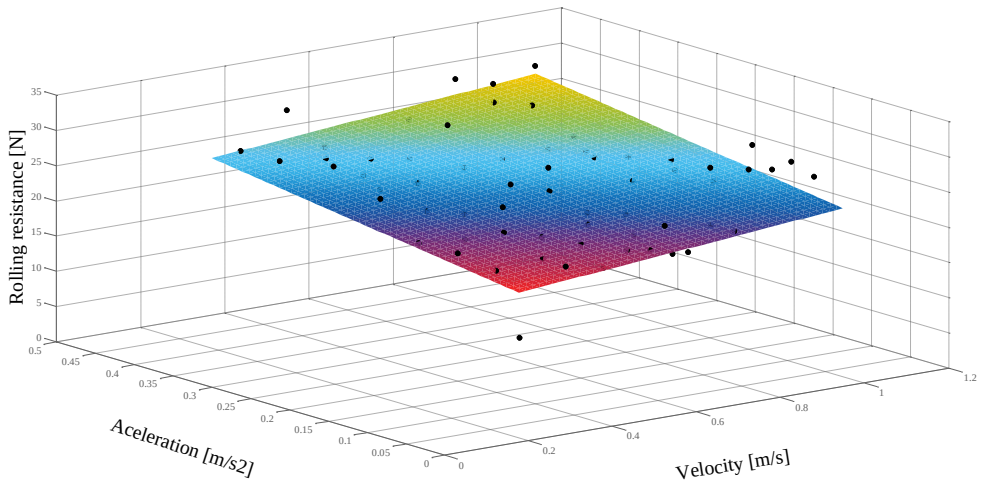

Figure 6.13 Best fit plane for rolling resistance at different values of velocity and acceleration.

To better observe the overall tendency of the data with respect to velocity, a lateral view of the plane is shown in figure 6.14. It can be seen that rolling resistance increases with velocity, as found in the constant velocity experiments. Similarly, to observe the overall tendency of the data with respect to acceleration, figure 6.15 show a different lateral view of the data points and best fit plane. Once again, the increasing tendency can be perceived.

The mapping of rolling resistance as a function of velocity and acceleration is original work presented in this thesis. One set of data was enough to create a cloud points and show overall tendencies. Greater precision can be obtained by repeating several tests and averaging their results. The AMPS ability to control the velocity and trajectory of a manual wheelchair was key to perform these tests and observe changes in rolling resistance during acceleration. Further work could compare similar mappings of rolling resistance for different wheels types and configurations.

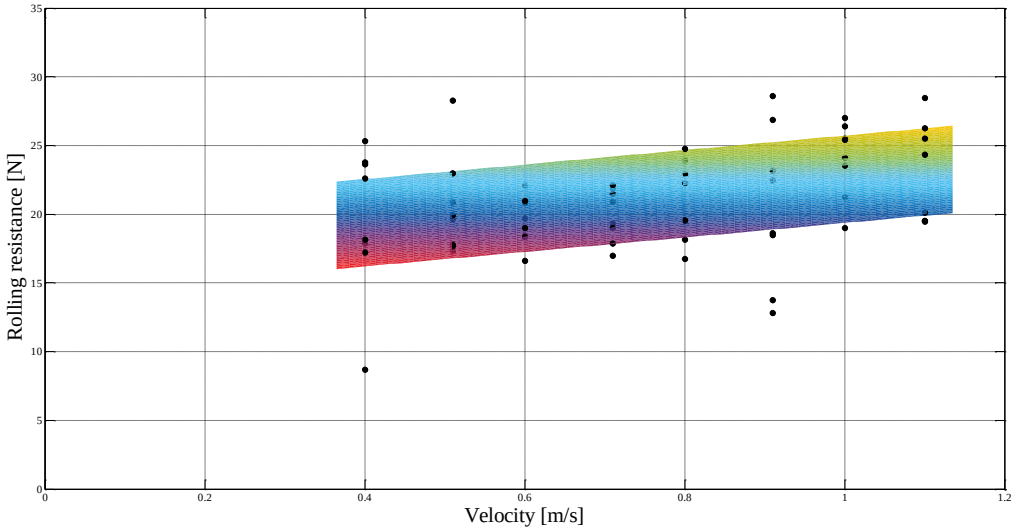

Figure 6.14 Rolling resistance and velocity for multiple experiments.

Rolling resistance increases as velocity increases.

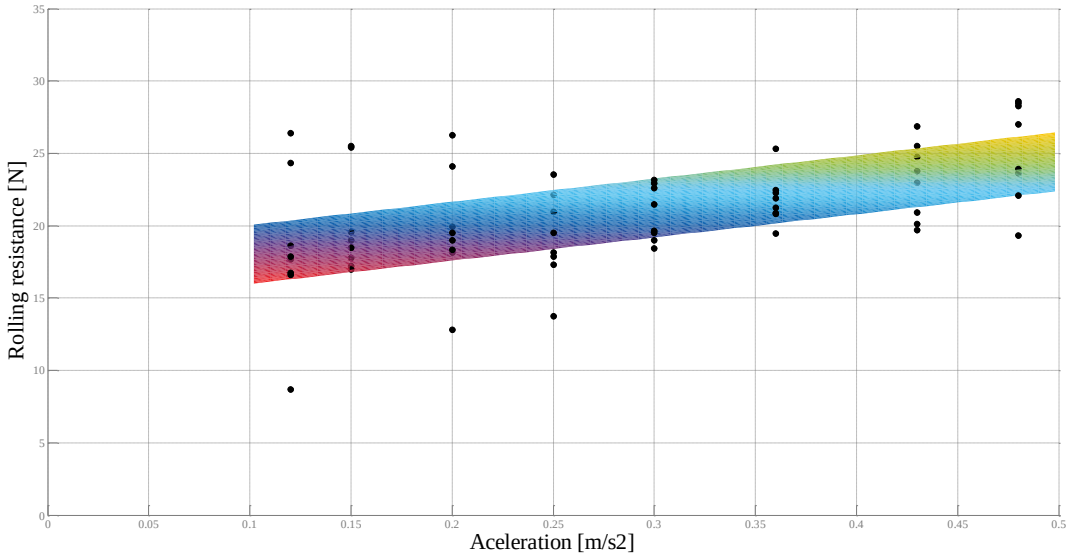

Figure 6.15 Rolling resistance and acceleration for multiple experiments.

Rolling resistance increases as acceleration increases.

6.2 Turning resistance experiments

Despite most of experiments regarding wheelchair dynamics are performed following straight paths, curvilinear maneuvers occur commonly on wheelchair users' daily activities. The dynamic analysis of such maneuvers is more complex but necessary to better understand everyday use of manual wheelchairs. The added complexity of the analysis of general curvilinear trajectory include: the need for measuring the location of center of mass (COM) of the wheelchair, determining the caster wheels orientation with respect to the frame, and the addition of tangential forces and resistive moments acting on the wheels as shown in chapter 2.

Turning resistance experiments comprised a series of circular maneuvers with a fixed center of rotation and constant linear (tangential) speed. These particular conditions greatly simplify the equations allowing to calculate total turning resistance.

Figure 6.14 AMPS performing a circular trajectory maneuver.

During turning maneuvers the caster wheels adopt different orientation relative to the rear wheels and frame. Experience demonstrate the tendency of caster wheels to align themselves tangentially to the instantaneous radius of curvature at any given point of the wheelchair's trajectory. However, mathematically modeling passive caster wheels such as the ones found in manual wheelchairs, is a challenging task. For the circular motion in these set of experiments the caster's orientation remained unchanged with respect to the frame. The α orientation angle of each caster visually confirmed the alignment of these wheels tangentially to the trajectory. In addition, work by Chénier [19] has shown a simplified model for wheelchair caster and is the one used in this thesis work for reference.

In general, the dynamic analysis of a curvilinear trajectory is more difficult than that of a straight path since more forces are present affecting the motion of the wheelchair. For a straight trajectory only rolling resistance has been considered so far. Each one of the four wheels contributed to the total rolling resistance, with the forces acting parallel and opposed to the wheelchair's straight motion. For a curvilinear path rolling resistance in all four wheels is not parallel any more since the caster wheels adopt different orientations with respect to the main body. Additionally, a turning resistive force appears as the wheels rotate scrubbing the floor while changing the wheelchairs orientation. To the knowledge of this thesis' author there are no publications measuring turning resistance on a moving wheelchair.

The dynamic analysis presented previously show that, in order to identify the effects of turning resistance on a curvilinear path, rolling resistance had to be previously determined. Otherwise it would be impossible to differentiate the effects of turning resistance from the total resistive forces acting against the wheelchair motion. Rolling resistance values needed for this set of experiments is found on section 6.1.1.

Experiments for determining turning resistance consisted of a series of circular trajectories with different radius of curvature. The linear forward speed was held constant during the trajectory. This implies that the angular velocity of the vehicle circling a center

point on the floor was held constant. Since the radius of the trajectory is fixed, the orientation of the caster wheels holds constant and can be measured directly.

The following figure shows the circular trajectory used in the experiments.

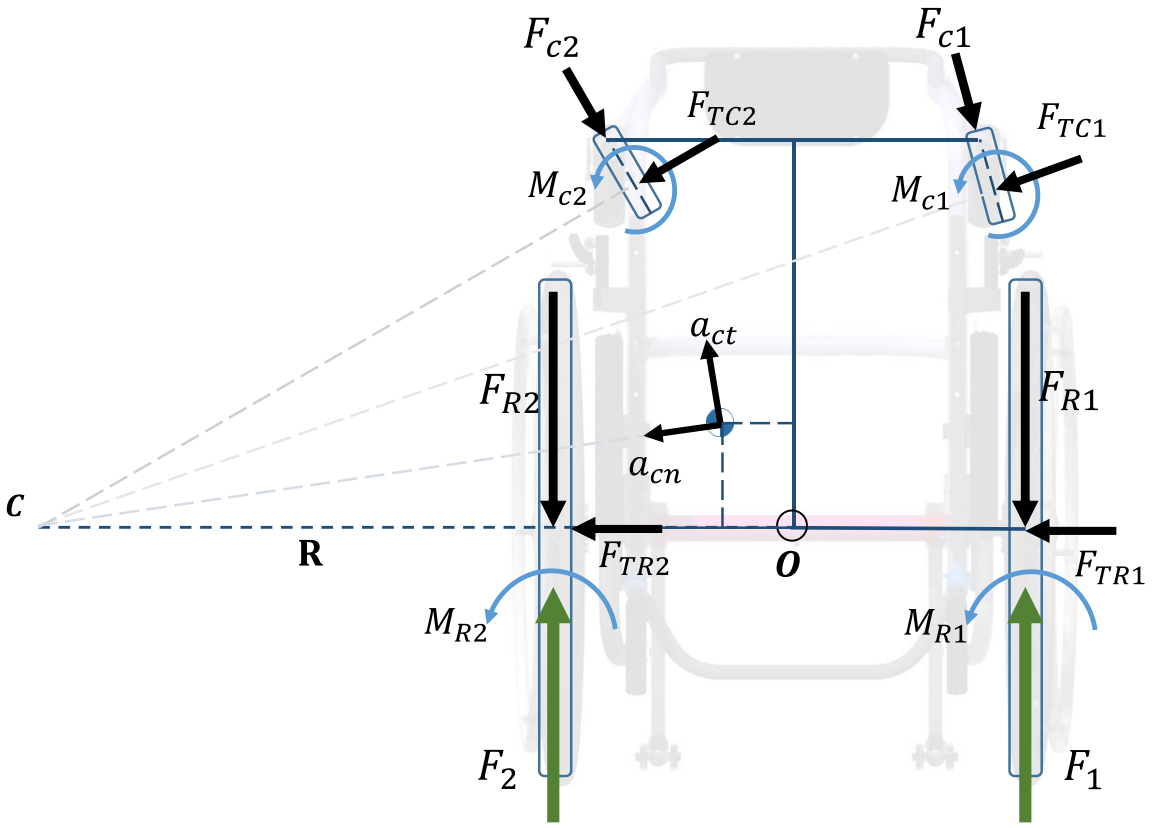

Figure 6.15 Dynamic analysis of a wheelchair moving on a circular trajectory.

Where a_{cn} is the centripetal acceleration and a_{ct} is the tangential acceleration of the COM with respect to the instantaneous center of rotation. The tangential acceleration is zero when the linear speed of the wheelchair does not change.

Taking the moments with respect to the instantaneous center of rotation allows to isolate the total turning resistance moment acting on the wheelchair.

$$\sum M_C = 0 \tag{6.18}$$

$$\sum M_C = (F_1 - F_{R1})\left(R + \frac{d_R}{2}\right) + (F_2 - F_{R2})\left(R - \frac{d_R}{2}\right) - F_{c1}R_{c1} - F_{c2}R_{c2} - (M_{R1} + M_{R2} + M_{c1} + M_{c2}) \quad (6.19)$$

$$T_{res} = M_{R1} + M_{R2} + M_{c1} + M_{c2} \quad (6.20)$$

$$T_{res} = (F_1 - F_{R1})\left(R + \frac{d_R}{2}\right) + (F_2 - F_{R2})\left(R - \frac{d_R}{2}\right) - F_{c1}R_{c1} - F_{c2}R_{c2} \quad (6.21)$$

Where T_{res} is the total turning resistance opposing the circular motion of the wheelchair.

The turning resistance experiments comprised circular trajectories with different radios of curvature from 0.3 to 1.8 m. Forward speed (tangential to the trajectory) was kept constant at 0.6 m/s. To keep consistency with the straight trajectory experiments, circle trajectory maneuvers were performed once in clockwise and counterclockwise direction. For each run turning resistance was calculated by using the aforementioned equation. The following figure shows the results of the experiments.

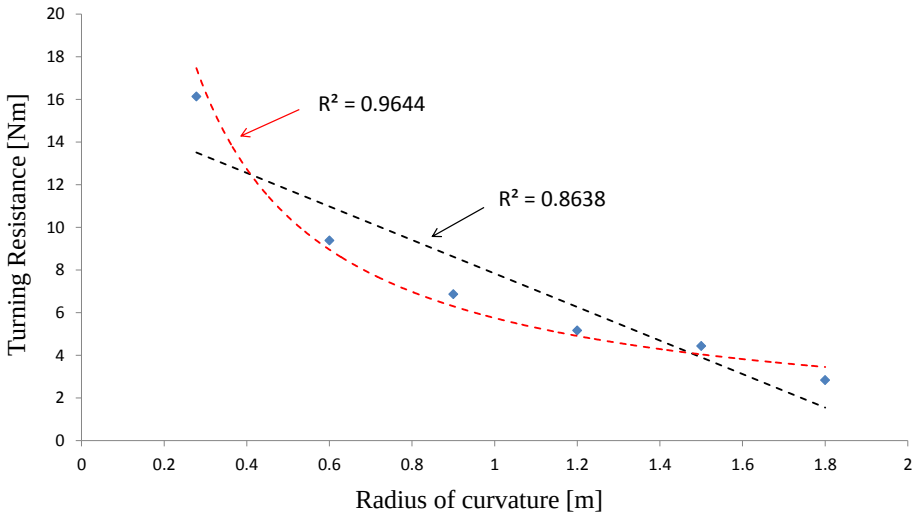

Figure 6.16 Turning resistance variation with radius of curvature.

Figure 6.16 shows the average turning resistance for a manual wheelchair following circular trajectories in two directions: clockwise turn and counterclockwise turn. Turning resistance varies from 2.8 to 16.1 Nm for an increasing radius of curvature of 0.28 to 1.8 m. Two trend lines are also shown in the graph. The straight line has correlation coefficient is 0.8638. The exponential curve fits better the data points with a correlation coefficient of 0.9644. It would be expected that turning resistance tend to zero as the radius of curvature increases, approaching a straight trajectory. An exponential curve shows better this asymptotical tendency.

6.3 Energy efficiency experiments

Various sets of experiments where performed to measure overall energy efficiency. Following the definitions of efficiency in chapter 6 some experiments where designed based on their significance of those metrics.

6.3.1 Energy conversion efficiency

For a mechanical system converting one type of energy into another, efficiency is the ratio between the useful output of the device and the input, in energy terms.

$$\eta = \frac{E_{output}}{E_{input}} \tag{6.22}$$

The AMPS transforms electric power fed to the motors into kinetic energy of the wheelchair. This conversion ratio is more significant during acceleration than during constant speed periods. In constant speed periods the kinetic energy of the system remains the same while the motors keep delivering energy to overcome the energy losses due to rolling resistance. Consequently, this definition of mechanical efficiency does not properly illustrates the system's behavior during constant velocity straight tests. However, during the acceleration phase it is interesting to observe how the delivered energy is transformed into kinetic energy through the wheelchair system.

The following figure shows energy data for a straight run during the acceleration phase.

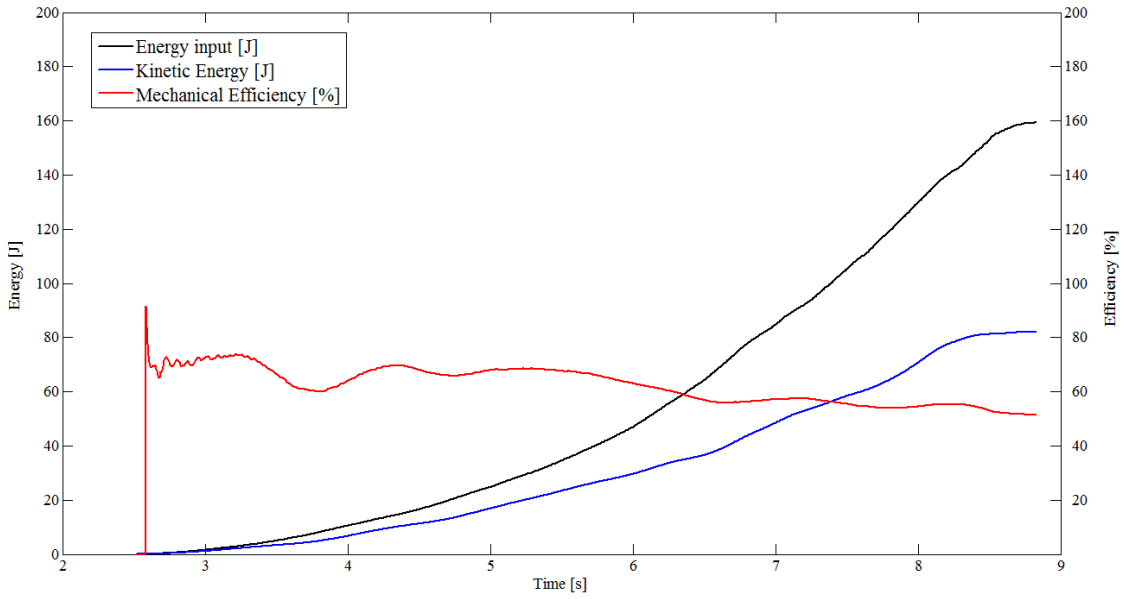

Figure 6.17 Energy input, energy output and energy conversion efficiency during a constant acceleration on a straight trajectory.

Efficiency is expressed in percentage of the ratio between the incrementing kinetic energy (output) and the incrementing mechanical power delivered by the motors (input). I remains somewhat constant during the whole acceleration phase.

Experiments were performed to characterize mechanical efficiency for different values of acceleration. The following figure shows the energy conversion efficiency for acceleration phases ranging from 0.12 to 0.48 m/s2.

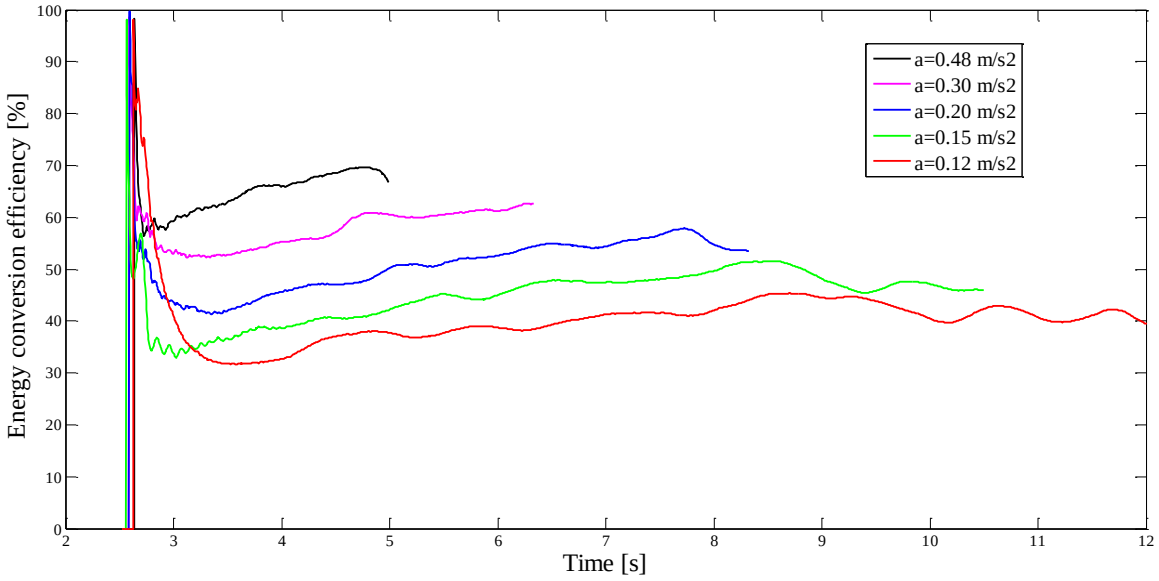

Figure 6.18 Energy conversion efficiency for various acceleration experiments.

It can be observed from figure 6.17 that energy conversion efficiency is greater with larger values of acceleration, meaning that the faster energy is delivered to the system, the more efficient it is in converting it that energy into motion. This is an interesting observation considering that rolling resistance is greater for larger values of acceleration.

6.3.2 Cost of Transport

Cost of transport (COT) was measured for straight maneuvers at constant speed and pulsatile propulsion. It was also used to compare curvilinear trajectories. In previous experiments it was found that rolling resistance incremented with velocity and acceleration. Also, that turning resistances increases as the turning radius decreases. The consequence of these findings is that the cost of transport should increase as the average velocity goes up or the curvature radius shortens, for the same travelled distance. The continuous periods of acceleration during a pulsatile propulsion are also expected to affect overall cost of transport even though the average speed and travelled distance are maintained.

Experiments for measuring COT where performed over a 15 meters straight path while maintaining a regular constant speed within ± 5% (figure 6.19).

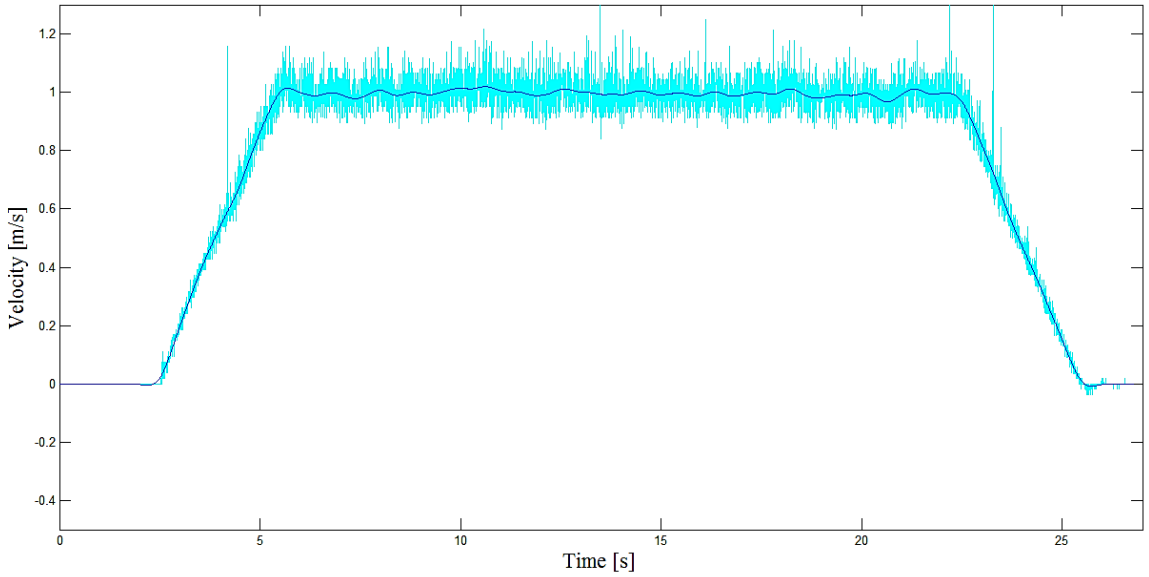

Figure 6.19 AMPS velocity profile during a COT experiment.

The equation for calculating COT is

$$COT = \frac{E_{input}}{Dm} \tag{6.23}$$

The travelled distance D is easily measurable both directly on the track and by using the encoder collected data. Calculating the energy input of the system is one of the most important advantages of using the AMPS versus performing tests with human beings. Since the AMPS uses electric motors the energy input can be calculated by

$$E_{input} = \int_0^t P(t)dt = \int_0^t T(t)w(t)dt = \int_0^t A(t)\, K_t\, w(t)dt \qquad (6.24)$$

Where $P(t)$ is the power delivered by the motors, $T(t)$ is the provided torque and $w(t)$ is the angular velocity of the motors' shaft. The provided torque is proportional to the current passing through the motors (figure 6.20) measured by Hall-Effect sensors.

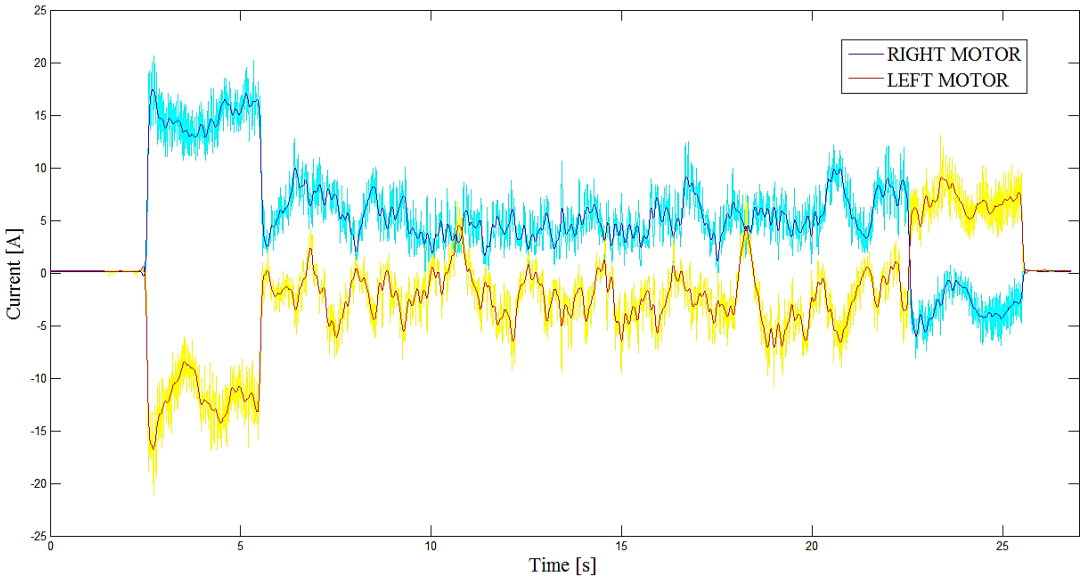

Figure 6.20 Motor current recorded during a COT experiment.

The angular velocity is calculated from the wheel encoders, which are mechanically connected to the motors. Figure 6.21 shows the total energy input provided to the wheelchair during the maneuver, along with total system kinetic energy and energy loss.

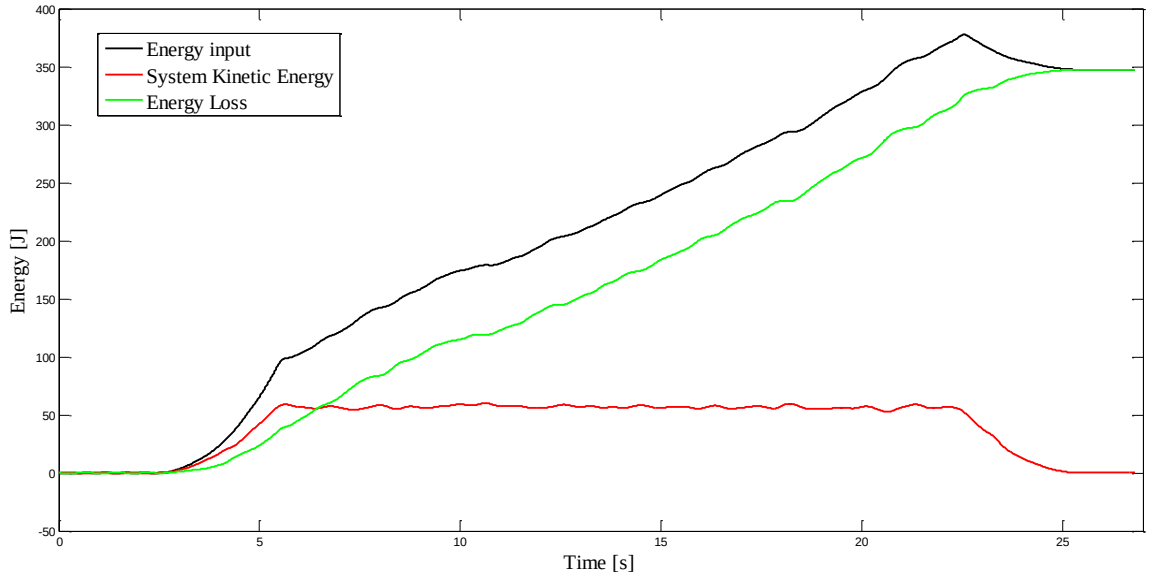

Figure 6.21 AMPS energy input, output and loss during a straight trajectory experiment.

In figure 6.21 three different data sets are presented. The black curve represents the total energy provided to the wheelchair through the motors, whose calculation was described above. The red curve represents the total kinetic energy of the system throughout the maneuver and it constitutes the energy output of the system at any given time of the straight trajectory. It is calculated with equation

$$KE = \frac{1}{2}mV^2 + \frac{1}{2}I_R\left(\dot{\theta}_{R1}^2 + \dot{\theta}_{R2}^2\right) + \frac{1}{2}I_C(\dot{\theta}_{C1}^2 + \dot{\theta}_{C2}^2) \qquad (6.25)$$

The third curve, in green, represents the accumulated energy loss during the maneuver. It is calculated by arithmetically subtracting the energy output from the input

$$E_{loss} = E_{input} - KE \qquad (6.26)$$

The results for cost of transport measured in straight maneuvers at different velocities are presented in the following figure.

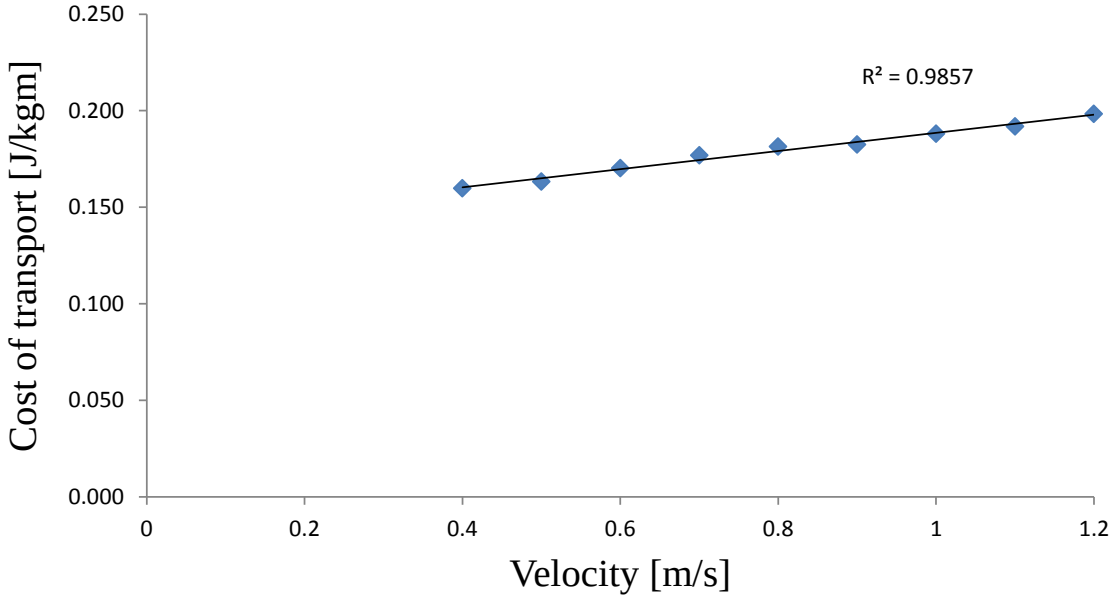

Figure 6.22 Cost of transport (COT) at various velocities along a straight trajectory.

It can be seen that COT increments with velocity. This means that the system is less efficient when velocity is incremented. This result is consistent with what was previously found, that rolling resistance increases with velocity. Since rolling resistance increments, the energy losses of the system also increases, diminishing its energetic efficiency.

Section 6.2.1 predicted that the COT of transport for a straight trajectory at constant speed should be very close to the value of rolling resistance.

$$COT = \frac{F_{Roll}}{m} + \frac{1}{D}\int_0^t V(t)a_y(t)dt \tag{6.27}$$

Figure 6.23 compares both COT and rolling resistance for straight path experiments at constant speed. Note that the units for rolling resistance and COT are equivalent and thus can be compared. The result show close results of rolling resistance and COT as expected.

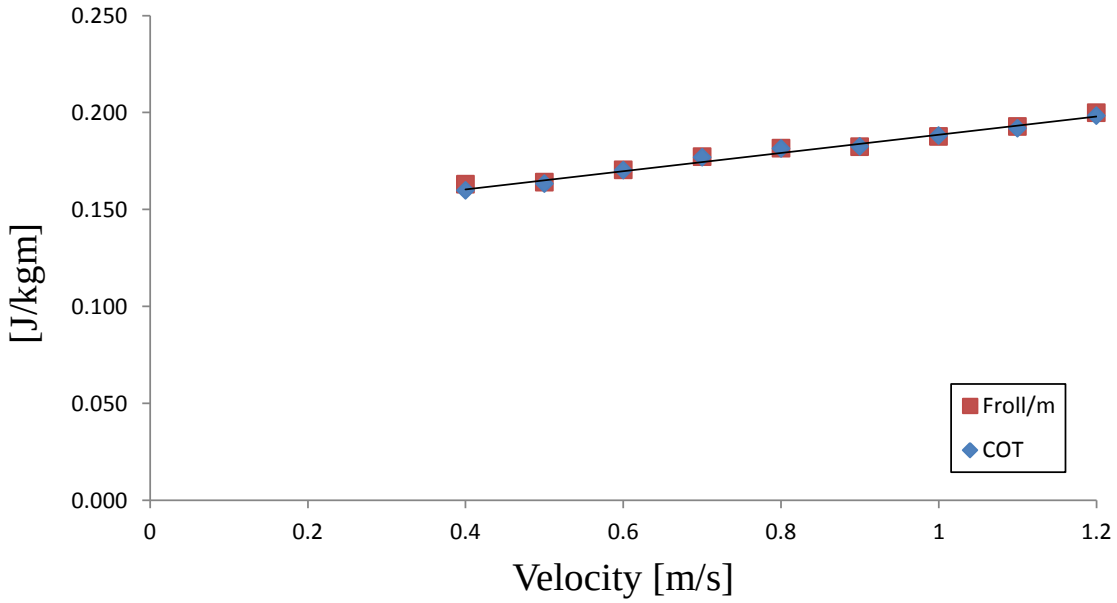

Figure 6.23 Comparison between cost of transport and average rolling resistance at different velocities during straight trajectory experiments.

The same COT calculation was performed on experiments including circular trajectories. This time the forward velocity was fixed at 0.6 m/s but the radius of curvature was increased from 0.28 to 1.8 m. Figure 6.24 show the result of this analysis.

It can be observed that the transition from a straight trajectory to a curvilinear trajectory has a great impact on the cost of transport. At 0.6 m/s on a straight path the COT averaged 0.17 J/kgm, however, for a radius of curvature of 1.8 m the COT increases to 0.40 J/m (135% increment). COT increases drastically as the radius of curvature approaches 0.28 m, a condition when one wheel remains in the same position. At this state the COT more than doubles, showing the increased effort necessary to move in such sharp curves.

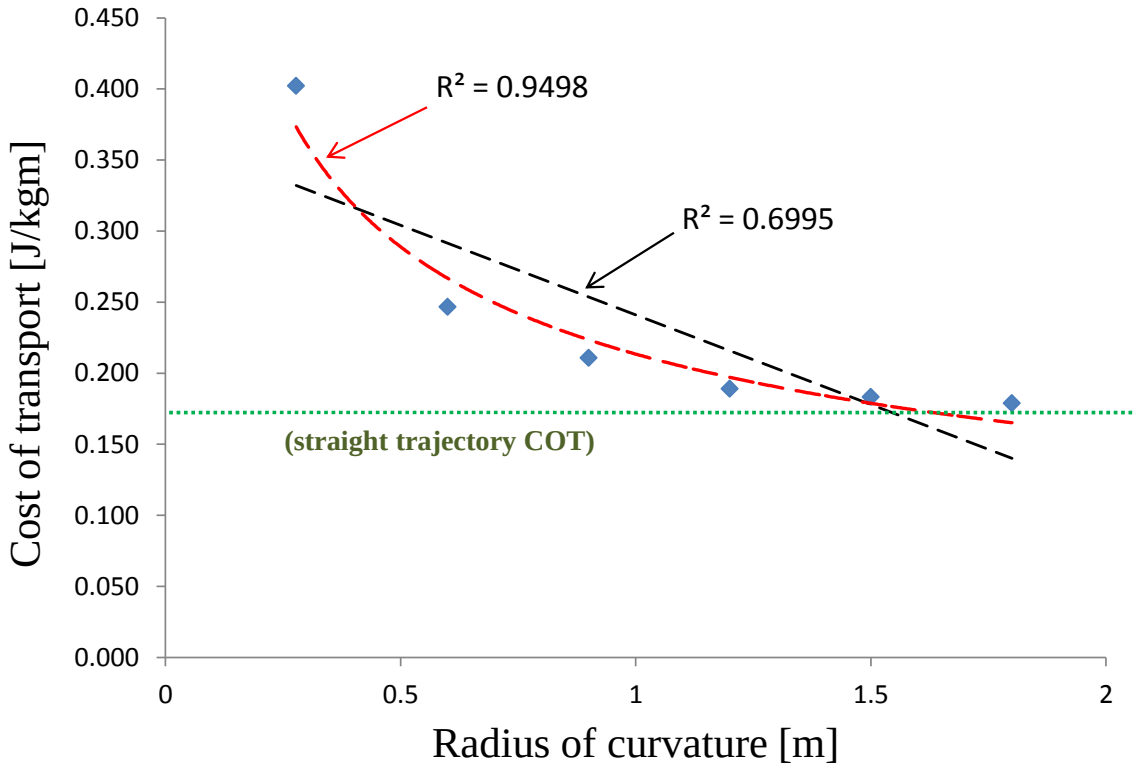

Figure 6.24 Cost of transport on a circular trajectory, various radios.

A possible explanation for this important increase in cost of transport with radius of curvature lies on the addition of turning resistance affecting the wheelchair, not present in the straight trajectory experiments. As turning resistance increases as instantaneous radius of curvature decreases, the system efficiency is expected to drop.

Two trend lines are shown on figure 6.24. The first is a straight line with correlation coefficient of 0.6995, indicating this curve fitting is deficient. An exponential curve fits better with the data presented, reaching a correlation coefficient of 0.9498. Not only this curve fits better but tends to an asymptotical value. It is expected that the COT of a circular trajectory would tend to match that of a straight trajectory as the radius approximates infinity. In figure 6.24 a green dotted line indicates the calculated COT for a straight line experiment. The data points seem to approximate this value asymptotically.

6.4 Pulsatile propulsion experiments

The experiments designed to measure rolling and turning resistance required a close-to-constant push from the motors in order to obtain wheelchair constant speed. However, human beings have a particular way of propelling manual wheelchairs due the interface between upper limbs and the wheels' handrims. The passenger's hands grab the handrims and apply force on them as the wheel rotates. After a finite arc length the passenger let go the handrims to return to the original position and push again. This strategy of propulsion consists in a series of pulses that increases the kinetic energy of the system, alternating with periods of freewheeling in which the wheelchair travels freely. A person can change the frequency or amplitude of the force pulses to follow a particular trajectory while keeping a manageable velocity.

Using the AMPS to emulate pulsatile propulsion requires two major features. One is the ability to emulate the freewheeling behavior while having the motors engaged to the handrims. The other is to calculate the appropriate pulse amplitude and frequency to obtain the desired trajectory in a given time.

6.4.1 Freewheeling

When a passenger let go the handrims during the propulsion cycle, the wheelchair keeps moving by its inertia and starts decelerating due to the resistive forces acting against the vehicle's motion. This condition is known as freewheeling.

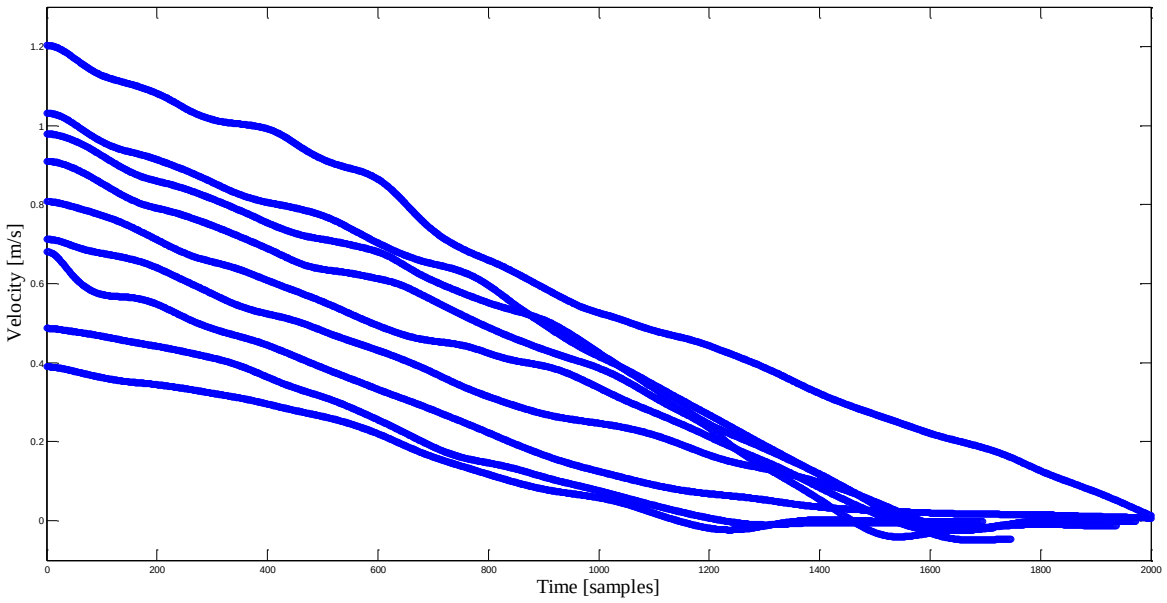

Figure 6.25 Wheelchair natural deceleration (freewheeling) for various initial velocities.

The AMPS have two electric motors constantly attached to the handrims, so it cannot ‘let go’ of them as a human passenger would. These electric motors have an internal friction that resists the rotation their shafts. This is clearly manifest when trying to push the AMPS with the motors engaged to the handrims. The wheelchair feels a lot ‘heavier’ than it would be without the motors, and decelerates much faster. To illustrate this, a set of deceleration curves can be plotted to contrast the natural freewheeling deceleration of the wheelchair without the friction of the motors, as opposed to the deceleration with the motors engaged.

Figure 6.25 shows in blue the natural deceleration of the wheelchair with the motors disengaged. The wheelchair was pushed until a maximum velocity was reached, and then let go. The velocity was calculated by numerically differentiating the angular position of the rear wheels collected by the encoders.

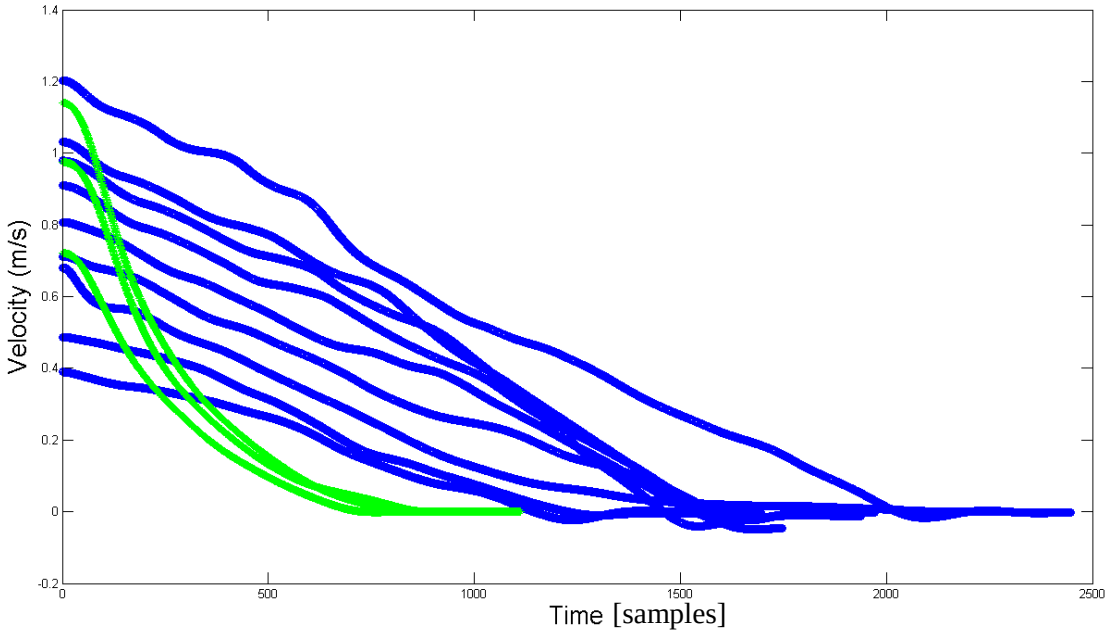

Figure 6.26 Natural deceleration compared to deceleration with motors engaged.

In order to achieve a natural freewheeling dynamics while the motors are engaged, the internal friction of the motors has to be cancelled. In this work the cancellation of the motors is based on the no-load current of the motors. No-load current is the amount of electric current flowing through the motor at a given velocity when no external load is attached to it. This current is proportional to the torque needed to overcome only the motor's internal friction. Theoretically, if an electric motor did not have any frictional resistance in its mechanical parts, no current should be necessary to keep it rotating at any speed. In actual equipment, the internal friction depends on the motors components and manufacturing. The strategy to achieve the motor cancellation effect needed to emulate freewheeling, is to supply the no-load current at any given angular velocity.

Testing was performed on each individual motor to determine no load current as a function of velocity. Figure shows the results. It is worth noting that the value of current when approaching zero RPM is hard to measure since the static friction of the motor varies slightly with the angular position of the shaft.

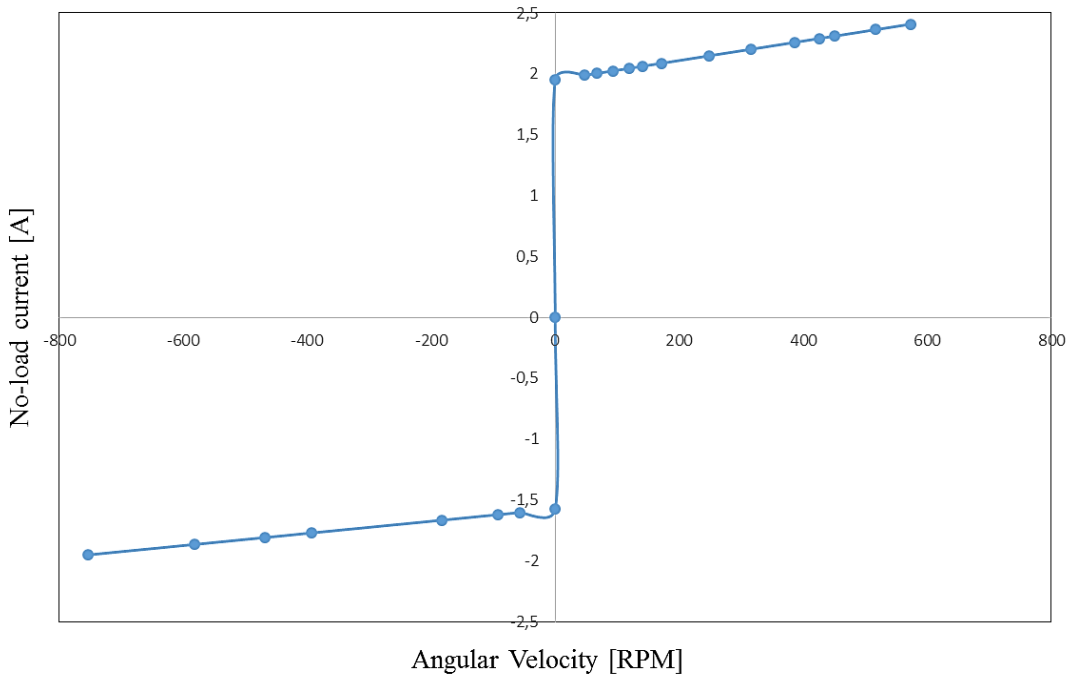

Figure 6.27 Motor no-load current versus angular velocity.

The AMPS controller keeps track of the velocity of the vehicle and angular speed of the motors at any moment. By applying the no-load current to the motors corresponding to the actual speed it was possible to cancel their braking effect. The following figure shows the application of motor cancelation based on no-load current.

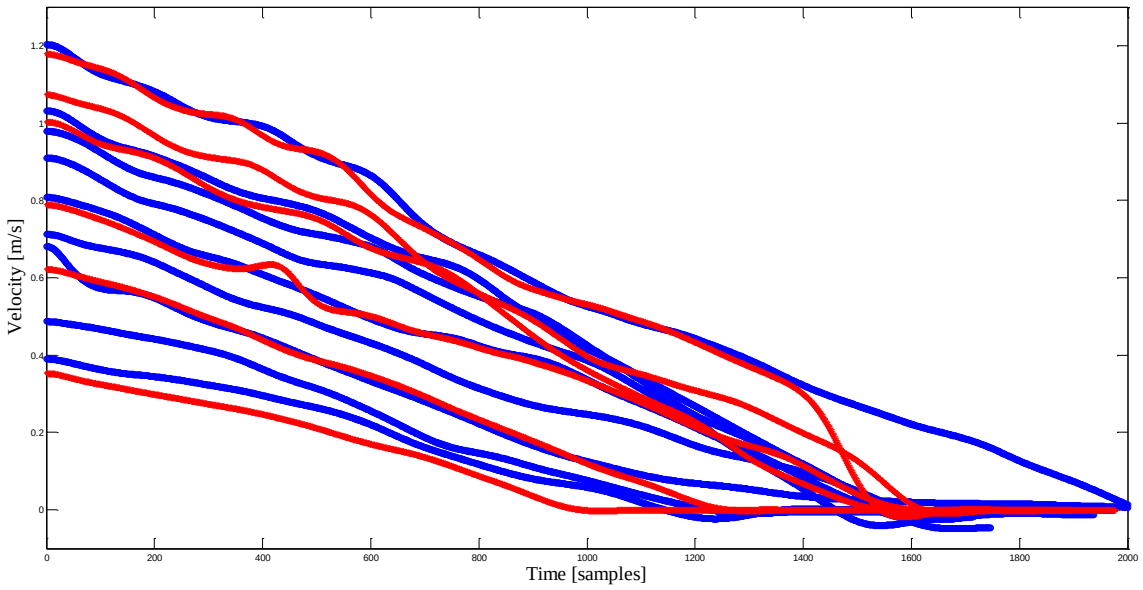

Figure 6.28 Comparison between natural deceleration (blue) and motor cancellation deceleration (red).

Figure 6 shows in the same graph both natural wheelchair acceleration and the one obtained through motor cancellation. Visual inspection find no noticeable difference between the natural and the 'artificial' one. Since freewheeling during maneuvers usually last less than two seconds, the error in traveled distance is very small.

Average natural deceleration (blue) starting near 1.2 m/s was -0.1259 m/s^2, while with motor cancellation (red) it was -0.1257 m/s^2, a difference of less than 1% in a 7 seconds period. Average natural deceleration (blue) starting near 0.4 m/s was -0.06623 m/s^2, while with motor cancellation (red) it was -0.07082364m/s^2, a difference of 7% in a 5 seconds period. Fluctuations in natural deceleration could be most likely explained by the influence of local imperfections on the floor, especially at low velocities.

6.4.2 Pulses calculation

The next challenge to achieve pulsatile propulsion with the AMPS was to determine the shape and magnitude of the pulses that would propel the wheelchair. Appendix 6 shows the details of the mathematical analysis that creates the pulses. The general strategy is described below.

The push generated by a person during a straight maneuver shows a bell-curve shape as showed in the following figure:

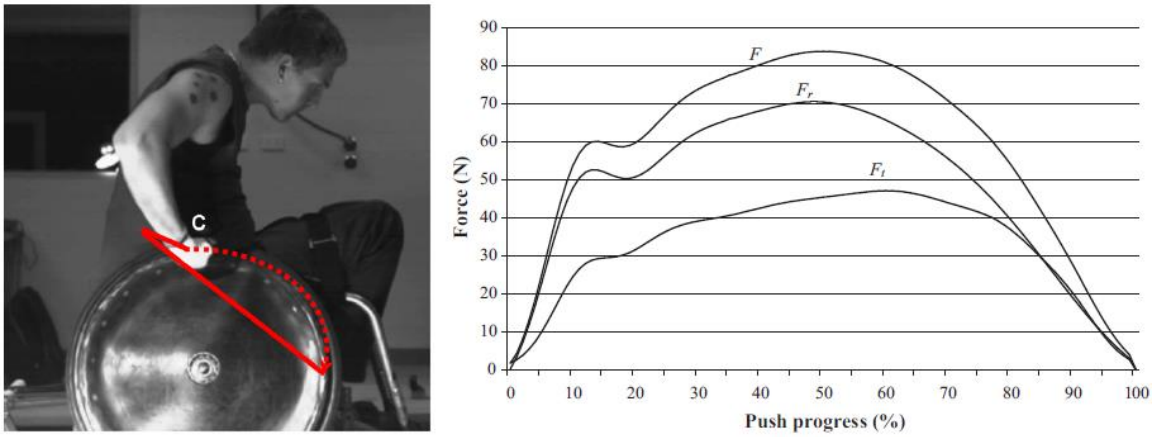

Figure 6.29 Individual pulsatile push applied by a human passenger on a manual wheelchair [24].

For the mathematical analysis the pulse's shape was assumed to be a parabola, which is the simplest function able to create a bell-type profile. Thus, pulsatile propulsion performed by the AMPS consists of a series of parabolic pulses of different amplitudes and frequencies, intercalated with periods of freewheeling.

Humans can vary both duration an amplitude of each pulse they apply, however, for the purposes of this study, the developed formulation requires to select a particular frequency of pushes and then the amplitude is calculated. Each pulse amplitude is

determined to achieve an approximate desired distance over a period of time, roughly maintaining a constant average velocity at the end of each cycle of pulse and freewheeling.

The determination of each pulse amplitude depends on the expected rolling resistance value at any given time. This work has explored the dependency of rolling resistance with velocity and acceleration and its general tendencies. However, it could not be expected that the calculated pulses would precisely achieve a near-constant velocity over a long straight path without any kind of feedback. The uniqueness of this propulsion strategy also required a unique kind of feedback system. Whatever correction on the input should be done in a way that does not interfere with the cycle of pulses and freewheeling, and that doesn't affect the frequency and parabolic shape of each individual pulse. The solution to this particular problem was to implement a correction signal with similar characteristics to the calculated set of pulses. Each pulse of the original correction signal has a unit amplitude. A gain K_p is calculated during the maneuver and multiplied times the correction signal to change its amplitude. It is later added to the original pre-calculated pulses to achieve the desired trajectory. K_p is calculated based on velocity error. The wheelchair is expected to maintain a certain average velocity. If the pulsatile propulsion is falling behind, the correction will increment the amplitude of the pulses. If it is going too fast, it will diminish them. Additionally, the AMPS keeps track of the orientation of the wheelchair at any given time. If the trajectory is moving to one side, the correction signal will increase the amplitude of the pulse on one side while reducing it on the other to correct the orientation

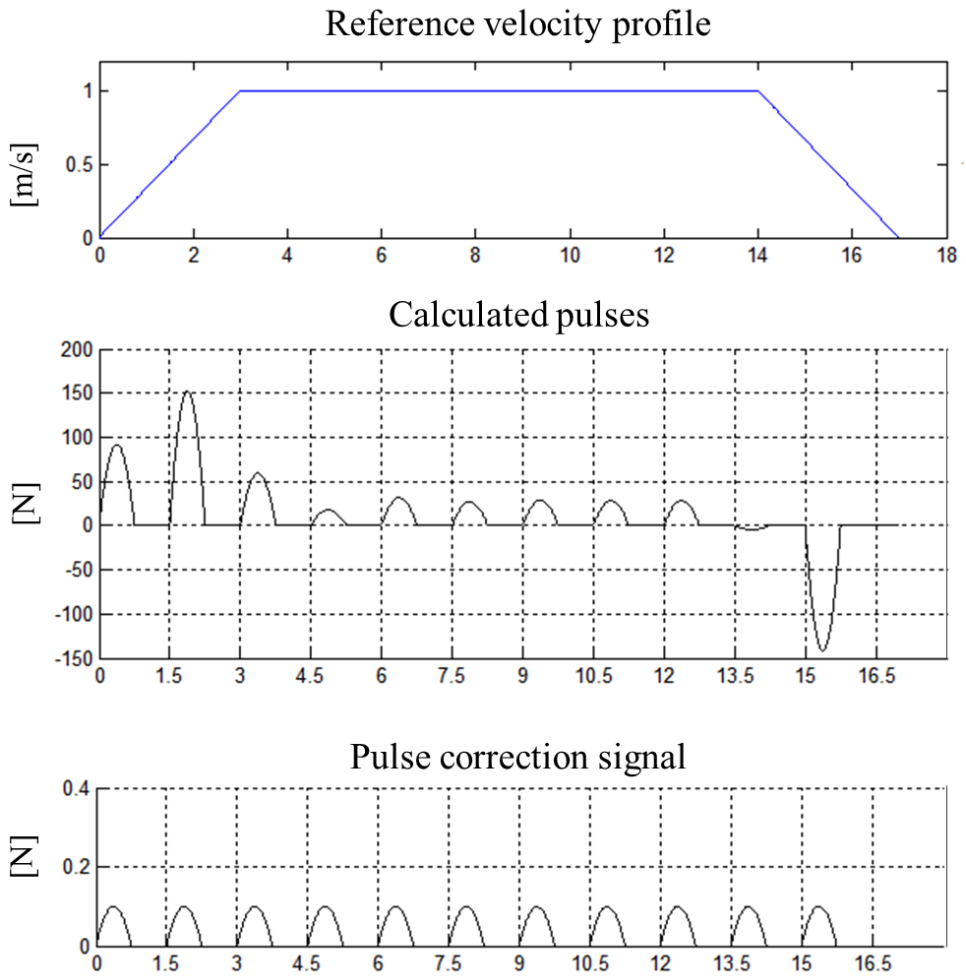

Figure 6.30 Pulsatile propulsion reference velocity profile, calculated pulses and correction feedback signal.

Experiments were performed with pulsatile propulsion to explore the changes in cost of transport at different frequencies of propulsion. One set was performed on the floor over a limited space available. The other set was performed on a dynamometer allowing for a longer duration of the tests.

6.4.3 Experiments performed on the floor

The following figures show trajectory, velocity, acceleration, motor current and energy input for a pulsatile propulsion experiment performed over the floor.

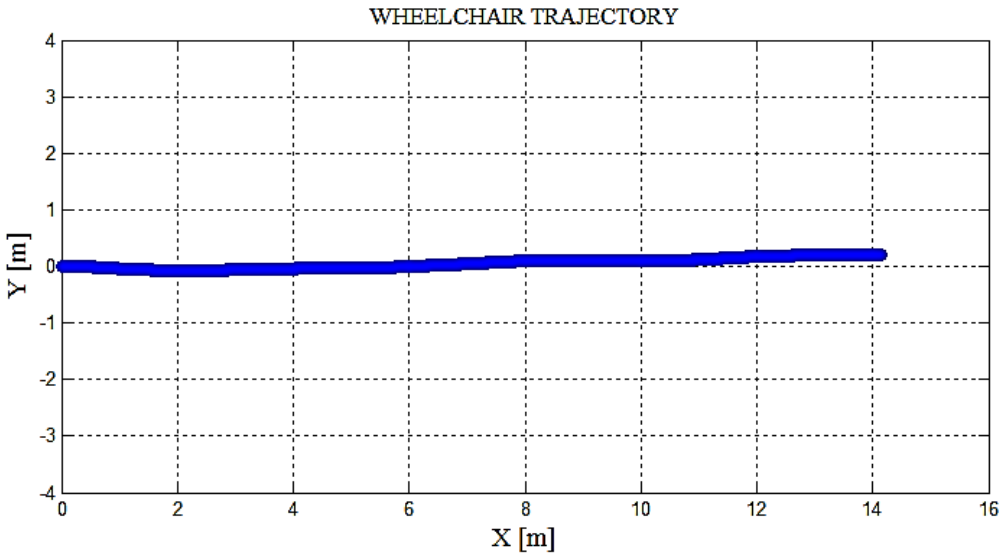

Figure 6.31 Pulsatile propulsion experiment resulting trajectory.

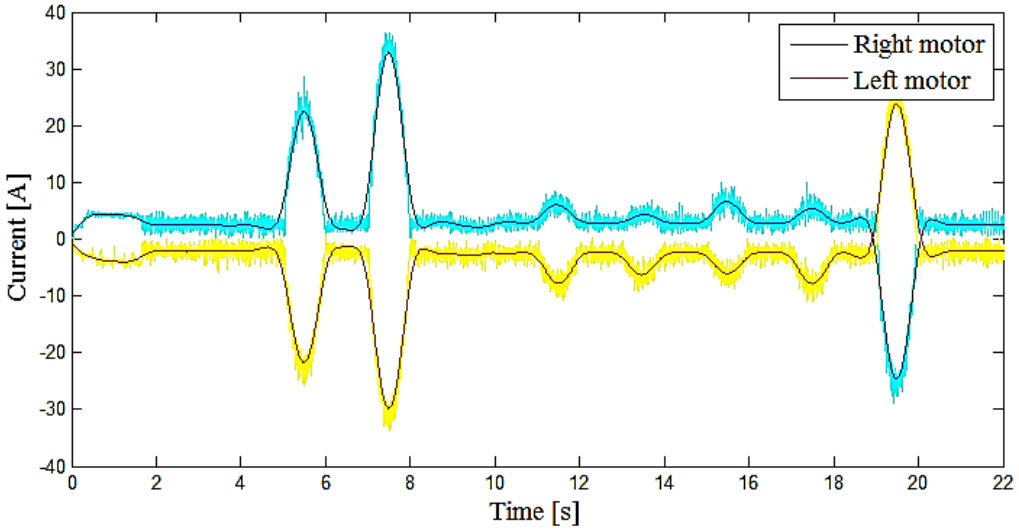

Figure 6.32 Pulsatile propulsion experiment recorded motor currents.

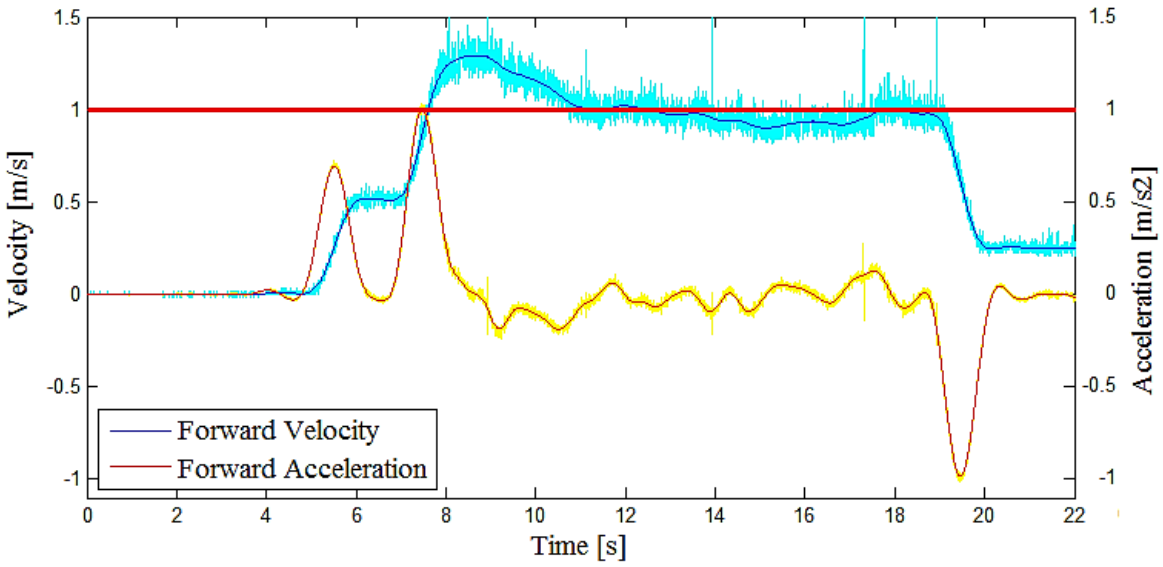

Figure 6.33 Velocity and acceleration in a pulsatile propulsion experiment.

(Red line indicates intended reference constant velocity.)

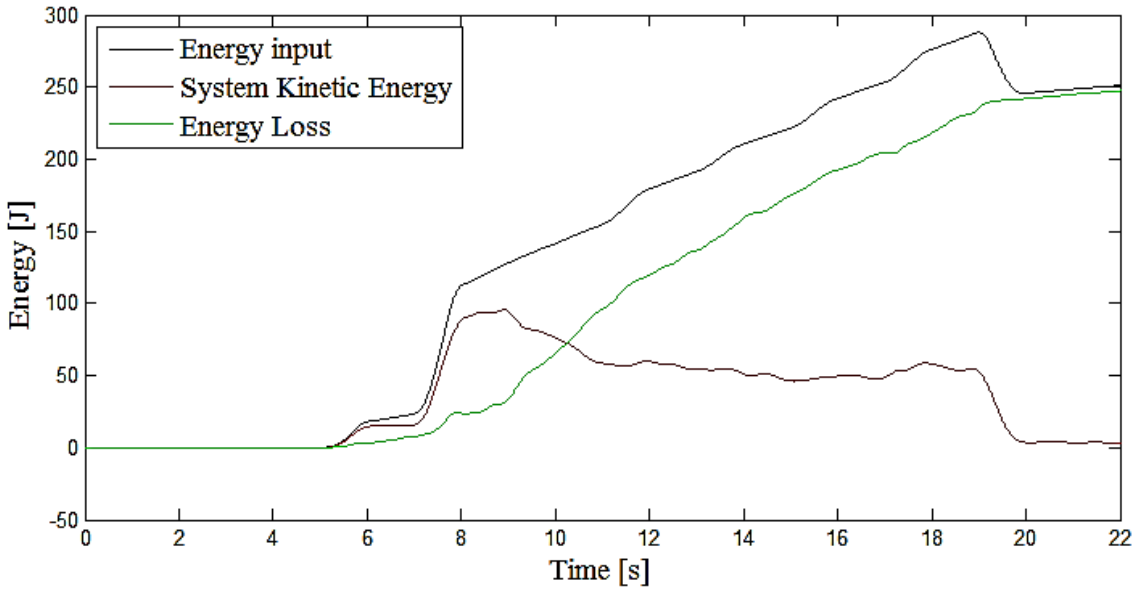

Figure 6.34 Energy input, output and loss in a pulsatile propulsion experiment.

It is observable on the figures that pulsatile propulsion is significantly different from the 'continuous' kind of push provided in previous experiments. It was of interest to determine if there is a significant difference in energy efficiency when comparing different frequencies of propulsion. Establishing the found COT for a continuous push as reference, the following table shows results for four different frequencies of propulsion. In addition, within each cycle the distribution of time between push and freewheeling can been varied. In this case 50% and 70% were chosen.

Table 6.1 COT for pulsatile propulsion at various frequencies

Freq [Hz]	cycle time [s]	Pulse duration [%]	mass [kg]	distance [m]	Energy spent [J]	COT [J/m]
1	Continuos propulsion		108.42	10.9	194.8	0.164
0.67	15	50	108.42	11.2	198.3	0.163
0.67	15	80	108.42	10.4	170.2	0.151
0.50	20	50	108.42	11.3	175.5	0.144
0.50	20	80	108.42	10.5	173.6	0.152
0.40	25	50	108.42	10.9	164.4	0.139
0.40	25	80	108.42	10.2	149.1	0.135
0.33	30	50	108.42	10.7	175.1	0.150
0.33	30	80	108.42	10.1	145.0	0.132

The same data is also presented in figure 6.35 along with trend lines for clarity. Data shows that the COT varies with frequency and could be significantly less than the continuous push case.

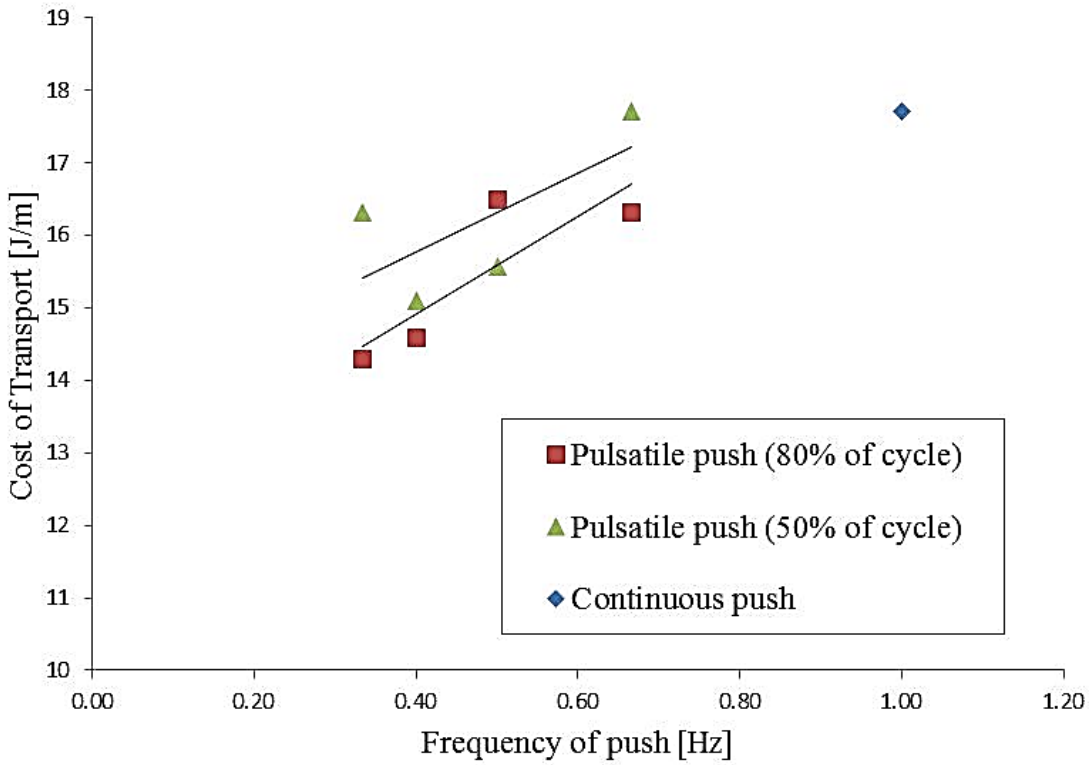

Figure 6.35 COT for pulsatile propulsion at various frequencies.

6.4.3 Experiments performed on the dynamometer

Performing experiments over a stationary dynamometer allowed to test the system for longer periods of time. This was convenient to better perceive differences among several frequencies of propulsion and freewheeling duration. However, there are some disadvantages of these tests. The dynamometer used had a single roller, restricting the propulsion to a single side, due to safety considerations on the electric motors. In addition, the dynamometer only generates rolling resistance on the rear wheels, excluding the casters, and does not produce the shifts in weight distribution that appear naturally with deceleration over the floor.

Regardless of these considerations, valuable information could be gathered from tests performed on a dynamometer. Figure 6.36 shows the AMPS setup on the single-roller dynamometer.

Figure 6.36 AMPS on a single-roller dynamometer.

Motor cancellation was again tested to ensure freewheeling on the dynamometer tests. Figure 6.37 show natural deceleration curves (blue) on the dynamometer with the motors disengaged and deceleration with motor cancellation (green). Some small modification of the no-load current (less than 10%) was necessary to match the natural deceleration on the dynamometer.

A series of tests were performed by changing the frequency of pulses and the proportion between pulse duration and freewheeling duration (duty cycle). Figure 6.38 show velocity and acceleration for one test. The periods of freewheeling are noticeable by the drop in velocity after each pulse.

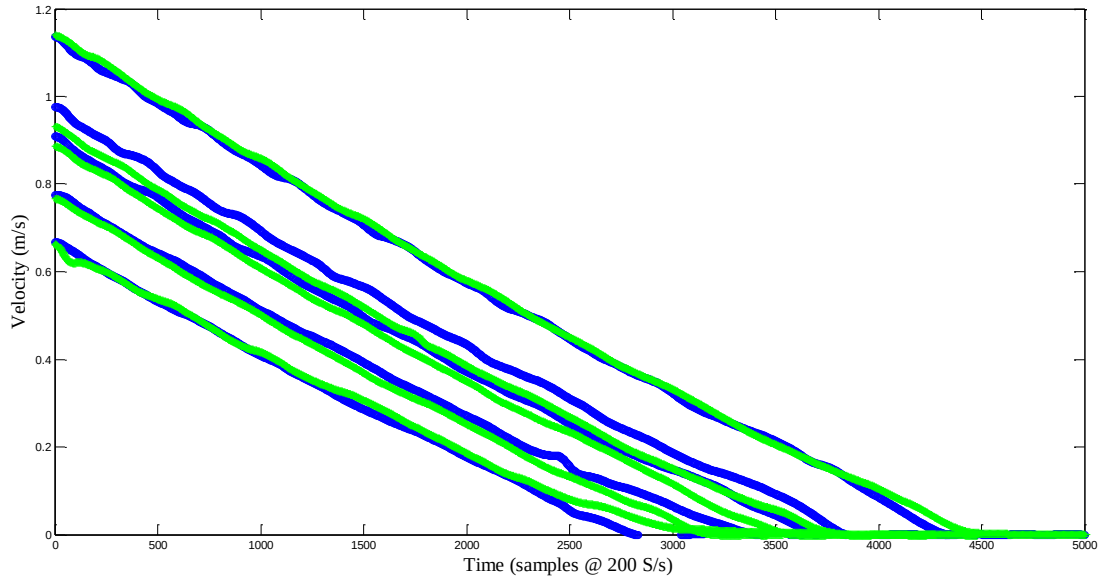

Figure 6.37 AMPS deceleration on a single-roller dynamometer.

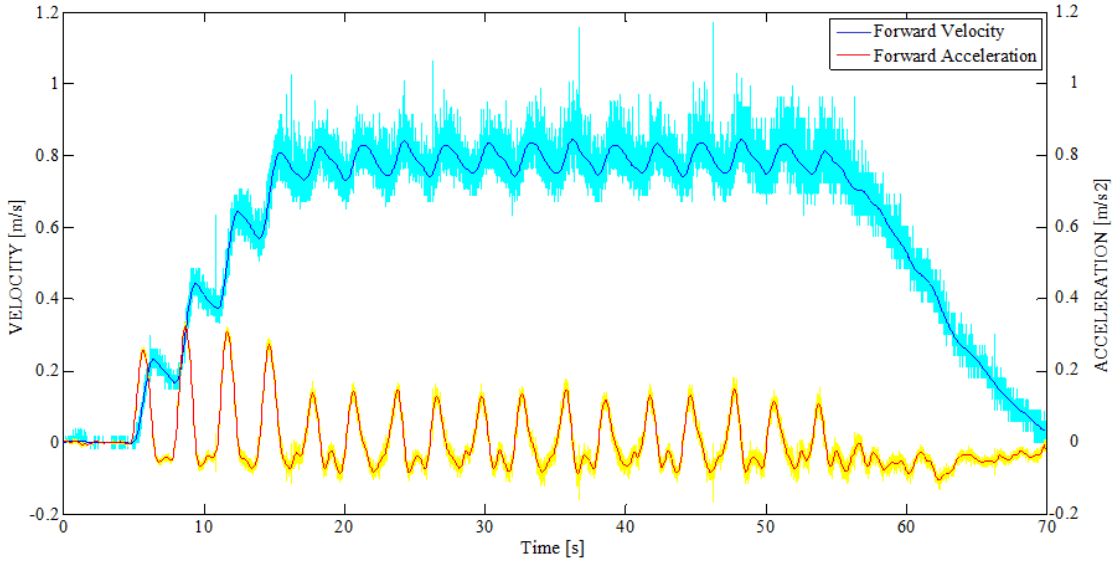

Figure 6.38 Velocity and acceleration for a pulsatile propulsion test on the dynamometer.

Energy analysis for the same test is shown in figure 6.39. The energy input remains unchanged when the system enter freewheeling mode since no push is applied, while the kinetic energy decreases due to resistive forces.

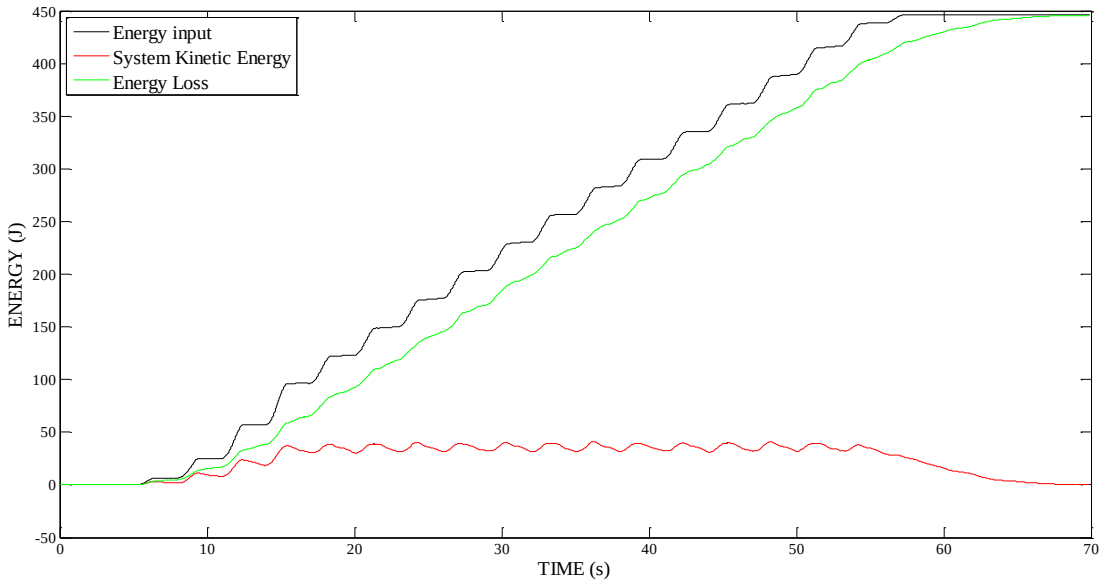

Figure 6.39 Energy analysis for a pulsatile propulsion test on the dynamometer.

Figure 6.40 show the current applied to the motor during the maneuver. Notice that the pulse amplitude remains nearly constant during the period of desired constant average velocity.

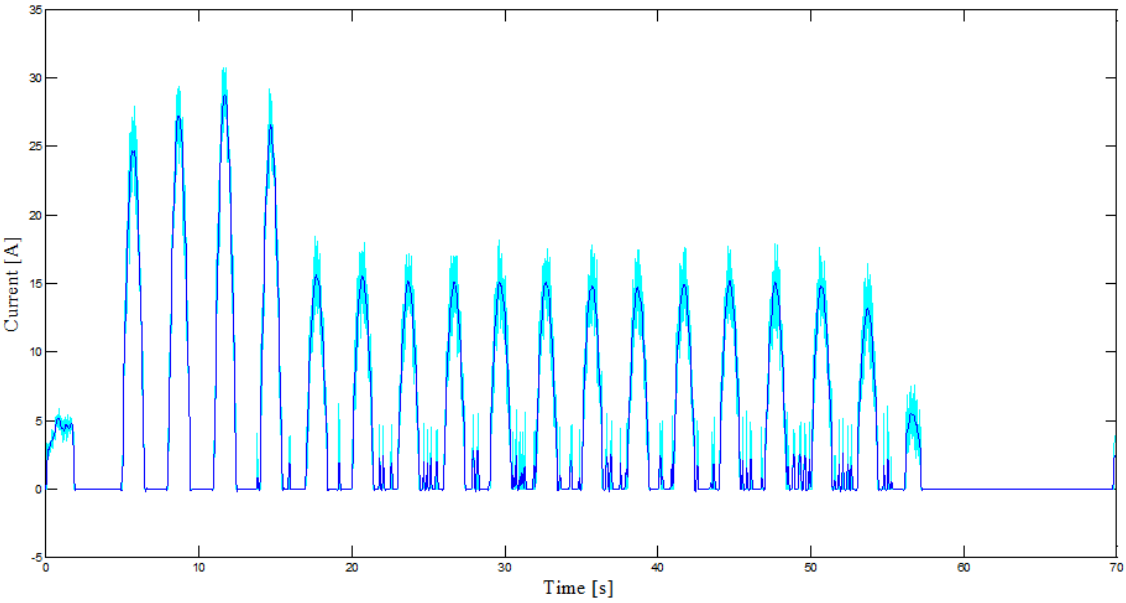

Figure 6.40 Motor current input for a pulsatile propulsion test on the dynamometer.

Having energy and velocity information allowed to calculate COT in the same way as previous sections. Table 6.2 shows COT for pulsatile propulsion at various frequencies and cycle durations. Different colors are used to group the trials in which the same pulse duration time was used. In each group the duration of freewheeling was changed. The calculated pulse amplitude was larger when freewheeling duration was longer, compensating for the greater periods of deceleration between pushes. As reference, the COT for a continuous push experiment was added at the end of the table.

Table 6.2 COT for pulsatile propulsion at various frequencies

half pulse (s)	pulse (s)	total cycle (s)	frequency (Hz)	Velocity (m/s)	mass (kg)	distance (m)	energy (J)	COT (J/Kgm)
0.75	1.5	3	0.33	0.791196	108.42	23.7427	266.888	0.104
0.75	1.5	4.5	0.22	0.809962	108.42	24.3043	233.413	0.089
0.625	1.25	2.5	0.40	0.791922	108.42	23.7637	260.87	0.101
0.625	1.25	3.75	0.27	0.808451	108.42	24.259	262.269	0.100
0.625	1.25	5	0.20	0.802982	108.42	24.096	240.06	0.092
0.5	1	2	0.50	0.786835	108.42	23.6112	259.034	0.101
0.5	1	3	0.33	0.806929	108.42	24.214	251.195	0.096
0.5	1	4	0.25	0.816678	108.42	24.5055	259.409	0.098
0.375	0.75	1.5	0.67	0.778115	108.42	23.3476	255.6	0.101
0.375	0.75	2.25	0.44	0.81026	108.42	24.3129	249.422	0.095
0.375	0.75	3	0.33	0.810648	108.42	24.3239	237.957	0.090
REF	REF	REF	1	0.795129	108.42	23.8594	325.175	0.126

Even though the data collected was limited, some tendencies in COT could be observed. Figure 6.41 suggests that COT tends to decrease as the freewheeling period increases, when the pulse duration time is kept constant. Figure 6.42 suggests that COT tends to increase as the pulse duration increases, when the total cycle time is kept constant. This partial results show that some interesting observations could be obtained when using this controller along with the AMPS.

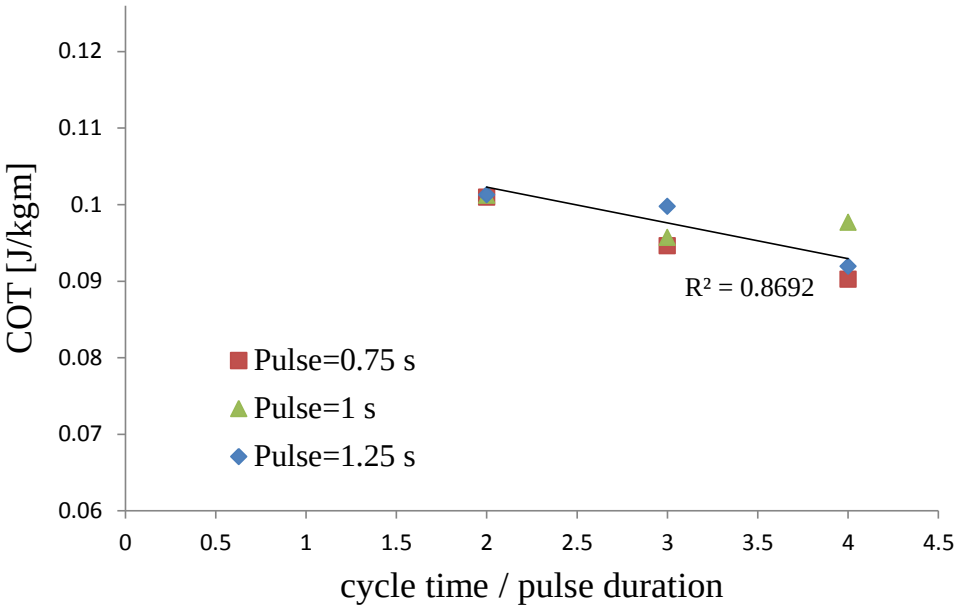

Figure 6.41 COT decreases as the freewheeling period increases.

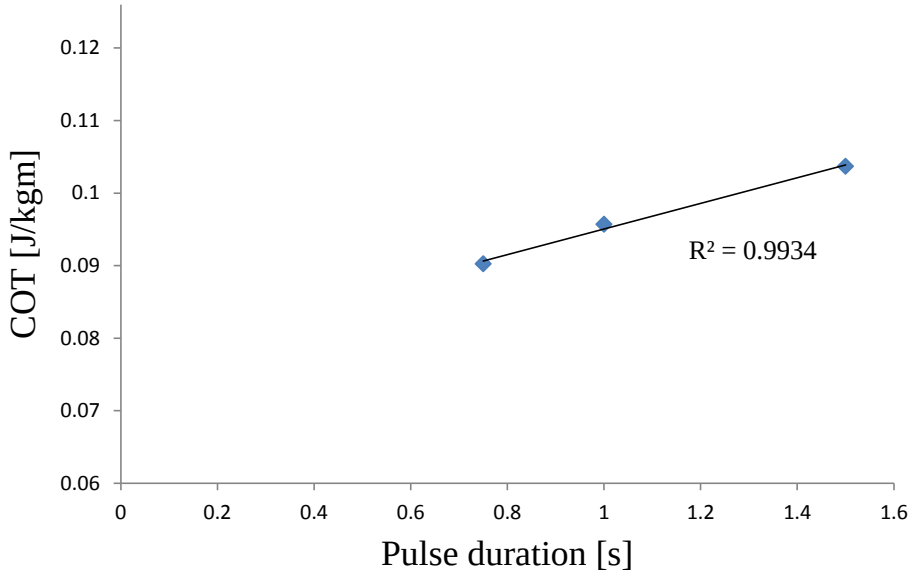

Figure 6.42 COT increases as the pulse duration increases.

CHAPTER 7

CONCLUSIONS AND FUTURE WORK

7.1 Conclusions

- The controller developed for the AMPS is capable of performing the maneuvers needed to complete this experimental work. It successfully accomplished straight trajectories, circles and a general curvilinear trajectory (slalom). This means that the AMPS is capable of performing virtually any trajectory needed wheelchair testing.
- The kinematic and dynamic analysis were fundamental to perform the feed-forward section of the controller and track the vehicle trajectory in real time. Since the AMPS' controller is model-based, any further improvement of the model could potentially translate into a more accurate control.
- The especial pulsatile controller included two challenges that are unique to the AMPS implementation. Obtaining a natural deceleration effect (freewheeling) with the motors engaged to the handrims proved to be a reasonable alternative to the use of mechanical clutches. The formulation for calculating pulses to create a straight trajectory is completely original as far as the author is concerned. The implementation of this controller opens the door to new types of testing based on different propulsion cycle frequencies and pulse duration.
- Rolling resistance was successfully measured with a new approach that appears to be more convenient than previous methodologies. The flexibility of the AMPS to control velocity, acceleration and trajectory allows us to perform a broad spectrum of experiments to understand better the effects of rolling resistance in manual wheelchairs. The experiments confirmed previous results of rolling resistance

increasing with velocity. They also showed that rolling resistance varies during acceleration, an original contribution of this work that increases our understanding of this resistive force.

- Consistently with rolling resistance experiments results, energy efficiency measured in the form of cost of transport decreases as wheelchair velocity increases.
- Using the AMPS for measuring turning resistance as a function of the trajectory's radius of curvature is a significant advance made by this considering the lack of publications concerning this topic. Since curvilinear trajectories are common in the everyday life of wheelchair users, having a better understanding of the forces affecting those maneuvers could help improve wheelchair design.
- Measuring different metrics of wheelchair mechanical efficiency could become a new standard for comparing performance among different wheelchair models and component configurations. Manufactures and consumers need objective ways to discern which products better fit their needs. The information produced with the AMPS about a specific wheelchair performance constitutes objective data that can be used for comparison. The lack of human variability involved during testing increase the dependability of the information gathered.

7.2 Future Work

- Use the gathered information about rolling and turning resistance to improve the mathematical wheelchair model in which the feed-forward controller is based. This should reduce the amount of controller effort necessary to perform general curvilinear trajectories.
- A set of primitive maneuvers of interest could be selected as a standard for comparison among wheelchair. Studying efficiency during these maneuvers would

provide useful information to the final user about wheelchair performance in daily manual wheelchair use.

- Pulsatile propulsion could be used for comparing the COT of a moving wheelchair over different surfaces. Diverse selection of propulsion frequencies and pulse duration could be explored to find the most efficient approach to propelling a wheelchair. These results could be later compared against human test-driven tests and search for consistency or correlation.
- The AMPS could be used to test the influence of floor side-slope in the effort required to drive a wheelchair.
- Additional instrumentation added to the AMPS could help further study the shift of weight distribution during the different maneuvers. Angular sensors attached to the caster wheels would greatly improve the study of wheelchair dynamics in general curvilinear maneuvers.
- Pulsatile propulsion control could be improved by implementing mathematical iteration in the pulses amplitude calculation. Obtaining controlled curvilinear trajectories with pulsatile propulsion constitutes a challenging problem since the number of variables increases significantly with respect to the straight trajectory case. However, achieving such a controller would help obtain results more closely related to the human everyday use of manual wheelchairs.

APPENDIX A

WHEELCHAIR FORWARD KINEMATIC ANALYSIS

In this appendix the kinematic analysis for a manual wheelchair is described. Figure A.1 shows a general kinematic description of a wheelchair following a general curvilinear trajectory with instantaneous center of rotation C.

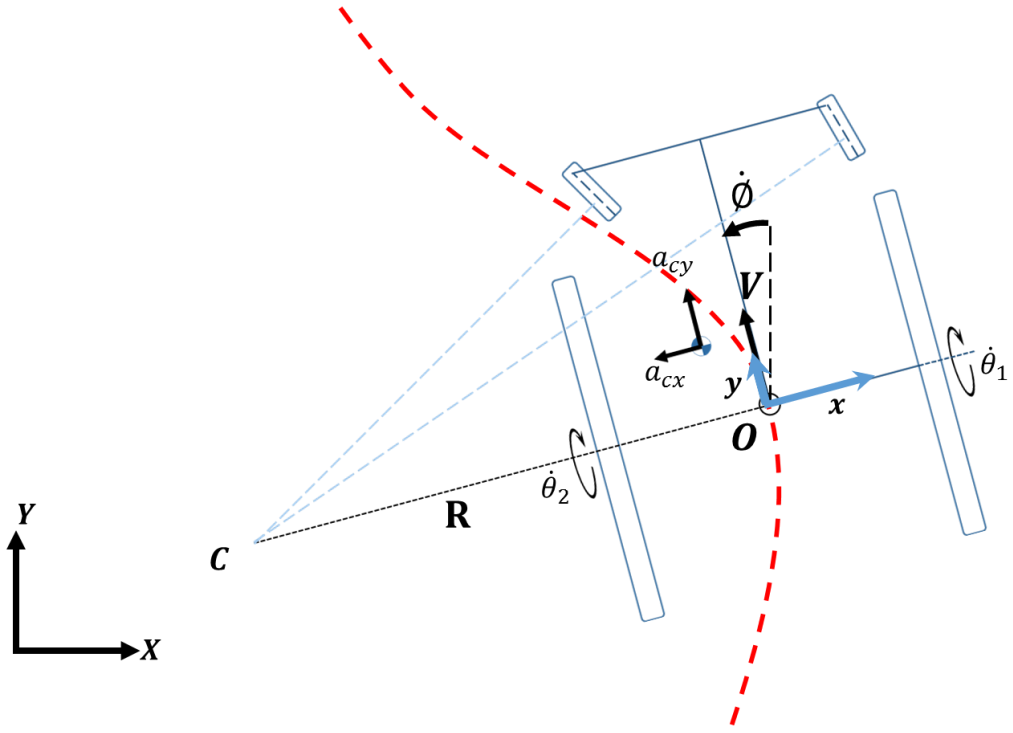

Figure A.1 Kinematic model of wheelchair following a curvilinear trajectory.

In figure A.1 there are two sets of coordinate frames. The xy coordinate frame is fixed to the wheelchair's rear wheel axis center and changes its orientation as the wheelchair turns. The XY coordinate frame is fixed to the ground and is the global reference frame for the wheelchairs absolute position and velocity.

The objective of forward kinematics is to describe the motion of the wheelchair based on the actions of the rear wheels. These wheels are the ones pushed by the passenger and their motion can be directly recorded from encoders located on their axis.

The analysis starts with an individual wheel rolling on the ground, as shown in figure A.2.

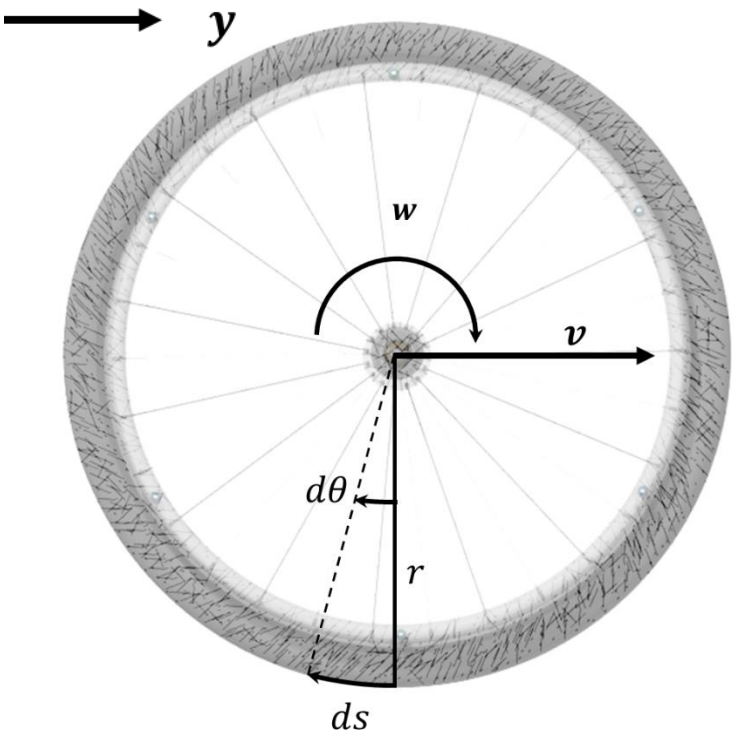

Figure A.2 Kinematic description of a rotating wheel (lateral view).

For a wheel moving forwards with linear velocity v the following equations can be stablished:

$$ds = r\, d\theta \tag{A.1}$$

Where ds is the linear displacement of the wheel produced by and angular displacement $d\theta$. Differentiating with respect to time we obtain

$$\frac{ds}{dt} = r\,\frac{d\theta}{dt} \tag{A.2}$$

$$\frac{d^2s}{dt^2} = r\,\frac{d^2\theta}{dt^2} \tag{A.3}$$

Which are equivalent to the more familiar expressions

$$v = r\,\dot{\theta} \tag{A.4}$$

$$a = r\,\ddot{\theta} \tag{A.5}$$

Now let us consider a top view of the wheelchair. The displacement of the two rear wheels can be related to the displacement of the center of the rear axis as shown in figure A.3.

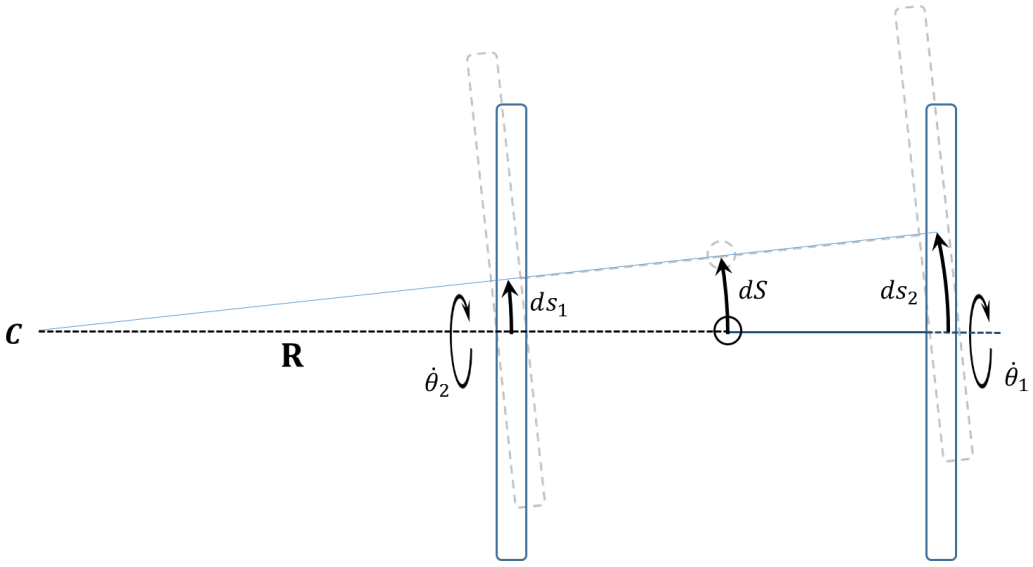

Figure A.3 Infinitesimal displacement of the wheelchair (top view).

The following relation can be stablished directly from the geometry shown of the previous figure.

$$dS = \frac{(ds_1 + ds_2)}{2} \tag{A.6}$$

Differentiating equation A.6 with respect to time we obtain

$$\dot{y} = V = \frac{(v_1 + v_2)}{2} \tag{A.7}$$

Or equivalently by using equation A.4 we obtain

$$\dot{y} = V = \frac{1}{2} r_R(\dot{\theta}_1 + \dot{\theta}_2) \tag{A.8}$$

Differentiating with respect to time once again we obtain

$$\ddot{y} = a_y = \frac{1}{2} r_R(\ddot{\theta}_1 + \ddot{\theta}_2) \tag{A.9}$$

Equation A.6, A.8 and A.9 calculates the linear displacement, velocity and acceleration of the wheelchair starting from the angular displacement, velocity and acceleration of the rear wheels.

Figure A.4 shows instantaneous linear velocities of three points along the rear wheel axis of a wheelchair following a curvilinear trajectory with instantaneous center of rotation C.

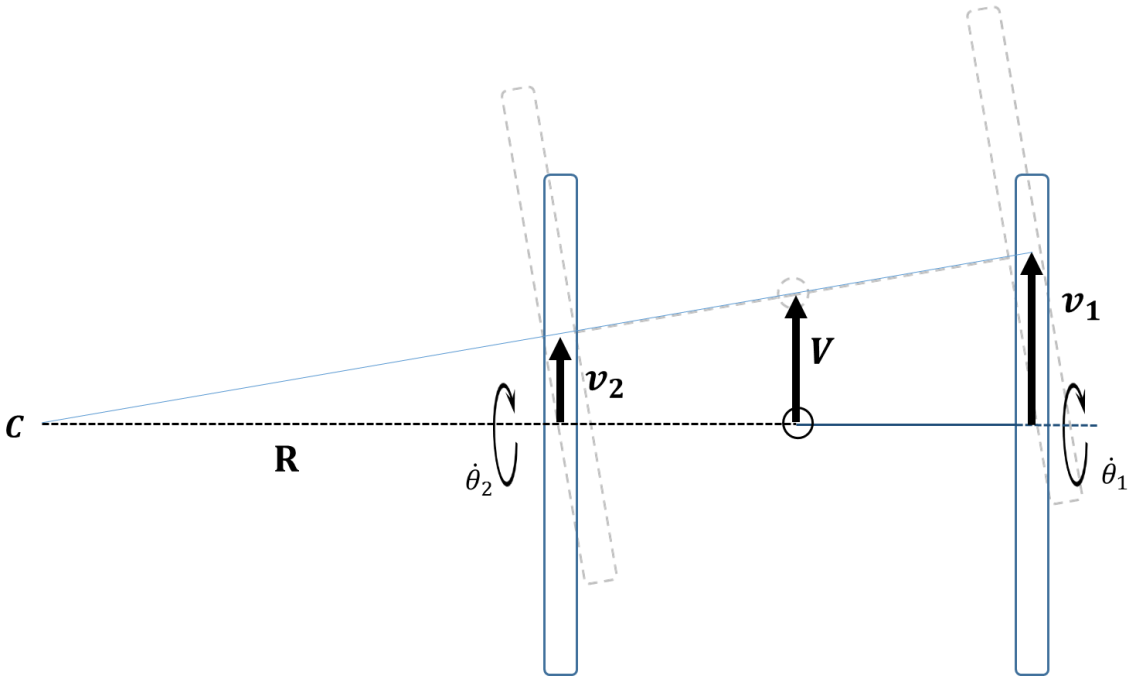

Figure A.4 Linear velocities of wheels and center of rear axis (top view).

Next, we consider the change of orientation of the wheelchair along the trajectory with respect to the ground-fixed XY coordinate frame. Figure A.5 shows the angle of rotation $\emptyset$ of the wheelchair during a turn. This angle is formed between the body-fixed y axis and the ground-fixed Yaxis and determines the absolute orientation of the wheelchair throughout the trajectory.

It can be seen that

$$\emptyset = \frac{dS}{R} = \frac{(ds_1 - ds_2)}{d_R} \tag{A.10}$$

$$R = \frac{dS}{\emptyset} \tag{A.11}$$

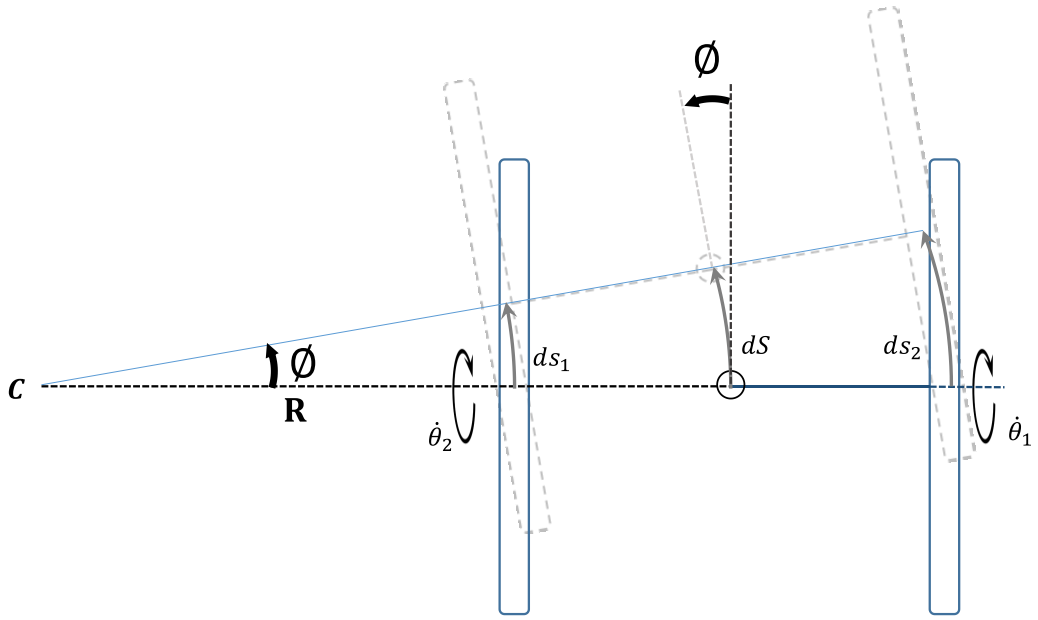

Figure A.5 Wheelchair change of orientation during a left turn (top view).

By differentiating equation A.9 with respect to time we find the following expressions:

$$\dot{\phi} = \frac{(ds_1/dt - ds_2/dt)}{d_R} \tag{A.12}$$

$$\dot{\phi} = \frac{(v_1 - v_2)}{d_R} \tag{A.13}$$

$$\dot{\phi} = \frac{(\dot{\theta}_1 - \dot{\theta}_2)}{d_R} r_R \tag{A.14}$$

$$\ddot{\phi} = \frac{(\ddot{\theta}_1 - \ddot{\theta}_2)}{d_R} r_R \tag{A.15}$$

Equations A.9, A.13 and A.14 describe the orientation angular displacement, velocity and acceleration of the wheelchair during a maneuver, starting from the rear wheels' angular displacement, velocity and acceleration respectively.

Additional useful expressions regarding the instantaneous radius of curvature can be found from figure A.5.

$$R = \frac{dS/dt}{\emptyset/dt} = \frac{V}{\dot{\emptyset}} \tag{A.16}$$

$$\dot{\emptyset} = \frac{V}{R} \tag{A.17}$$

For the dynamic analysis it is necessary to calculate the accelerations of the center of mass (COM) for use in the dynamic analysis. Figure A.6 shows the location of the COM and its acceleration components in the xy frame.

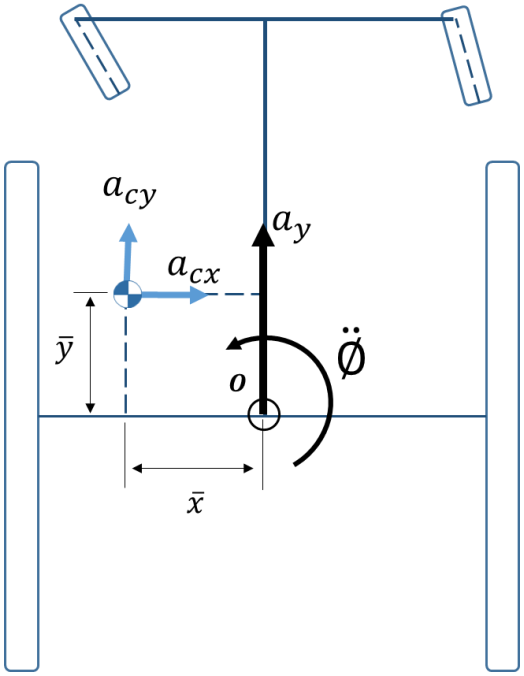

Figure A.6 Wheelchair center of mass (COM) acceleration components.

The acceleration of the COM is described by the following equations.

$$a_{cx} = -\bar{y}\,\ddot{\emptyset} \tag{A.18}$$

$$a_{cx} = -\bar{y}\,\frac{r_R}{d_R}\,(\ddot{\theta}_1 - \ddot{\theta}_2) \tag{A.19}$$

$$a_{cy} = a_y - \bar{x}\,\ddot{\emptyset} \tag{A.20}$$

$$a_{cy} = \frac{r_R}{2}\left(1 - \frac{2\bar{x}}{d_R}\right)\ddot{\theta}_1 + \frac{r_R}{2}\left(1 + \frac{2\bar{x}}{d_R}\right)\ddot{\theta}_2 \tag{A.21}$$

Finally, we are interested in expressions that calculate the absolute position and velocities of the wheelchair rear axis center from the ground-fixed XY reference frame. Velocities are calculated by

$$\dot{Y} = \dot{y}\,\cos\emptyset = V\,\cos\emptyset \tag{A.22}$$

$$\dot{X} = \dot{x}\,\sin\emptyset = V\,\sin\emptyset \tag{A.23}$$

For calculating the absolute position on the ground-fixed XY reference frame let's consider a small advance of the wheelchair.

$$\Delta Y = \Delta S\,\cos\emptyset \tag{A.24}$$

$$\Delta Y = \frac{1}{2} r_R(\Delta\theta_1 + \Delta\theta_2)\,\cos\left(\frac{r_R}{d_R}(\Delta\theta_1 - \Delta\theta_2)\right) \tag{A.25}$$

The absolute position of the wheelchair with respect to the ground-fixed XY reference frame after n small advances is

$$Y_n = \sum_{i=1}^{n} \Delta Y_i = \sum_{i=1}^{n} \frac{1}{2} r_R (\Delta\theta_{1i} + \Delta\theta_{2i}) \cos\left(\frac{r_R}{d_R}(\Delta\theta_{1i} - \Delta\theta_{2i})\right) \quad \text{(A.26)}$$

$$X_n = \sum_{i=1}^{n} \Delta X_i = \sum_{i=1}^{n} \frac{1}{2} r_R (\Delta\theta_{1i} + \Delta\theta_{2i}) \sin\left(\frac{r_R}{d_R}(\Delta\theta_{1i} - \Delta\theta_{2i})\right) \quad \text{(A.27)}$$

APPENDIX B

WHEELCHAIR INVERSE KINEMATIC ANALYSIS

The process of inverse kinematics starts by defining the trajectory the wheelchair should perform. Even though the curve can be defined analitically by a parametric function, this demonstration assumes that such function is unknown, so only the points of the curve are known. Figure B.1 shows the desired trajectory S of a wheelchair with starting and ending points.

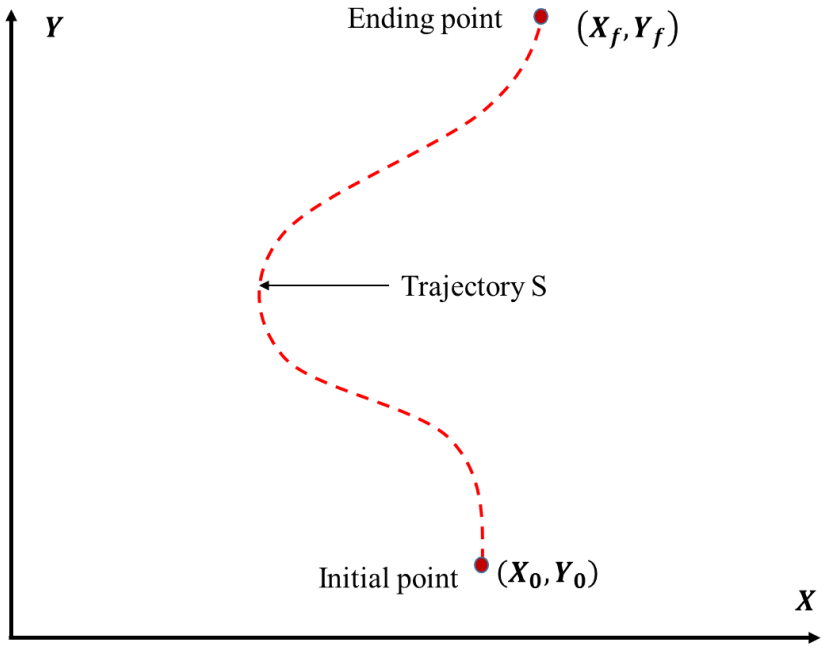

Figure B.1 Wheelchair trajectory for the inverse kinematic analysis.

Also, the desired forward velocity profile needs to be defined. (Otherwise, there would be an infinite amount of solutions on how to achieve the proposed path.) In this case a simple velocity profile was selected and shown in figure B.2.

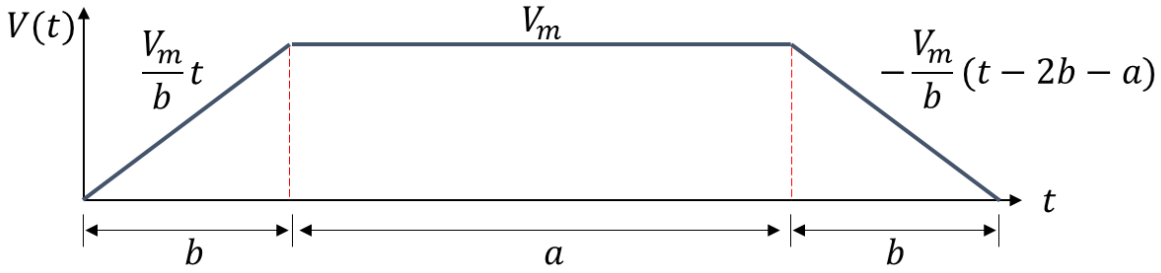

Figure B.2 Desired wheelchair velocity profile for the inverse kinematic analysis.

This velocity profile consists in a constant acceleration phase, followed by a period travelling at constant velocity V_m and ending with a constant deceleration phase. This profile has one degree of freedom, variable a, to be determined further in the process. All the other variables are previously selected. At this stage the total length of the trajectory is still unknown and thus the complete velocity profile cannot be fully defined.

The next step is analyzing the curve to obtain the total length of the trajectory and the wheelchair orientation at any point. Figure B.3 shows an infinitesimal section of the trajectory.

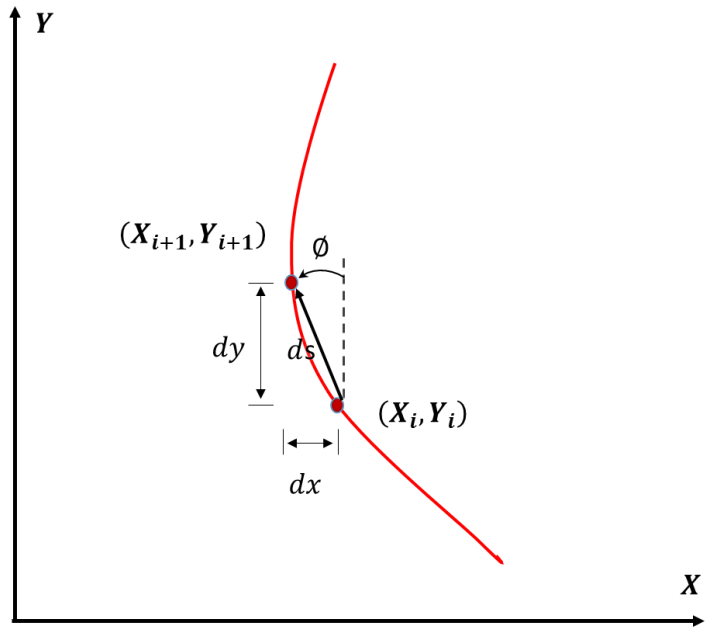

Figure B.3 Infinitesimal section of the trajectory with displacements.

Simple geometric relations from figure B.3 allow us to find the displacement ds between points and the wheelchair orientation $\emptyset$ at each point:

$$ds = \sqrt{(\Delta x)^2 + (\Delta y)^2} \tag{B.1}$$

$$\emptyset = \tan^{-1}\frac{\Delta x}{\Delta y} \tag{B.2}$$

This equations allows to create a mapping between each point (X_i, Y_i) of the curve and a value of $\emptyset_i$ and ds_i. Now, the total length of the curve can be calculated as

$$L = \sum_{i=1}^{n} ds_i = \sum_{i=1}^{n} \sqrt{(\Delta x_i)^2 + (\Delta y_i)^2} \tag{B.3}$$

The precision of this calculation depends on how small is each division of the curve. With the total length of the trajectory known, the velocity profile can be fully defined by finding the parameter a. The integral of the velocity is equal to the length of the curve.

$$L = \int_0^{a+2b} V(t) \tag{B.4}$$

$$L = \int_0^b \frac{V_m}{b} t \, dt + \int_b^{a+b} V_m \; - \; \int_{a+b}^{a+2b} \frac{V_m}{b}(t - 2b - a) \, dt \tag{B.5}$$

$$L = (a + b)V_m \tag{B.6}$$

$$a = \frac{L}{V_m} - b \tag{B.7}$$

Integrating the velocity profile results in a function of time for the displacement along the curve as shown in figure B.4. This means that for every time t_i we can find on which point S_i along the trajectory is the wheelchair located.

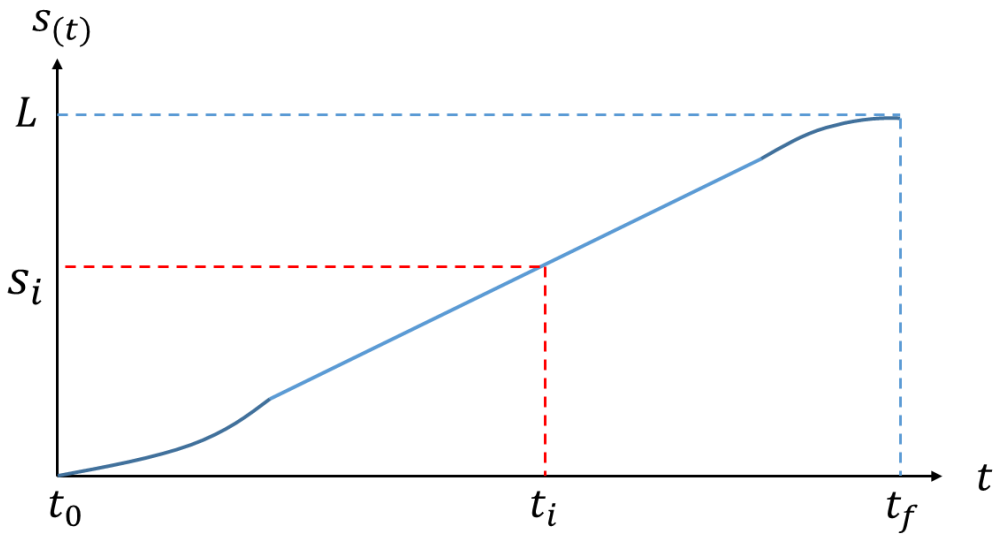

Figure B.4 Wheelchair forward displacement as function of time.

As stated previously, a mapping exists between displacement S_i and wheelchair orientation $\emptyset_i$. This means that for any time t_i we can now determine the linear velocity $V(t)$ and the and the wheelchair orientation $\emptyset(t)$.

The wheelchair orientation angular velocity could be further obtained by considering small changes in orientation and time.

$$\dot{\emptyset} = \frac{\Delta\emptyset}{\Delta t} \tag{B.8}$$

This way we have enough information to determine the rear wheels angular velocity as a function of time.

$$\theta_1 = \frac{V}{r_R} + \frac{\dot{\phi}\, d_R}{2r_R} \tag{B.9}$$

$$\theta_2 = \frac{V}{r_R} - \frac{\dot{\phi}\, d_R}{2r_R} \tag{B.10}$$

Finally, for use in the dynamic analysis, equations B.9 and B.10 can be further differentiated to obtain accelerations.

$$\ddot{\theta}_1 = \frac{a_y}{r_R} + \frac{\ddot{\phi}\, d_R}{2r_R} \tag{B.11}$$

$$\ddot{\theta}_2 = \frac{a_y}{r_R} - \frac{\ddot{\phi}\, d_R}{2r_R} \tag{B.12}$$

APPENDIX C

PULSATILE PROPULSION FORMULATION

In this appendix a formulation for defining a pulsatile propulsion with the AMPS is developed. It is worth noting that this analysis is limited to the straight trajectory motion. The result presented is an approximation that has proven succesful so far. Recommendations about improvements to this method are stated at the end.

The methodology for creating a pulsatile propulsion with the AMPS starts with some esential information regarding the motion we want to obtain.

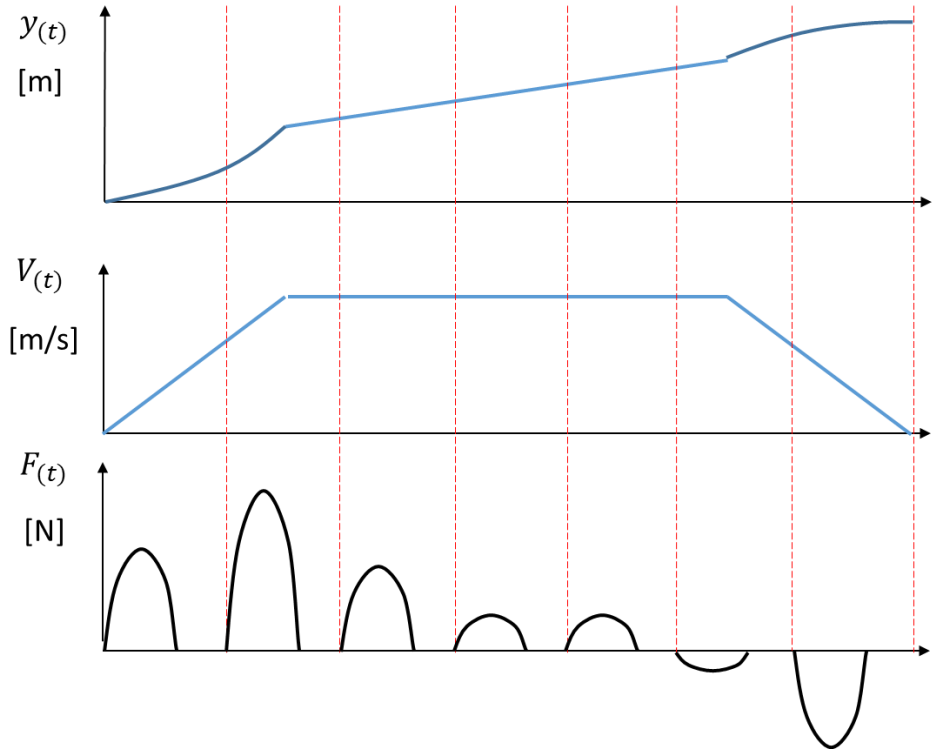

Figure C.1 Pulsatile propulsion analysis initial information.

Figure C.1 shows a series of pulses we want to create to obtain a straight trajectory. Each pulse is separated by a period of freewheeling, creating a cycle of propulsion that is

repeated throughout the maneuver. The method requires to have a reference of velocity as a function of time. This approximate description of the final motion gives us vital information for calculating the pulses' amplitude. Note that the frequency of cycles as well as the duration of the pulses can be determined freely.

Isolating one cycle of pulse and freewheeling allows us begin the analysis.

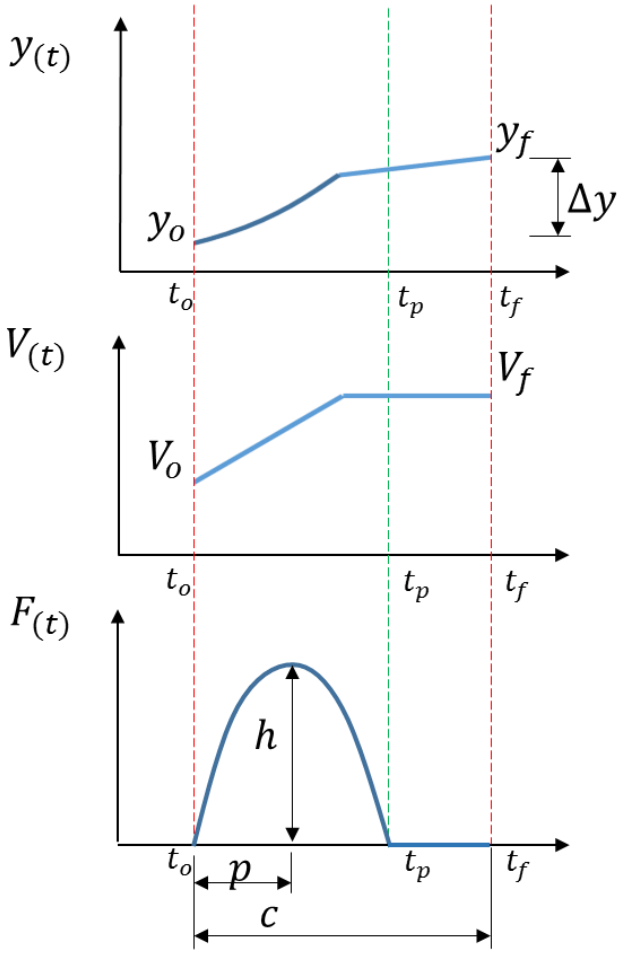

Figure C.2 Individual pulse description and reference information.

The pulse was modeled as an inverted parabola for two reasons: it resembles the bell-shaped push created by a human, and is the simplest function we can select to complete the mathematical analysis. The duration of the whole cycle (pulse + freewheeling) is determined by the variable c, while the duration of the pulse is determined by p. Notice

that the pulse will not create the same position and velocity curves as the ones provided initially. They have been established as a useful reference that helps us determine the final outcome of the new pulsatile propulsion maneuver.

From the dynamic analysis of a wheelchair travelling on a straight path we have:

$$a_y(t) = \frac{1}{m}(F_{(t)} - F_{roll(t)}) \tag{C.1}$$

We can determine the position and velocity of the wheelchair by integrating.

$$V_{(t)} = \int_{t_o}^{t_f} a_y(t)dt \tag{C.2}$$

Since the pulse function $F_{(t)}$ has two sections, $a_y(t)$ has different definitions for the intervals (t_o, t_p) and (t_p, t_f). The integration of this two-part function introduces a total of two integration constants. Two initial conditions (initial and final velocity) taken from the reference profiles permits us to fully define the new functions.

An important simplification on this analysis is assuming the value of the rolling resistance force $F_{roll(t)}$ as approximately constant during the pulse duration. This assumption helps the equations become simpler.

The pulse function $F_{(t)}$ has a parabola shape as stated before. The equation for this parabola is:

$$F_{(t)} = -\frac{h}{p^2}(t-p)^2 + h \tag{C.3}$$

The function $F_{(t)}$ is zero for initial time $t_o = 0$ and for the end of the pulse at $t_p = 2p$. For the rest of the period $F_{(t)} = 0$. Now we can introduce $F_{(t)}$ in the acceleration equation and proceed with the calculations.

For the time period $(t_o, t_p) = (0,2p)$

$$a_y(t) = \frac{1}{m}\left(-\frac{h}{p^2}(t-p)^2 + h - F_{roll}\right) \tag{C.4}$$

$$V_{1(t)} = \int a_y(t)dt = \int \frac{1}{m}\left(-\frac{h}{p^2}(t-p)^2 + h - F_{roll}\right)dt \tag{C.5}$$

This results in the following

$$V_{1(t)} = \frac{1}{m}\left(-\frac{h}{3p^2}(t-p)^3 + (h - F_{roll})t + k_1\right) \tag{C.6}$$

With initial conditions $v_{(0)} = V_o$ the integration constant k_1 can be determined.

$$k_1 = mV_o - \frac{hp}{3} \tag{C.7}$$

Next, for the time period $(t_p, t_f) = (2p, c)$

$$a_y(t) = \frac{-F_{roll}}{m} \tag{C.8}$$

$$V_{2(t)} = \int a_y(t)dt = \int \frac{-F_{roll}}{m} dt \tag{C.9}$$

This results in the following expression

$$V_{2(t)} = \frac{1}{m}(-F_{roll}t + k_2) \tag{C.10}$$

With initial condition $V_{(c)} = V_f$ the integration constant k_2 can be determined.

$$k_2 = mV_f + cF_{roll} \tag{C.11}$$

Finally, to find the amplitude of the pulse h we apply the condition of continuity of the velocity function.

$$V_{1(2p)} = V_{2(2p)} \tag{C.12}$$

From here we can calculate the amplitude of the impulse necessary to travel such distance.

$$h = \frac{3m}{4p}\left(V_f - V_o + \frac{cF_{roll(t)}}{m}\right) \tag{C.13}$$

With this analysis, each impulse of the maneuver can be determined to achieve an approximate velocity profile. Notice that some error was introduced when assuming rolling

resistance as a constant throughout the propulsion cycle. To compensate for this error, the AMPS controller uses a special feedback that corrects each pulse amplitude based on the difference between expected and real average velocity. Section 6.3.3 explains how a unit-amplitude input signal is used to modify the original pulse calculation.

One way to improve the accuracy of this method is by having a more detailed mapping of rolling resistance as a function of velocity and acceleration. Such function can be obtained by performing several experiments like the ones described at the beginning chapter 6. However, this increases the calculation complexity. Velocity and acceleration would have to be known to accurately introduce the values of rolling resistance at each time, which cannot be determined exactly until the input force has been calculated. A way to overcome this issue would be to use the reference velocity profile to estimate rolling resistance and calculate a force input. Later, the actual velocity produced by this force would be used again to recalculate a more appropriate assumption of rolling resistance. Repeating the process many times would constitute an iterative method with possibly better results.

APPENDIX D

ROLLING RESISTANCE AND TURNING RESISTANCE

Two resistive forces affecting wheelchairs are explored in the present thesis work: rolling resistance and turning resistance. Rolling resistance occurs due to the deformation of the ground and tire as a wheel is rolling, resisting its advance. Turning resistance occurs due to the sliding friction between tire and floor as the wheel rotates vertically when the wheelchair makes a turn. This appendix describes basic knowledge regarding rolling and turning resistance as an introduction to the experiments performed on chapter 6.

D.1 Rolling resistance fundamentals

Rolling resistance is a resistive force acting against the motion of a rolling wheel due to materials inelastic characteristics. It is described, in physical terms, as a hysteretic energy loss that occurs as the elastic materials of a tire and ground deform in the wheel-floor interface during rotation [25-26].

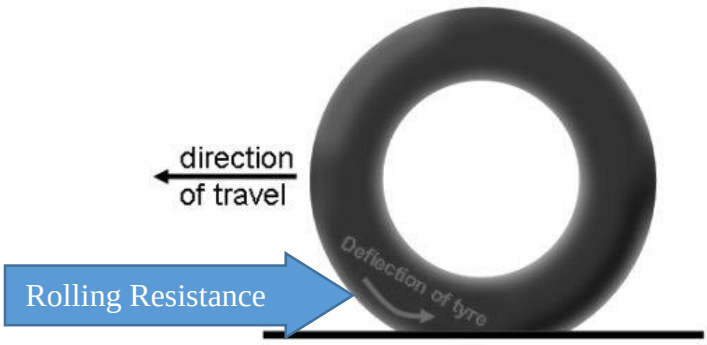

Figure D.1 Rolling resistance force on a deforming tire.

This natural phenomenon affects any vehicle using wheels and determines how much ‘push’ it is necessary to keep it moving. Rolling resistance’s relationship with deformation and elasticity is commonly experienced while riding a bicycle: when a tire loses air pressure it deforms more, requiring a greater effort to keep it in motion. A similar effect is experienced when transitioning from a rigid floor (such as concrete) to a soft and deformable floor (such as grass or sand). The effort increases considerably over softer, more deformable surfaces.

In vehicle dynamic analysis (chapter 2) rolling resistance is traditionally represented as a force acting against the wheel motion. However, when modelling rolling resistance at the wheel level, the usual representations is more detailed. Figure 5.2 shows the free body diagram for a wheel moving at a constant speed.

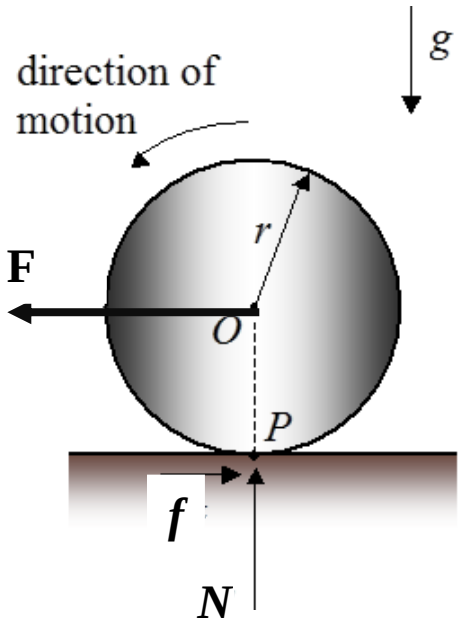

Figure D.2 Rolling resistance force free body diagram representation.

By adding forces in the horizontal direction the dynamic equation is:

$$\sum F_y = ma_y = 0 = F - f \tag{D.1}$$

By calculating the sum of moments around the wheel center we have:

$$\sum M_o = I\ddot{\theta} = 0 = fr - N\lambda \tag{D.2}$$

$$f = \frac{N\lambda}{r} = F \tag{D.3}$$

Where r is the radius of the wheel, N is the normal force, f is the rolling resistance force and λ is known as rolling resistance parameter (RRP).

The normal force is not perfectly aligned with the vertical load applied to the wheel. This is explained due to a shift of the contact pressure centroid while a wheel is in motion, as shown in figure D.3. This is a product of the elastic characteristics of the wheel and the floor.

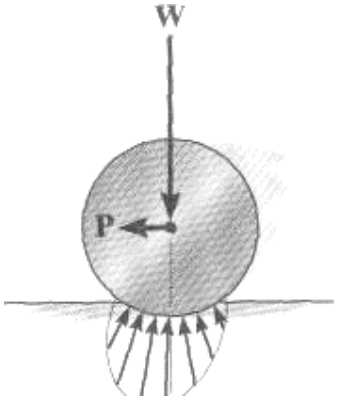

Figure D.3 Normal forces during wheel rolling motion.

The rolling resistance parameter λ has to be determined experimentally and is unique to a particular wheel rolling on a particular floor. Since rolling resistance depends on the deformation of tire and ground, λ acquires different values for different combinations. Tire material, shape and inflation pressure affect rolling resistance and thus

the rolling resistance parameter. In general the more deformable the wheel and floor, the greater the rolling resistance and associated RRP.

Manual wheelchair research is particularly focused rolling resistance since it is the dominant force affecting a wheelchair motion. Many methods are used each with their advantages and disadvantages. Figure D.4 shows a test performed over a dynamometer [27-29]. This procedure only allows to measure rolling resistance on the rear wheels and is unable to test different floor surfaces.

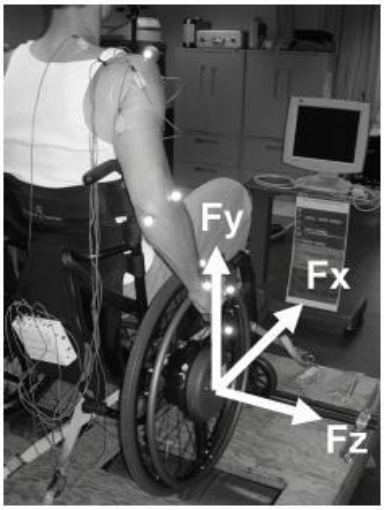

Figure D.4 Rolling resistance test using a dynamometer.

Figure D.5 shows a wheelchair test performed on a treadmill. This method allows to measure rolling resistance for the rear wheels and casters over a flat surface, and the velocity can be precisely controlled [30-33]. However, it doesn't allow to test the wheelchair in common floor surfaces such as carpet.

Figure D.5 Rolling resistance test using a treadmill.

Other methods of measuring rolling resistance are performed over the ground by adding sensors to the wheelchair, such as rotary encoders and accelerometers, or by the use of instrumented wheels, such as SmartWheels [29-32]. These methods are usually restricted to a particular set of maneuvers. The disadvantage of using human beings for testing have been previously discussed. In some experiments weights are added to the wheelchair and pushed to initialize motion. Unfortunately the maneuvers are very restricted.

Figure D.6 Rolling resistance test using an instrumented wheelchair.

The results of these experiments coincide that rolling resistance increments if the normal forces are increased (adding weight to the wheelchair). They also show that rolling resistance increases with velocity. Figure D.6 shows the result of an extended number of experiments relating rolling resistance parameters and velocity [38]. Since RRPs are directly proportional to rolling resistance it can be appreciated that rolling resistance changes non-linearly with velocity.

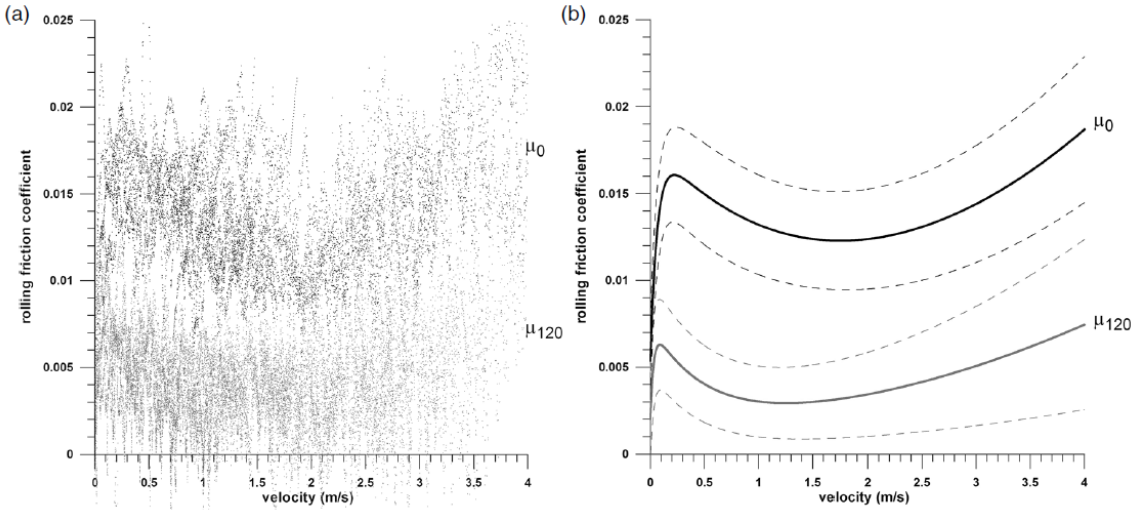

Figure D.7 Rolling resistance parameters variation with velocity [38].

The study of rolling resistance by using the AMPS is a novel and unique technique that allows testing on actual daily-used flooring while keeping the precise control obtained through more restrictive tests. It is expected that the AMPS experiments show new information otherwise unattainable with previous methodologies.

D.2 Turning resistance fundamentals

Turning resistance originates from the sliding friction between a wheel and the floor as the former rotates about its vertical axis while the wheelchair changes its orientation. A simplified model of this resistive force was presented by Thacker [38]. In figure D.8 an idealized contact area between the tire and the floor is depicted.

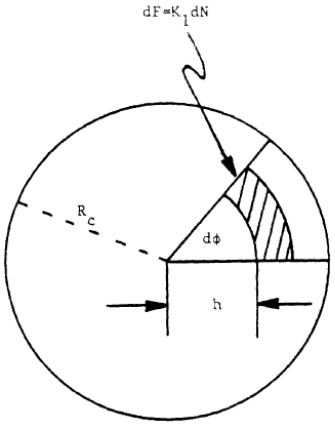

Figure D.8 Representation of the contact area between wheel and floor [38].

According to this model, the total resistive moment is

$$M = \frac{2}{3} KNR_c \qquad \text{(D.4)}$$

Where M is the turning resistance, N is the normal force, R_c is the radius of the contact patch and K is an experimental constant.

The only work known by the author regarding measurement of rolling resistance on manual wheelchair tires was written by T.G. Frank [8]. He used a special device (figure D.9) designed to measure the torque generated by a wheel rotating against a surface. His results can be observed on figure D.10 and present the change of turning resistance with the load applied to each wheel.

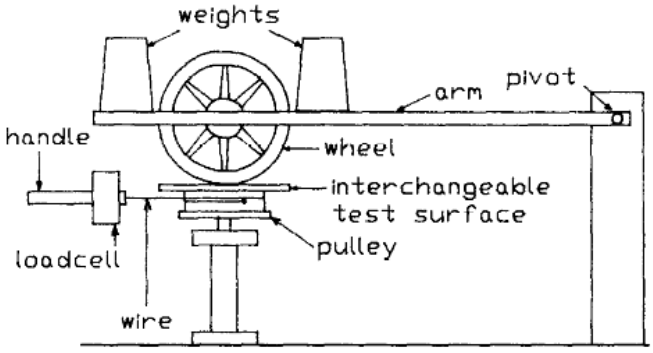

Figure D.9 Turning resistance device used by T.G. Frank [8].

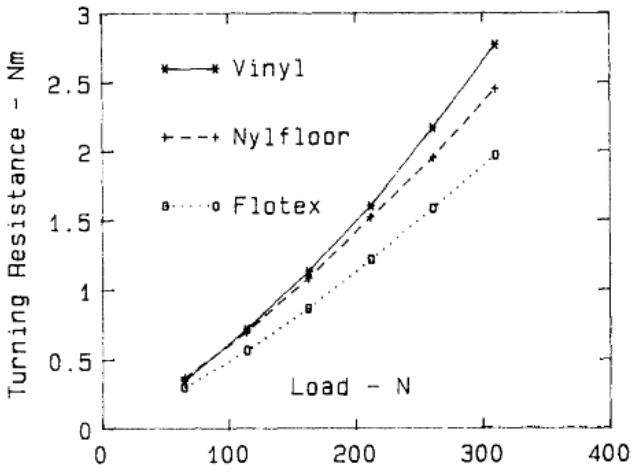

Figure D.10 Turning resistance measured for different loads and floor types [8].

Frank's device was limited by the fact that the wheel was not rolling as it changed direction with respect to the floor. The dynamics of a wheel rotating vertically as it rolls on a surface is complex and this work does not intend to model it. Instead, by using the AMPS we expect to find evidence of the resistance effect over a turning wheelchair.

APPENDIX E

EXPERIMENTS RESULTS TABLES

E.1 Rolling resistance experiments

E.1.1 Constant velocity experiments

In section 6.1.1 rolling resistance was measured for a straight path maneuver travelling at constant velocity. The protocol requires to do measurements of opposite directions of the same track. Results for both directions were averaged and used to calculate total rolling resistance.

Table E.1 Rolling resistance in constant velocity experiments

	Direction 1		*Direction 2*			
Wheelchair Velocity (m/s)	**Right motor average current (A)**	**Left motor average current (A)**	**Right motor average current (A)**	**Left motor average current (A)**	**Total average current (A)**	**Rolling resistance Force (N)**
0.4	4.38	3.46	5.29	2.47	7.79	17.26
0.5	3.41	4.89	3.41	4.89	8.30	18.29
0.6	4.53	3.63	5.19	2.42	7.88	17.97
0.7	4.27	4.13	4.97	3.03	8.20	18.51
0.8	4.75	3.80	5.47	2.66	8.34	18.82
0.9	4.35	4.17	5.13	2.83	8.24	18.76
1.0	4.82	3.71	5.55	2.56	8.32	18.77
1.1	4.72	3.98	5.55	2.66	8.45	19.17
1.2	4.83	4.18	5.78	3.05	8.92	19.85

Additional experiments were performed with different weight distributions. Original weight distribution was used in table E.1. Table E.2 shows added weight on the front, center and rear of the wheelchair.

Table E.2 Alternate weight distributions

Original		Added front		Added center		Added rear	
Front [kg]	Rear [kg]	Front [kg]	Rear [kg]	Front [kg]	Rear [kg]	Front [kg]	Rear [kg]
28.1	78.9	44.0	75.3	27.7	88.9	24.0	96.6

Table E.3 Rolling resistance with weight added at the front

	Direction 1		*Direction 2*			
Wheelchair Velocity (m/s)	Right motor average current (A)	Left motor average current (A)	Right motor average current (A)	Left motor average current (A)	Total average current (A)	Rolling resistance Force (N)
0.4	3.60	4.87	5.42	2.42	8.15	17.75
0.6	3.43	5.33	5.33	2.58	8.34	18.98
0.8	3.50	5.68	5.99	2.19	8.68	19.23
1.0	3.56	5.98	5.67	2.67	8.94	19.70
1.2	3.40	5.78	6.24	3.06	9.24	21.62

Table E.4 Rolling resistance with weight added at the center

	Direction 1		*Direction 2*			
Wheelchair Velocity (m/s)	Right motor average current (A)	Left motor average current (A)	Right motor average current (A)	Left motor average current (A)	Total average current (A)	Rolling resistance Force (N)
0.4	3.45	4.77	4.93	2.79	7.97	17.56
0.6	3.67	5.27	5.14	2.97	8.52	18.78
0.8	3.93	5.29	5.32	2.73	8.63	19.02
1.0	3.98	5.45	5.47	2.79	8.85	19.49
1.2	4.20	6.04	5.72	3.45	9.71	21.39

Table E.5 Rolling resistance with weight added at the rear

	Direction 1		*Direction 2*			
Wheelchair Velocity (m/s)	Right motor average current (A)	Left motor average current (A)	Right motor average current (A)	Left motor average current (A)	Total average current (A)	Rolling resistance Force (N)
0.4	3.40	4.91	4.79	2.71	7.90	17.41
0.6	3.84	5.17	4.90	2.98	8.45	18.61
0.8	3.91	5.26	5.09	2.81	8.54	18.81
1.0	3.86	5.47	5.29	2.79	8.70	19.17
1.2	4.16	5.48	5.64	3.49	9.38	20.68

E.1.2 Constant acceleration experiments

In section 6.1.3 rolling resistance was measured for a straight path maneuver travelling with constant acceleration. Results for both directions were averaged and used to calculate total rolling resistance.

Table E.6 Rolling resistance in constant acceleration experiments

	Direction 1		*Direction 2*			
Wheelchair Acceleration (m/s2)	**Right motor average current (A)**	**Left motor average current (A)**	**Right motor average current (A)**	**Left motor average current (A)**	**Total average current (A)**	**Rolling resistance force (N)**
0.12	6.90	7.85	8.13	6.03	14.45	19.17
0.15	7.55	9.04	9.10	6.56	16.13	19.64
0.20	8.85	9.84	10.04	8.03	18.38	19.24
0.25	10.34	11.62	11.46	9.51	21.47	20.69
0.30	11.83	13.35	12.51	10.84	24.27	21.51
0.36	13.29	14.94	14.04	12.54	27.41	22.00
0.43	15.90	16.43	16.58	15.06	31.98	24.60
0.48	17.13	18.16	18.08	16.32	34.84	25.55

E.2 Turning resistance experiments

In section 6.2 turning resistance was measured for a wheelchair travelling at constant velocity on a circular trajectory. The experiments were repeated in both directions of the circle: clockwise and counterclockwise.

Table E.7 Turning resistance for different circular trajectories

			Clockwise turn		*Counterclockwise turn*		
Radius of curvature (m)	**Caster 1 orientation (degrees)**	**Caster 2 orientation (degrees)**	**Right motor average current (A)**	**Left motor average current (A)**	**Right motor average current (A)**	**Left motor average current (A)**	**Average Turning resistance (Nm)**
1.8	12.32	15.90	7.21	0.45	1.72	6.28	2.83
1.5	14.35	19.39	7.90	-0.30	0.49	7.23	4.43
1.2	17.16	24.72	8.34	-1.37	-0.42	7.65	5.16
0.9	21.28	33.58	9.97	-3.30	-1.47	8.44	6.86
0.6	27.76	49.76	10.93	-6.43	-4.64	9.82	9.38
0.3	40.11	81.18	11.68	-17.83	-14.42	10.74	16.13

E.3 Cost of transport

In section 6.3.2 cost of transport (COT) was measured for a wheelchair travelling at constant velocity on straight trajectory. COT was additionally compared to the ratio between average rolling resistance and the mass of the system.

Table E.8 Cost of transport for straight trajectories

		direction 1		*direction 1*		*average*		
Velocity (m/s)	**mass (kg)**	**distance (m)**	**Energy input (J)**	**distance (m)**	**Energy input (J)**	**COT (J/kgm)**	**Froll (N)**	**Froll/m (N/kg)**
0.4	108.4	14.7	213.9	14.3	287.7	0.160	17.7	0.163
0.5	108.4	14.0	206.0	13.7	283.3	0.163	17.8	0.164
0.6	108.4	13.6	204.6	13.3	290.3	0.170	18.5	0.170
0.7	108.4	12.9	202.3	12.6	286.1	0.177	19.2	0.177
0.8	108.4	13.0	210.2	12.8	296.5	0.181	19.7	0.182
0.9	108.4	12.8	207.6	12.6	293.3	0.182	19.8	0.182
1	108.4	12.1	201.4	11.9	288.5	0.188	20.3	0.188
1.1	108.4	12.2	207.6	12.0	295.5	0.192	20.9	0.193
1.2	108.4	12.0	214.7	11.9	299.5	0.198	21.7	0.200

A similar analysis procedure was done for a wheelchair travelling at constant velocity on a circular trajectory. The experiments were repeated in both directions of the circle: clockwise and counterclockwise.

Table E.9 Cost of transport for circular trajectories

			Clockwise turn		*Counterclockwise turn*		
Velocity (m/s)	**Radius (m)**	**mass (kg)**	**Energy input (J)**	**distance (m)**	**Energy input (J)**	**distance (m)**	**Average COT (J/kgm)**
0.60	1.8	108.42	174.76	9.03	166.36	8.56	0.18
0.61	1.5	108.42	151.38	7.54	147.97	7.53	0.18
0.60	1.2	108.42	108.24	5.25	104.85	5.14	0.19
0.61	0.9	108.42	87.59	3.69	81.37	3.70	0.21
0.63	0.6	108.42	99.82	3.62	95.16	3.68	0.25
0.60	0.278	108.42	100.56	2.23	82.89	1.97	0.40

REFERENCES

[1] World Health Organization. "Guidelines on the provision of manual wheelchairs in less resourced settings." (2008).

[2] Brault, Matthew W. *Americans with disabilities*: 2010. US Department of Commerce, Economics and Statistics Administration, US Census Bureau, 2012.

[3] Boninger, M.L., et al., "Manual wheelchair pushrim biomechanics and axle position." *Archives of physical medicine and rehabilitation*, 2000. 81(5): p. 608-613.

[4] Van der Woude, L. H. V., et al. "Optimum cycle frequencies in hand-rim wheelchair propulsion." *European journal of applied physiology and occupational physiology* 57.6 (1979): 625-632.

[5] Van der Woude, L. H., et al. "Wheelchair racing: effects of rim diameter and speed on physiology and technique." *Medicine and science in sports and exercise* 20.5 (1988): 492-500.

[6] Van der Woude, L.H., et al., "Measurement of wheelchair rolling resistance with a handle bar push technique." *J Med Eng Technol*, 2003. 27(6): p. 249-58.

[7] Kauzlarich, J.J. and J.G. Thacker, "Wheelchair tire rolling resistance and fatigue." *J Rehabil Res Dev*, 1985. 22(3): p. 25-41.

[8] Frank, T. G., and E. W. Abel. "Measurement of the turning, rolling and obstacle resistance of wheelchair castor wheels." *Journal of biomedical engineering* 11.6 (1979): 462-466.

[9] Frank, T. G., and E. W. Abel. "A technique for the accurate measurement of low values of rolling resistance." *Proceedings of the Institution of Mechanical Engineers*, Part D: Journal of Automobile Engineering 202.4 (1977): 251-255.

[10] Kwarciak, Andrew M., et al. "Evaluation of wheelchair tire rolling resistance using dynamometer-based coast-down tests." *Journal of Rehabilitation Research & Development* 46.6 (2009).

[11] Beekman, C.E., L. Miller-Porter, and M. Schoneberger, "Energy cost of propulsion in standard and ultralight wheelchairs in people with spinal cord injury." *Physical therapy*, 1999. 79(2): p. 146-158.

[12] International Standards Organization, ISO 7176 Wheelchair Standards- Section 11: Test Dummies, 2012, International Standards Organization.

[13] Walter, J. D., and F. S. Conant. "Energy losses in tires." *Tire Science and Technology* 2.4 (1964): 235-260.

[14] Bascou, Joseph, et al. "A method for the field assessment of rolling resistance properties of manual wheelchairs." *Computer methods in biomechanics and biomedical engineering* 16.4 (2013): 381-391.

[15] Patterson, Murray G. "What is energy efficiency?: Concepts, indicators and methodological issues." *Energy policy* 24.5 (1996): 377-390.

[16] Shi, Wei, Douwe Stapersma, and Hugo T. Grimmelius. "Comparison study on moving and transportation performance of transportation modes."

[17] Johnson, Barry W., and James H. Aylor. "Dynamic modeling of an electric wheelchair." *Industry Applications*, IEEE Transactions on 5 (1975): 1274-1293.

[18] Bascou, Joseph, et al. "A method for the field assessment of rolling resistance properties of manual wheelchairs." *Computer methods in biomechanics and biomedical engineering* 16.4 (2013): 371-391.

[19] Chénier, Félix, Pascal Bigras, and Rachid Aissaoui. "An Orientation Estimator for the Wheelchair's Caster Wheels." *Control Systems Technology*, IEEE Transactions on 19.6 (2011): 1317-1326.

[20] Hofstad, M. and P.E. Patterson, "Modelling the propulsion characteristics of a standard wheelchair." *Journal of Rehabilitation Research and Development*, 1994. 31(2): p. 129-37.

[21] Eicholtz, M.R., et al., "Test method for empirically determining inertial properties of manual wheelchairs." *J Rehabil Res Dev*, 2012. 49(1): p. 51-62.

[22] AmpFlow motor A40-300 Performance Chart. http://www.ampflow.com/A40-300_Chart.png.

[23] Teran E and Ueda J. "Evaluation of Wheelchair Rolling Resistance Using a Robotic Device." *Proceedings of the 2014 IEEE Workshop on Advanced Robotics and its Social Impacts (ARSO 2014)*. 2014. Evanston, IL.

[24] Leary, M., et al. "A fundamental model of quasi-static wheelchair biomechanics." *Medical engineering & physics* 34.9 (2012): 1278-1286

[15] Clark, Samuel Kelly, and Richard N. Dodge. "A handbook for the rolling resistance of pneumatic tires." (1979).

[26] Roberts, G. B. "Power Wastage in Tires." *Proceedings of the International Rubber Conference.* 1959.

[27] Theisen, Daniel, et al. "A new procedure to determine external power output during handrim wheelchair propulsion on a roller ergometer: a reliability study." *International journal of sports medicine* 17.08 (1996): 564-571.

[28] Faupin, Arnaud, et al. "The effects of rear-wheel camber on the mechanical parameters produced during the wheelchair sprinting of handibasketball athletes." *Journal of rehabilitation research and development* 41.3B (2004): 421-428.

[29] Kwarciak, Andrew M., et al. "Evaluation of wheelchair tire rolling resistance using dynamometer-based coast-down tests." *J Rehabil Res Dev* 46.7 (2009): 931-38.

[30] Kauzlarich, J. J., and J. G. Thacker. "Wheelchair tire rolling resistance and fatigue." *Journal of rehabilitation research and development* 22.3 (1985): 25-41.

[31] Brubaker, C. E. "Wheelchair prescription: an analysis of factors that affect mobility and performance." *J Rehabil Res Dev* 23.4 (1986): 19-26.

[32] Woude, Lhv Van Der, et al. "Wheelchair ergonomics and physiological testing of prototypes." *Ergonomics* 29.12 (1986): 1561-1573.

[33] Van der Woude, Lucas HV, Sonja de Groot, and Thomas WJ Janssen. "Manual wheelchairs: Research and innovation in rehabilitation, sports, daily life and health." *Medical engineering & physics* 28.9 (2006): 905-915.

[34] Coutts, Kenneth D. "Drag and sprint performance of wheelchair basketball players." *Journal of rehabilitation research and development* 31 (1994): 138-138.

[35] Hoffman, Martin D., et al. "Assessment of wheelchair drag resistance using a coasting deceleration technique." *American journal of physical medicine & rehabilitation* 82.11 (2003): 880-889.

[36] Bascou, J., et al. "Error estimations of wheelchair deceleration tests using a 3D accelerometer." *Computer Methods in Biomechanics and Biomedical Engineering* 13.S1 (2010): 21-22.

[37] Sauret, C., et al. "Repeatability of wheelchair deceleration tests using a 3-D accelerometer." *Computer Methods in Biomechanics and Biomedical Engineering* 13.S1 (2010): 137-138.

[38] Chua, J. J. C., F. K. Fuss, and A. Subic. "Non-linear rolling friction of a tyre-caster system: analysis of a rugby wheelchair." *Proceedings of the Institution of Mechanical Engineers*, Part C: Journal of Mechanical Engineering Science 225.4 (2011): 1015-1020.

[39] J. G. Thacker, "Lecture notes on wheelchair dynamics," Univ. of Virginia, 1980.